論文 / 著書情報
Article / Book Information

題目(和文)	
Title(English)	COMPACT ODOR SENSING SYSTEM BASED ON INSECT OLFACTORY RECEPTORS AND FLUORESCENT INSTRUMENTATION ROBUST AGAINST DISTURBANCE
著者(和文)	MujionoTotok
Author(English)	Mujiono Totok
出典(和文)	学位:博士（工学）, 学位授与機関:東京工業大学, 報告番号:甲第10321号, 授与年月日:2016年9月20日, 学位の種別:課程博士, 審査員:中本 高道,岩本 光正,山田 明,間中 孝彰,宮島 晋介,神崎 亮平
Citation(English)	Degree:, Conferring organization: Tokyo Institute of Technology, Report number:甲第10321号, Conferred date:2016/9/20, Degree Type:Course doctor, Examiner:,,,,,
学位種別(和文)	博士論文
Type(English)	Doctoral Thesis

TOTOK MUJIONO

COMPACT ODOR SENSING SYSTEM BASED ON INSECT OLFACTORY RECEPTORS AND FLUORESCENT INSTRUMENTATION ROBUST AGAINST DISTURBANCE

A THESIS SUBMITTED IN PARTIAL FULFILLMENT OF THE REQUIREMENTS
FOR THE DEGREE OF DOCTOR OF ENGINEERING

DOCTORAL THESIS

Supervised by

Professor Takamichi Nakamoto

Department of Physical Electronics

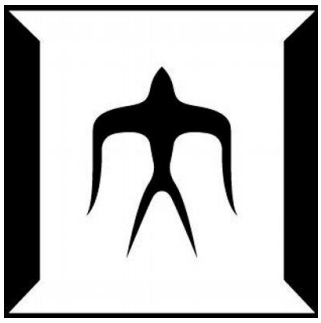

Tokyo Institute of Technology

2016

ABSTRACT

Recently, the demands on various odor detection system in many areas of application are growing significantly. The development of odor sensor based on olfactory receptor (OR) of human or animal olfaction system is a promising approach for realizing highly selective and highly sensitive sensor since the performance of a current artificial sensor is insufficient. Among the techniques available in biosensor transducer, fluorescence microscopy offers advantages of noninvasive technique with high sensitivity. However, the main problem of this technique is the presence of ambient light when the measurement is not performed in dark condition since the intensity of fluorescence light is very weak. A lock-in measurement technique can be applied to the system to acquire a weak fluorescent signal buried under the strong ambient light and noises. Furthermore, a compact, low power, and robust measurement system is very demanding. The purpose of the research is to develop a portable fluorescent instrumentation system robust against ambient light using lock-in measurement technique.

The system consists of a cell based biological sensing element, an optical transducer, a lock-in amplifier, and a microfluidic system (MFS) chamber. Sf21 cell expressing the insect OR and calcium ion (Ca^{2+}) indicator fluorescent protein was used as sensing element. The bindings of odorant molecules by the OR triggers the increase of intracellular Ca^{2+} concentration since the OR and co-receptor forms an ion channel. The fluorescent protein is used to monitor the activity of Ca^{2+}. The higher odorant concentration is, the more Ca^{2+} influx is. Then, the increase of Ca^{2+} concentration makes the cell emit higher fluorescent intensity when it receives the excitation light. The optical system is used to provide the cell sensor with the proper blue (488nm) excitation light from laser diode and to capture the emitted green (512nm) fluorescent light on a complementary metal–oxide–semiconductor (CMOS) camera. Processing the fluorescent intensity and performing the lock-in technique were done using Matlab on PC. Cell immobilization and odorant exposure were performed in an acrylic chamber for static system and a MFS made of glass and polydimethylsiloxane (PDMS) for flow system. The cell immobilization was done by letting the cell be adsorbed firmly at the base on the chamber.

Both static and flow systems were evaluated in this study. First, several experiments were performed on the static system. Both cells, expressing Or56a and BmOR3, responded to geosmin and bombykal with concentrations from 5μM to 100μM, respectively. It was difficult to obtain the responses to odorant with concentration smaller than 5μM in static system since it was almost the artifact level due to odorant dropping.

Then, the apparatus for flow system consists of pump, micro pipe, flow chamber, solenoid valve and sink. Two types of pumps were used, micro-pump and syringe-pump. The applied flowrate of odorant should be kept less than 400μl/min to avoid the cell removal. Typical

characteristics of micro-pump are small size and low power dissipation. Thus it is suitable for realizing a portable system. However, micro-pump cannot be used for the experiment on small concentration since it produces the artifact. Experimental results show that microfluidic system using micro-pump was suitable for measuring odorant concentration between 5μM and 100μM (or above). Syringe pump has precise and stable flowrate. However, it cannot be used for portable applications because of its weight and dimension. In low flowrate (100μl/min.), almost no artifact was produced by syringe pump. Syringe-pump was used to investigate the detection limit of the cells response to the odorant. Experimental results show that the detection limit of Or56a cell lines to the geosmin odorant was 100nM while the detection limit of Or13a cell lines to the 1-octen-3-ol odorant was 50nM in the dark condition.

A lock-in measurement technique was incorporated into the system to avoid the influence of the ambient light. In the ambient light condition, the CMOS camera captures not only the fluorescent light, but also unwanted light such as background, offset, and noise. Lock-in measurement technique consists of fluorescent signal modulator, high-pass filter (HPF), phase sensitive detector (PSD), reference signal, and low-pass filter (LPF). The fluorescent signal was modulated by the laser diode system. The other blocks were implemented offline using Matlab. Experimental results in dark condition show that application of lock-in measurement technique slightly improved the detection limit down to 50 nM geosmin concentration and 25nM 1-octen-3-ol concentration for Or56a and Or13a, respectively. Compared with dark condition, applying the lock-in technique to both low (500 flux) and high (1000 flux) ambient light conditions, the limits of detections were almost the same for both cell lines with their associate odorants. The improvement of the detection limit reached approximately three orders of magnitude under the ambient light condition. Without lock-in technique, the limit of detection deteriorates much in ambient light condition.

Several improvement should be made by implementing the image and lock-in technique processing on FPGA platform to improve the speed, power dissipation, and compactness in the near future. Moreover, the cells with two or more OR types can be captured in one image to form a sensor array. Thus the system can be used to implement a compact and sensitive odor sensing system.

ACKNOWLEDGEMENT

I deeply appreciate my advisor, Professor Takamichi Nakamoto, for his guidance, mentoring, and encouragement throughout my whole PhD studies. He giving me an opportunity to conduct a world class researches in his laboratory to broaden my field and build my multidisciplinary knowledge. I respect his professional attitude to research and development, and his tremendous experience and acknowledge that helped me not only to complete my degree but also to develop myself as a researcher.

I would like to express my special gratitude and appreciation to Professor Ryohei Kanzaki of Tokyo University. I am thankful for allowing me to use “his cells”, which is an important part on my research, and being a committee member of my PhD study. Furthermore, the opportunity to interact with his laboratory members was a wonderful experience.

My sincere thanks to Professor Mitsumasa Imamoto for being my mentor and one of committee members of Phd study.

My sincere thanks are to the committee members of my PhD study, Professor Takaaki Manaka, Professor Shigeki Nakagawa, Professor Akira Yamada, Professor Shinsuke Miyajima, and Professor Nam Hai Pham for their mentoring, valuable suggestions and advices.

Special thanks to Dr. Hidefumi Mitsuno of Tokyo University for his invaluable help during my research. We had many discussions.

I would also like to thank the present and the past members of Nakamoto Laboratory Barto-san, Harada-san, Iseki-san, Suzuki-san, Kakizaki-san, Sukekawa-san, and many more. I am feeling at home because of them. They help me a lot.

I would like to send my great thanks to Japanese Government, Department of Agriculture and JASSO, for financing my research study.

Finally, I thanks to my wife (Drg. Ariesta Widiastuti), my children (Nafisa Damayanti Mujiono, Kurnia Ramadhani Mujiono, and Arya Pramudhita Mujiono), and our parents in Indonesia. Their enormous love and spiritual encouragement help me to realize my dream. This dissertation and my PhD degree could not be accomplished without their invaluable support.

Table of Contents

Chapter 1
Introduction

1.1 Background and Motivation

Smell or odor sensing system is beneficial for quality control in many areas of industry such as fragrance [1], food, and beverage [2]. The odor detection is found important in the environmental monitoring [3], chemical purity analysis, medical diagnosis [4], or even in drug and explosive material detection, etc. [5]. Currently, the artificial odor sensing system is not adequate for most of applications and most of odor related activities are performed by human or animal such as dogs [6]. With enough training, both human and dog have capability with most of important characteristics of sensing system such as selectivity, sensitivity and real time. They suffer from subjectivity since their performance depends on physical and physiological wellness [7]. Thus, they lack in repeatability and unavailability for mass production. Another drawback of using living body as a sensor is the expensive training cost. There are growing demands and area of applications for selective, sensitive and real time odor sensing system.

Most of the odors are composed of mixtures of many odorant molecules with different concentrations [8]. Therefore, individual gas sensor is not adequate for the purpose of odor detection. Inspired by human olfactory system composed of many types of odor receptors, an array of sensors forms an odor sensing system called electronic nose (e-nose) [9]. The first e-nose was reported by Wilkens and Hatman in 1964 [10]. However, the concept of e-nose as an intelligent chemical sensor appeared 20 years later [11]. Since then the artificial odor sensors have been developed for many areas of applications. However, the performance of artificial odor sensor is inferior to living organism capability [12]. Utilization of odor biological sensor is intended to meet the performance requirement of e-nose. The olfaction sensory organ of living creature has been developed through long time of evolution, the smell (odor) detection contains useful information for sustaining their life such as danger, food, mating [13]. Utilization of olfactory organ as a sensor expected to exceed the capability of living creature. Possibility of using olfactory organ as a sensor becomes realistic by discovery of olfactory receptor (OR) [14] and advanced development of bio engineering to express an OR on in another cell or organ [15].

OR based sensing element coupled with optical fluorescent technique is one of the well-known techniques for odor biosensor since it is sensitive, non-invasive techniques and easy to prepare or immobilized [16]. In response to the odorant, biosensor produce the biological signal in the form of increasing calcium ion inside cell expressing

OR and fluorescent protein. A transducer based on fluorescent microscopy is used to detect the change of calcium ion activity. Basically, the cell illuminated by an excitation light emits the fluorescent light with intensity which reflects the concentration of odorant. The main problem of optical fluorescent technique is the presence of background light (disturbance) when it is used under ambient light condition since the intensity of fluorescent light is very small [17]. Special instrumentation technique called lock-in amplifier or lock-in measurement can be applied to the system where the signal is buried under the noise [18]. Another current issue in designing an electronic system is portability [19] which has characteristic small in dimension, low-power and light weight. This research is intended to develop a compact odor sensing system based on insect olfactory receptors and fluorescent instrumentation robust against disturbance.

1.2 Mechanism of olfaction

Olfaction, According Mirriam-Webster dictionary, is the sense of smell or the act of smelling. Any substance that have distinctive smell known as odorant, a volatile chemical compound. The organ or nerve concerned with the sense of smell known as olfactory organ. Olfaction contained many important/useful information. The olfactory perception consist of four-step process: (1) stimulation – an odorant stimulus impinge on an odorant receptor; (2) transduction - the stimulus energy produces electrochemical nerve impulses in the dendrites of the sensory neuron; (3) transmission - the axon of the sensory neuron conducts action potentials along an afferent pathway to the central nervous system (CNS) or brain; and (4) interpretation - the brain creates a sensory perception from the electrochemical events produced by afferent stimulation [20]. Basically, the odorant receptor (OR), the olfactory receptor neuron (ORN), glomeruli, and olfactory cortex (brain) are responsible for each step.

There are two types of olfactory system of terrestrial creature (air breathing), insect and vertebrate. In vertebrate, OR and ORN are located in olfactory ephithelium while glomeruli located in olfactory bulb. In insect, OR and ORN are located in antenna and maxillary pulp while glomeruli located in antennal lobe.

Figure 1.1 shows the schematic diagram of human olfactory system which is typical for vertebrate. The process of olfaction begins when odorants are inhaled and get through an aqueous medium (mucus) layer prior to contact with the olfactory epithelium. The odorant binding protein (OBP) carries the odorants towards cilia where the odorant molecules bind its associate OR and start the signal transduction mechanism [21]. There are several theories describing the mechanism by which odorants bind to the ORs which are based on shape, vibration, and tunneling [22].

Figure 1.2 shows the process of signal transduction mechanism of vertebrate. When the odorant molecules bind to the ORs, their attachment induces a change in the shape of the olfactory receptor [23]. The modification in the structure of the receptor induces their binding to the G-protein (comprised of α, β, and γ) which activates the adenylyl cyclase (AC). The AC converts adenosine triphosphate (ATP) into cyclic-3',5'-Adenosyl monophosphate (cAMP), known as second messenger. As the intracellular concentration of cAMP increases, it activates the gated ion channel (cyclic nucleotide-gated, CNG channel) which permits the entry of extracellular ions (Na^+ and Ca^{2+}) which causes the inside of cell to become less negative. The Ca^{2+} influx causes an opening of calcium-gate chloride channels, resulting in Cl^- efflux that causes depolarization which activates the action potentials of the receptor cell and provides the neural signals to the olfactory bulb. Sensory information received from olfactory receptors is processed (decoded) in olfactory bulb before it is transmitted to the olfactory cortex located on the brain for odor identification [24]. Most of odors are composed of multiple odorant molecules and each of them activates several ORs. There are more than 400 ORs on human olfactory organ [25].

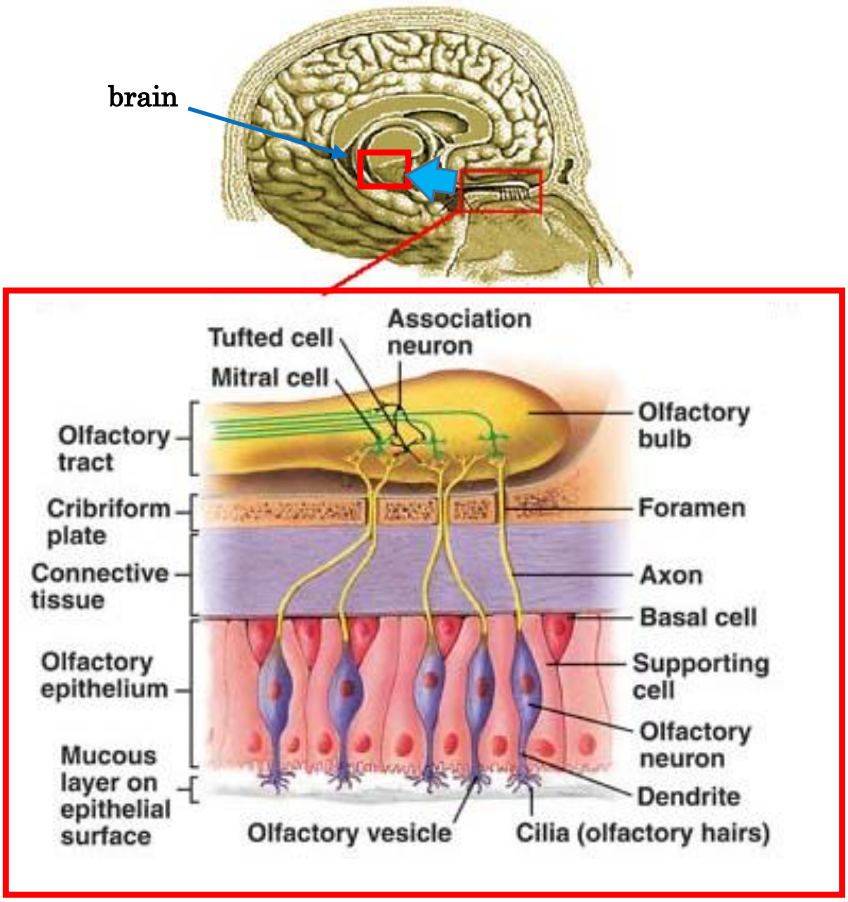

Figure 1.1 Schematic diagram of the human olfactory system [21].

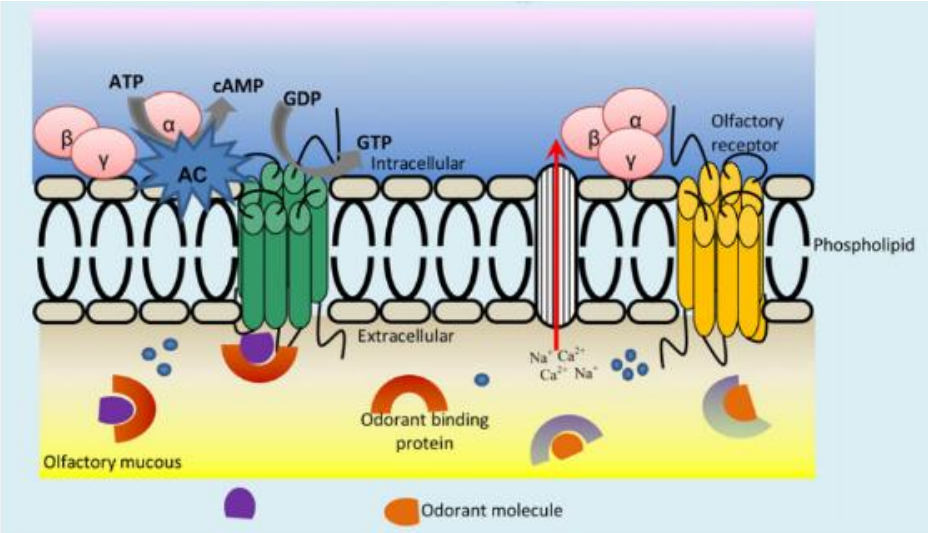

Figure 1.2 Schematic diagram of the signal transduction in vertebrate [23].

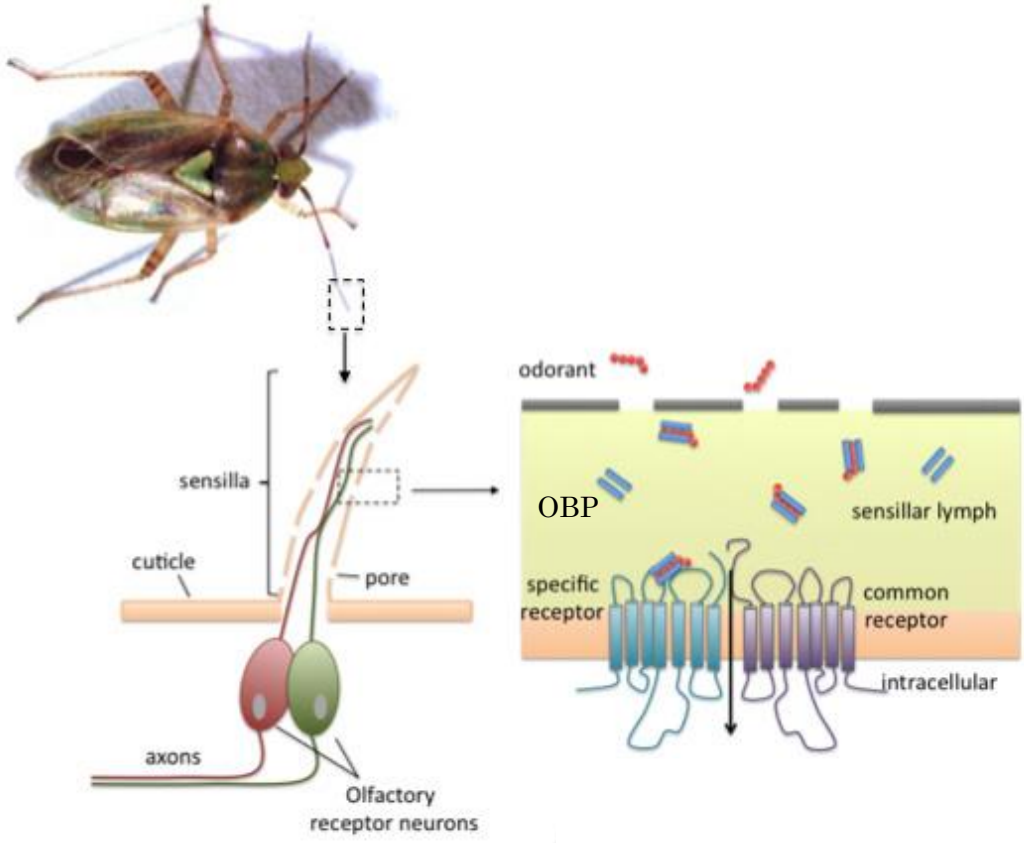

Figure 1.3 Olfaction mechanism in insect [27]

The mechanism of olfaction in insect begins in antenna and maxillary pulp when odorants molecules get through the pores and then aqueous medium (lymph) layer prior to contact with the receptor. The OBP assists the molecules to go towards sensila where the odorant molecules bind its associate receptor (ORx) and start the signal transduction mechanism [26]. The mechanism of signal transduction in insect is simpler than human (vertebrate). Figure 1.3 (right) shows the signal transduction model in insect. Specific receptor (ORx) forms heteromeric complex with the common receptor (Orco) and function as an odorant-gated ion channel [27]. When the ORx bind the odorant molecule, odorant-gate ion channel become an "open" gate and allows the calcium ion influx from extracellular to intracellular. Calcium ion act as a signal transduction which activates the action potentials of the receptor cell and provides the neural signals to the glomeruli located in antennal lobe. Sensory information received from olfactory receptors is processed (decoded) in glomeruli before being transmitted to the olfactory cortex located on the brain for odor identification [28]. There are more than 60 types of ORs available in insect.

1.3 Related work

1.3.1 Odor Sensor for E-nose.

Odor is a mixture of molecules that are able to stimulate odorant receptor when it is in contact with sensory systems. Odorant molecules have some basic characteristics such as: light (relative molecular masses up to approximately 300 Dalton), small, polar, and mostly hydrophobic [29]. Simple odor such as alcohol, contains only one chemical component while complex odor can be made up of hundreds or even thousands of different molecules each in varying concentration. Table 1.1 shows several examples of common simple odorant with their main chemical constituents [30]. The threshold is for the detection by normal and healthy person, which have wide range of values. Most of natural smells, perfumes, and flavors are complex mixtures of chemical species. Table 1.2 shows the chemical components included in coffee aroma [31]. People can detect coffee aroma easily, but it has many constituents which may change over time.

Mimicking the biological olfaction system, which employs a large number of OR types, odor sensor is developed. Odor sensor or e-nose is a sensing system using an array of sensors with partially overlapping specificities to a wide range of odorants [32]. The collection of data obtained from many sensors is then processed using an appropriate pattern recognition system. Typical schematic diagram of e-nose system with its associate organ in human olfactory system is shown in Figure 1.4 [33].

Table 1.1. Some examples of simple odor [30].

Odor type	**Main chemical species**	**Threshold (ppb in water)**
Beer	Diacetyl	500
Green leaves	Trans-2-hexenal	316
Rose	Geraniol	290
Thyme	5-Isopropyl-2-methylphenol	86
Lemons	Limonene	10
White fish	Cis-4-heptenal	0.04
Butter	Octa-1,5-diene-3-one	0.01
Green papers	2-Isobutyl-3-methoxypyrazine	0.002
Grape fruit	α-Therpinethiol	0.00002

Table 1.2. Constituents of coffee aroma by chemical class [31]

Class of chemical species	**Number in class**
Furans	108
Pyrazines	79
Pyrroles	74
Ketones	70
Phenols	44
Hydrocarbons	31
Esters	30
Aldehydes	28
Oxazoles	28
Thiazoles	27
Thiophenes	26
Amines	21
Acids	20
Alcohols	19
Pyrydines	13
Thiols/Sulfides	13
Total	**631**

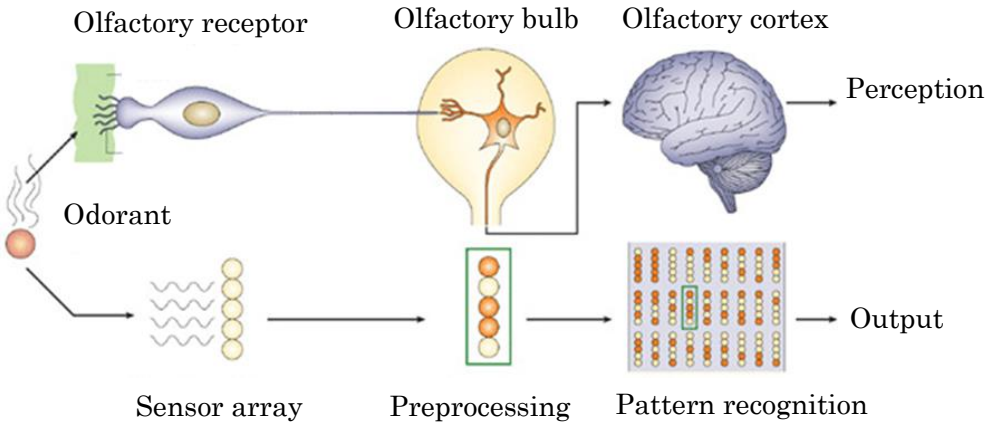

Figure 1.4. Typical schematic diagram of e-nose system (below) with associated block of human olfactory system (above) [33].

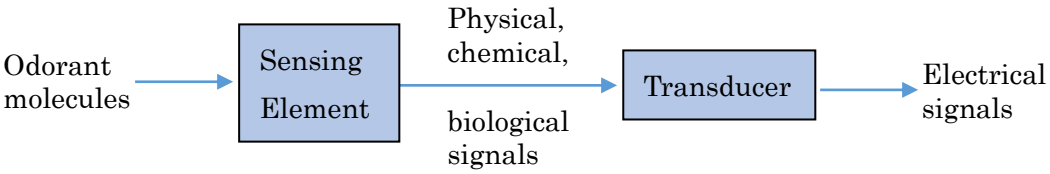

Figure 1.5. Typical schematic diagram of sensor used in a sensor array.

Sensor technology for e-nose has developed rapidly over the past decades. Figure 1.5 shows the schematic diagram of typical sensor. It consists of sensing element and transducer. Odorant molecules interact with the sensing element by either binding, absorption, adsorption, or chemical reactions [34]. There are two types of sensing elements, artificial and biological ones. Artificial sensing element normally interacts with odorant molecules in the gas phase and produces physical or chemical changes. As in human or animal olfaction system, biological sensing element normally works in the liquid phase and resulted in biological change after the interaction with odorant molecules. The non-electrical signals (physical, chemical, and biological signal) produced by sensing elements are then converted to electrical signal by transducer for further processing.

The sensors employed for e-nose should meet several criteria. They should have broad selectivity and high sensitivity to different types of chemical species (analyte), fast response time, short recovery time, low sensitivity to physical and environmental variable, robust, stable, and reproducibility [35]. Small size and low power sensor system are also desired for portable device implementation.

1.3.1.1 Artificial sensor for e-nose.

The most common sensing elements to capture odorant molecules in artificial sensor is chemical interactive material [36]. Several common physical properties change due to the interaction between odorant molecules and sensing element summarized in Table 1.3. A brief description of some sensor technologies given next. Most of the commercial artificial system are based on conductivity, piezoelectric, and MOS sensors.

Table 1.3. Physical changes in the sensor and the sensor devices used to transduce them into electrical signals

Physical changes	**Sensor type**	**Sensor**
Conductivity	Conductivity sensor	Conducting polymer [37,38].
Mass	Piezoelectric sensor	QCM [39,40], SAW [41,42].
Work function	Metal oxide sensor	MOSFET [43], MESFET [44]
Optical	Optical sensor.	Fluorescent detector[45]

1.3.1.1.1 Conducting polymer sensor

Conducting polymer sensor is based on measuring the conductivity or resistance of a thin-film polymer coated between two electrodes when the odorant molecules are adsorbed or absorbed into the polymer. The sensor response is correlated with the concentration of odorant. Sensor is fabricated by forming electro-polymerizing thin polymer films across a narrow electrode gap. Figure 1.6 shows the basic schematic diagram of conducting polymer sensor.

Conducting polymer material such as polypyrrole, polythiophene and polyaniline are typically used for e-nose sensing [46]. Several examples of gasses detected by conducting polymer are CH_4, $CHCl_3$ and NH_4 [47]. Several features of conductive polymer include fast and reversible response, easy to produce, long lifetime and low power. The main drawback of conducting polymer is the sensitivity toward humidity and temperature.

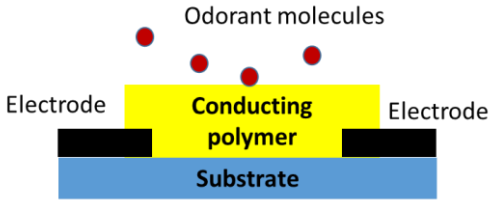

Figure 1.6. Schematic diagram of conducting polymer sensor.

1.3.1.1.2 Piezoelectric sensor

Piezoelectric sensor exploits the stable frequency resonance of piezoelectric materials such as quartz when acoustic wave passes through the crystal. The adsorption of gas molecules onto the coating film on the surface induces a shift in the oscillation frequency that is directly related to the mass of the adsorbed compound [48]. There are two types of piezoelectric sensors used in odor sensing, the surface acoustic wave (SAW) device and the quartz crystal microbalance (QCM). The SAW device produces a surface acoustic wave that travels along the surface of the piezoelectric substrate while the QCM produces a bulk acoustic wave that travels through the bulk of the sensor.

Figure 1.7 shows the schematic diagram of SAW sensor composed of piezoelectric substrate with an input and output interdigital transducer deposited on top of the substrate [49]. A gas sensing film is coated on the area between both transducers and an alternating current (AC) signal is applied to the input transducer creating a wave that propagates along the surface of the substrate. When the film interacts with analyte gas it has mass change and the frequency of the wave become changed. The materials for substrate are normally prepared from ZnO on silicon substrate, lithium niobate or quartz while for the sensitive membrane is usually polymer, liquid crystal, phospholipids or fatty acids. SAW sensor can detect a broad spectrum of odors due to the wide range of gas sensitive coatings available with high sensitivity and fast response times [50]. However, SAW devices suffer from poor signal to noise performance and high sensitivity to humidity and temperature [51].

Quartz crystal microbalance (QCM) sensors works on the same principle as SAW sensor. Figure 1.8 shows the schematic diagram of QCM sensor is made of a quartz disc coated with the adsorbing polymer layer and a set of gold electrodes evaporated onto both side of the polymer/quartz structure [52]. An AC voltage is applied to the piezoelectric quartz crystal and make the material oscillates at its resonant frequency. The wave produced, travels through the entire bulk of the crystal. When the sensor is exposed to vapor and the crystal adsorbs the associated molecules, its mass increases and alters the resonant frequency of the quartz crystal. A QCM coated with Polyvinylpyrrolidone has been used to detect various organic vapors and had a linear frequency shift with concentration of ethanol, n-heptane and acetone [53]. The advantages of using QCMs are fast response times. However, QCM gas sensors have disadvantages in poor signal to noise ratio [54].

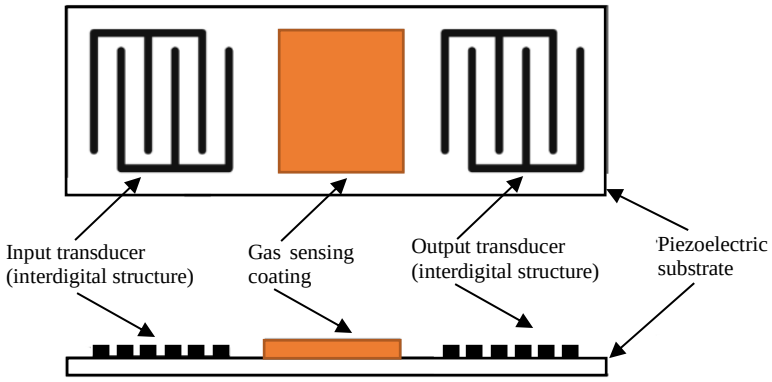

Figure 1.7. Schematic diagram of SAW sensor.

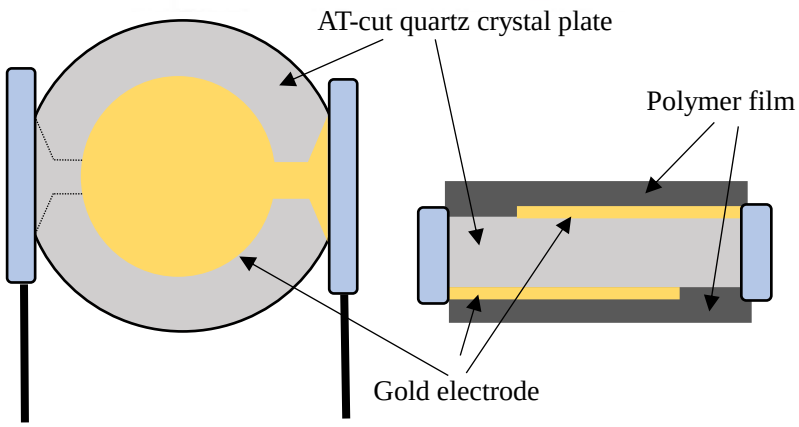

Figure 1.8. Schematic diagram of QCM sensor.

1.3.1.2 Odor biosensor

An odor sensor based on biological phenomena (biological sensor or biosensor) currently gains more attention since its performance is expected to exceed the artificial sensor [55]. An animal, for example, a dog is able to detect odorant much more accurately and faster than the current artificial sensors [56]. Biosensor consists of two parts, sensing element and transducer. The sensing element is biological components taken from biological olfactory systems that can recognize biological or chemical analytes (odorant molecules) in solution (liquid phase) or in atmosphere (gas phase) [57].

The sensing element may be a tissue, a cell, a receptor (OR), a sensory neuron, a protein, or a gene. The transducer is used to convert the biological signal produced by sensing element to electrical signal for further processing. Examples of common

transducer used for odor biosensor includes: microelectrode, SPR (surface plasmon resonance), Field Effect Transistor (FET), and optical fluorescent.

1.3.1.2.1 Sensing element of odor biosensor

A sensing element responds to the external stimuli, odorant molecules, and generates a biological signals as follows,

- Specific odorant receptor bind its associate odorant molecule and activates the specific receptor (intracellular or extracellular).
- Odorant receptor triggers a biochemical chain of events inside the cell.
- The cell elicits the response, such as: generating the nerve signal, alter the cell metabolism, shape, gene expression, or ability to divide.

Typical common organ used as sensing element are tissue, cell, or odorant receptor (OR) [58]. Some examples of olfactory organ tissue that can be used for sensing element are olfactory epithelium and olfactory bulb. Figure 1.9 shows the schematic diagram of both tissues. There are two types of cells used as sensing element, olfactory receptor neuron (ORN) cell and host cell expressing receptor or protein as illustrated in Figures 1.10(a) and (b). Figure 10(b) shows as Sf21 cell expressing ORx and fluorescent protein GCaMP6s. ORx and Orco form an ion channel. Figure 1.11 shows illustration of odorant receptor (OR) sensing elements. Odorant receptor belongs to G protein coupled receptor (GPCR) family which contain 7 hydrophobic transmembrane domain [59]. It is suggested that the binding of odorant molecule occurs in an odorant binding pocket formed by the third, fifth, sixth transmembrane domain. Table 1.4 summarizes the advantages and disadvantages of several types of odor biosensor characteristics.

Table 1.4. Characteristics of several types of odor biosensors [58]

Type	**Advantage**	**disadvantage**	**Remarks**
Tissue	Low cost, easy to use, and more natural	Less specificity, varies, difficult to maintain.	Need to kill animal
Cell	High selectivity and sensitivity.	Necessity of culturing, difficulty of handling	
Receptor	Stable, high selectivity and sensitivity.	Difficulty in purification and isolation, less natural.	

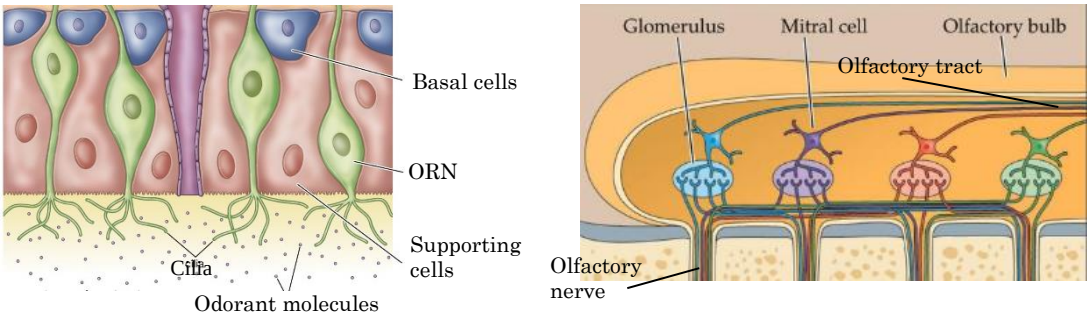

Figure 1.9. Schematic diagram of some olfactory organ tissues. (a) Olfactory epithelium [60] (b) Olfactory bulb [61].

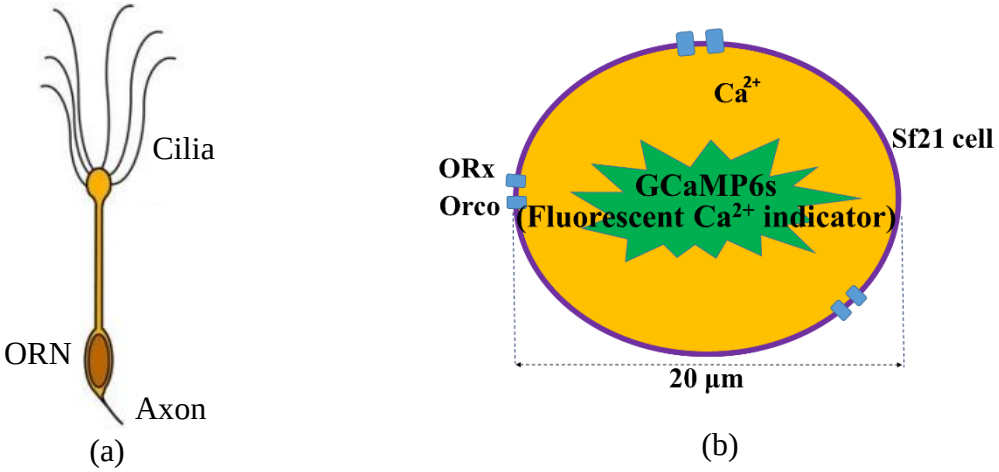

Figure 1.10. Schematic diagram of some olfactory organ cells. (a) ORN cell. Sf21 cell expressing ORx and GCaMP6 fluorescent protein [62].

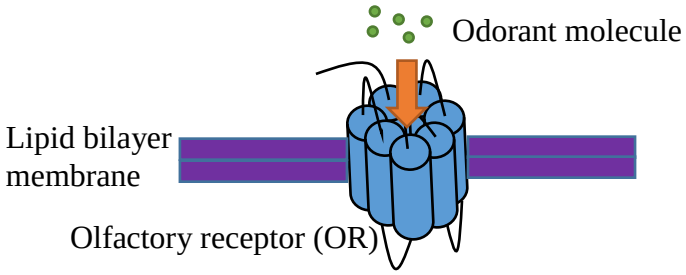

Figure 1.11. Schematic diagram of some olfactory organ olfactory receptor (OR).

1.3.1.2.2 Transducers for odor biosensor.

Several techniques can be used to convert biological signal to electrical signal such as electrochemical, optic, acoustic, colorimetric techniques, etc. A living cell of *Xenopus* oocyte expressing an olfactory receptor (OR) with amperometric transducer was successfully used as an odor sensor [63]. This technique requires inserting electrodes into a cell (invasive technique). It makes the cell easily damaged in addition to the short life span of the cells. One of the non-invasive technique is optical fluorescent one [64]. The non-invasive technique is useful since the cells are very small and easy to be damaged. Fluorescent technique is one of the non-invasive optical techniques suitable for a cell-based sensing system. The cell response to the odorant is obtained by detecting the intensity of fluorescent light emitted by the cell when it is illuminated by the excitation light. Thus, the cell should be prepared with the fluorescent protein inside it. Table 1.5 summarizes several types of transducers commonly used for odor biosensor.

Table 1.5 Several types of odor biosensor transducer.

Type	**Principles**	**Reference**
Microelectrode array (MEA)	- Electrodes inserted to the cell to extract the electrical signal. - Invasive method.	[65]
Quartz crystal microbalance (QCM)	- Its functionalized surface coated with OR. - Increase in mass by the binding of Odorant and OR, causes reduction of resonant frequency.	[66]
surface plas-mon resonance (SPR)	- SPR is an optical phenomenon that occurs when polarized light hits a prism covered with gold surface, at a specific incident angle.	[67]
Field Effect Transistor (FET)	- Ion or charge sensitive gate layer. - Detect potential change.	[68]
Optical (fluorescent)	- Additional fluorescent dye (protein) at biological element. - Fluorescent intensity change with ion activities.	[69]
Electro anten-nogram (EAG)	- Measuring the average output of an insect antenna t for a given odor	[70]
Light address-able potentio-metric sensor (LAPS)	- Light can induce photo current in semiconductor. - Detect the potential variation caused by an electrochemical event.	[71]

1.3.1.2.3 Classification of odor biosensor

a. Tissue based odor biosensor

Living body organ itself can be used for detection of several volatile components. The advantages of tissue based sensor is easy to fabricate, easy to immobilize, and low cost. The disadvantages are need to kill animal, difficulty in storage, olfactory fatigue, individual difference, and lack of specificity. Figure 1.12 shows the basic principle of one of the olfactory epithelium (tissue) based odor sensor. The specific response of olfactory epithelium can be detected and analyzed when the membrane depolarization is triggered due to the interaction between odorants molecules and ORs on cilia [72]. Connected to olfactory nerve, MEA (Microelectrode Array) was used to record the electrophysiological activity of the olfactory receptor as shown in Figure 1.12. Table 1.6 shows several types of tissue based odor biosensor.

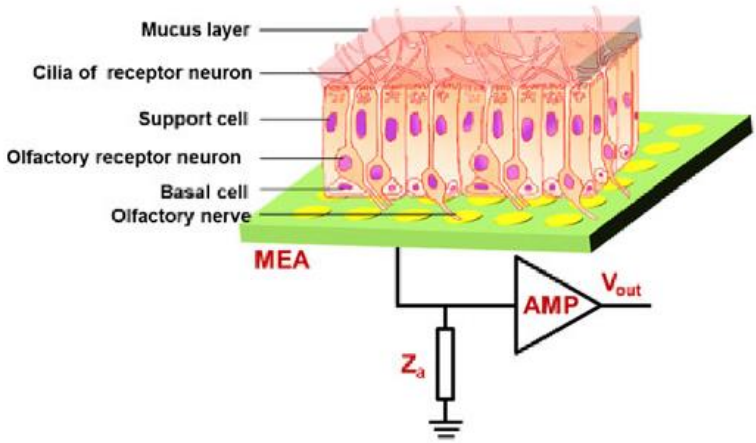

Figure 1.12. Schematic view of olfactory epithelium (tissue) based odor sensor with MEA transducer [72].

Table 1.6 Several types of tissue based odor biosensor.

Tissue type	**Transducer**	**Odorant**	**Notes**	**Lit**
Olfactory epithelium (Sprague dawley rat)	MEA	Acetic acid, etc.	Fast, Gas phase	[73]
	LAPS	Acetic acid, etc.	Fast, liquid phase	[74]
Olfactory bulb (Wistar rat)	MEA	Glutamic acid	Fast, liquid phase	[75]
	EAG	Hexanoic acid, etc.	Fast, gas phase	[76]

b. Cell based odor biosensor

In cell based odor biosensor, the cell utilize for sensing element can be a cultivated olfactory receptor neuron (ORN) cell or host cells which express the olfactory receptor (OR). ORN cells from insect antenna and mouse cilia have been used for biosensing application [77]. Typical cells for OR expression are human embryonic kidney cell (HEK293), *Xenopus laevis* oocyte, Sf21 (*Spodoptera frugiperda*), and a yeast (*Saccharomyces cerevisiae*). Table 1.7 shows some examples of cell based odor biosensor both from cultivated ORN cells (without OR) and host cells expressing OR. The advantages of cell based odor sensor are easy isolation and transformation, high sensitivity and high selectivity. The disadvantages are difficulty of long term handling, low stability, and necessity of culturing [59].

Biological signal produced by OR including:

- Conformational (shape) change in OR caused by the binding of a ligand.
- Dissociation of α-subunit of G-protein from activated OR.
- Ions (Ca^{2+}, Na^{+}, Cl^{-}) influx caused by signal transduction in cells.

Figure 1.13 shows as example of cells based odor sensor with light addressable potentiometric (LAPS) transducer [78]. LAPS has a structure of electrolyte-insulator (SiO_2)-semiconductor (Si). The light from the laser illuminates the silicon wafer to generate the photocurrent. When the extracellular potential of ORNs cultured on silicon changes due to odorant molecules binding to OR, the photo current generate corresponding signal. Thus, the change of extra cellular potential can be monitored by the measurement of photocurrent fluctuation.

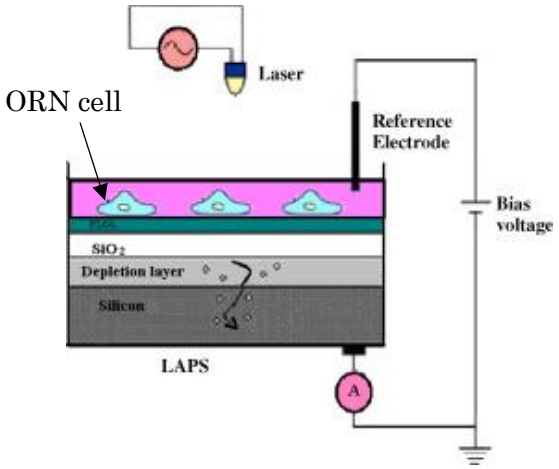

Figure 1.13. Schematic view of cell based odor sensor with light addressable potentiometric sensor (LAPS) transducer [78]

Table 1.7 Several examples of cell based odor biosensor.

Cell type	OR	Transducer	Odorant	Ref
ORN (insect)	-	EAG	Hexanol, butyric acid	[79]
ORN (rat)	-	LAPS	Acetic acid, oxtanol, hexanol.	[80]
ORN (pig)	-	Optical fluorescent	TNT, RDX,	[81]
Neuronal cell (wistar rat)	BmOR1	Optical fluorescent Ca^{2+}(EGFP)	Bombykol	[82]
HEK-293 (human)	I7	QCM	Helional, heptanal, Octanal	[83]
S. cerevisiae (yeast)	I7	Optical fluorescent Ca^{2+}(EGFP)	Helional, heptanal, Octanal	[84]
Xenopus oocytes (mammals)	BmOR3	Conductivity	Bombykal	[63]
Sf21 (insect)	BmOR3	Optical fluorescent Ca^{2+}(EGFP)	Bombykal	[85]

c. Receptor based odor sensor.

In receptor based odor sensor, the odorant receptor protein is used as sensing element to detect the odorant. There are several methods of odorant receptor protein production including extraction (isolated) from olfactory organ, overexpression in heterologous cell lines, cell free production and chemical synthesis [86]. Heterologous expression is commonly used for the production of large amount of odorant receptor protein.

Following its production, the protein immobilized on the surface of transducer. Currently, there are three methods are mainly used to immobilize the odorant receptor protein on the surface of transducer: physical adsorption, self-assembled monolayer (SAM), and SAM with biotin/avidin interaction [59]. The first method, physical adsorption is the most common method due to its simplicity.

The advantages of receptor based biosensor including high selectivity and sensitivity and longer term stability while the disadvantage is difficulty of olfactory receptor protein purification and isolation [59]. Figure 1.14 shows the example of the receptor based odor sensor [87]. An OR17-40 (human) and a G_{α} protein were expressed in *Saccharomyces cerevisiae* cells from which membrane nanosomes were prepared and then immobilized via interaction on the surface of gold film. Using a surface plasmon resonance (SPR), OR

stimulation by an odorant, with the presence of *guanosine triphosphate* (GTP), can be evaluate quantitatively by a shift of the SPR response level.

Table 1.7 shows several types of receptor based odor biosensor. Their transducer are piezoelectric, CPNT-FET (carboxylated polypirrole nanotubes-field effect transistor), SPR, EIS (electrolyte-isolator-semiconductor), swCNT-FET (single wall carbon nanotube-field effect transistor), and QCM.

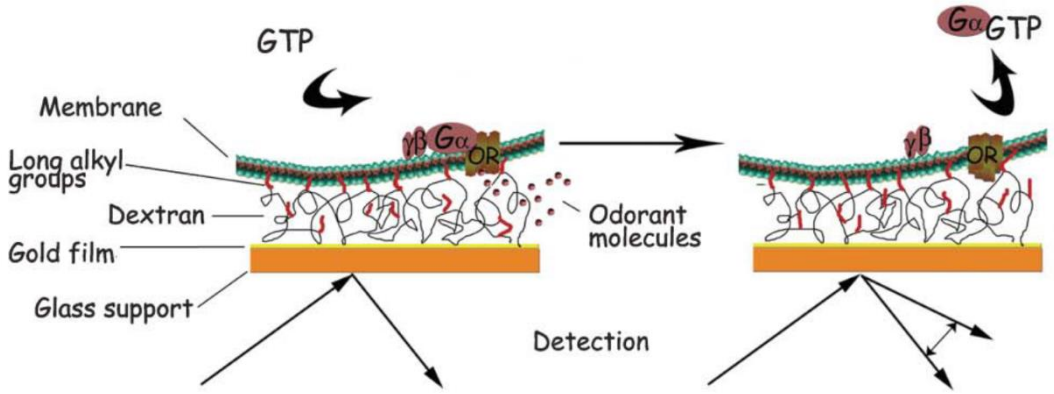

Figure 1.14. Detection mechanism of olfactory receptor based odor sensor with SPR transducer [87].

Table 1.8 Several types of receptor based odor biosensor.

OR type	**Production**	**Transducer**	**Odorant**	**Notes**	**Ref.**
Bullfrogg OR protein	Isolated (extracted)	Piezoelectric	n-Caproic acid, etc.	10^{-7}–10^{-6} (detection range)	[88]
hOR2AG1 (human)	Heterologous expression on *E. coli*.	CPNT-FET	Amyl butyrate	100fM (detection limit)	[89]
OR17-4 (human)	Cell free	SPR	Undecanal	1.2-100μM	[90]
OR17 (rat)	Heterologous expression on *S. cerevisiae.*	EIS	Octanal, heptanal, helional	10^{-13} – 10^{-4} (detection range)	[91]
Polypeptides (OR binding sites)	Chemical synthesis	swCNT-FET	Trimethylamine	10fM-1μM (detection range)	[92]
Polypeptides (OR binding sites)	Chemical synthesis	QCM	1-hexanol, 1-pentanol	2-3 ppm 3-5 ppm (det. limit)	[93]

1.3.2 Microfluidic system.

The dimension of biological sensing element (tissue, cell, receptor, etc.) is in the order of micrometer or less. A chamber with the scale of μm^3 dimension is needed to immobilize the biological element and to expose it to the analyte (odorant). Thus, a microfluidic system (MFS) is needed for a sensing system. The microfluidic is a miniaturized platform with advantages such as small dimension, low sample (cells) volume, low reagent (odorant) consumption, short processing time (because of rapid mixing), high throughput, enhanced analytical performance, less waste, low unit cost, and reduced energy consumption [94]. The requirements for chamber material used for biosensor are:

- Compatibility with biological element which is non-toxic to the elements..
- Possibility of immobilizing the cells.
- Possibility of precise control of odorant concentration.
- In case of optical fluorescence instrumentation the material should be transparent to allow excitation light to reach the cell

Several types of materials available with those requirement such as acrylic, glass and PDMS (polydimethylsiloxane) [95]. Microfluidic systems (MFS) for biosensor normally consist of a set of fluidic operation procedures that allow odorant molecules to be detected and assayed in an easy and flexible way. MFS is capable of sampling, filtration, pre-concentration, separation, restacking, and detection for odorant molecules. MFS normally consists of micro-pump, micromixer, valve, separator and concentrator [96]. Based on their flow type, MFS can be categorized into two main types, discrete and continuous one. The discrete microfluidic system based on droplet, while the continuous microfluidic system based on continuous flow of liquid (odorant) [97].

In case of odorant sensing system, continuous microfluidic system offers a more similarity to the real world problem compared to discrete microfluidic system. As a results, with more complicated system and more reagent needed compared to discrete microfluidic system. Continuous system suffers from the problems of mixing and reagent diffusion. Figures 1.15(a)-(c) shows an example of microfluidic system used for investigation of the OR space using microfluidic micro-well array [98]. There are around 2900 cells involved in the simultaneous investigation using calcium imaging technique (Figure 1.15(a) and (b)). Figure 1.15(c) shows how to arrange the cells on array of 20 μm-diameter, 10 μm-depth wells. First, the cells were loaded into the assembled device gently (top). Then the flow was stopped to allow cells to deposit into the well (middle). Finally, the flow was continued with saline to flush the movable cells (bottom). The process leaving ~70–90% of the wells filled with the cells for further experiment.

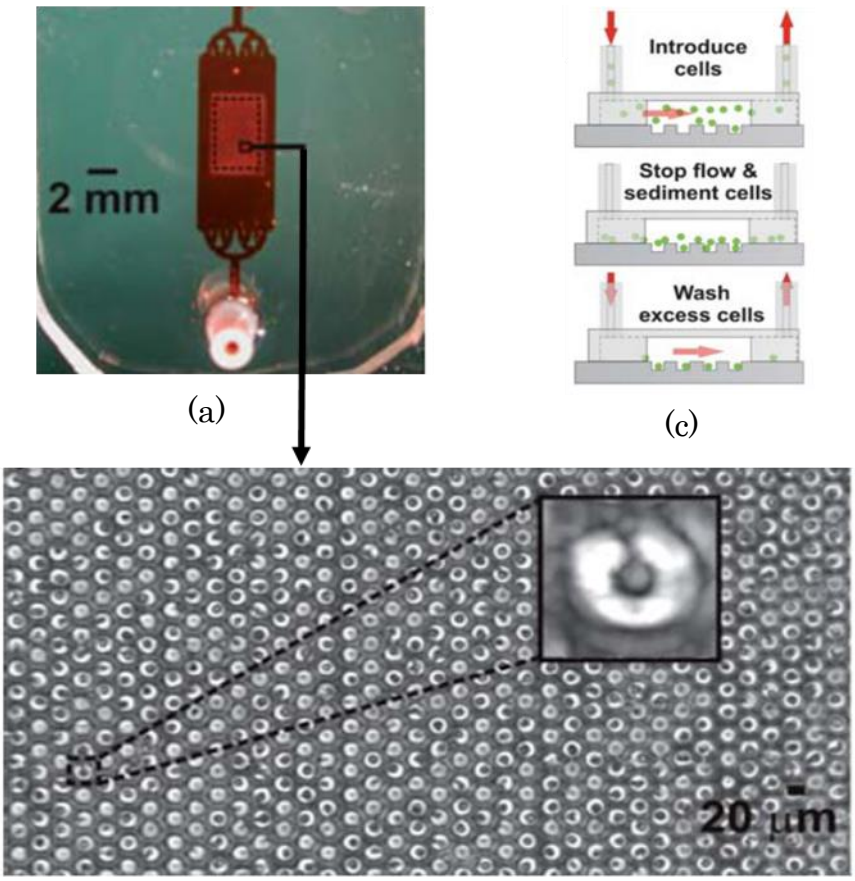

Figure 1.15. Example of microfluidic system (MFS) [98]. (a) Photo of the MFS, (b) Magnification of MFS, and (c) How to arrange the cells on the chamber.

1.3.3 Fluorescent Instrumentation

Fluorescence is the emission of light (photon) by a substance that has absorbed an excitation light or other electromagnetic radiations. The emission light has a longer in wavelength than the excitation light and known as Stokes shift. Fluorescent instrumentation takes advantage of this shift phenomenon which enables separation of both lights using appropriate optics [99]. The intensity, spectrum, life time, and polarization of the fluorescent are typically measured by the instrumentation [17]. Typical fluorescent instrumentation consists of excitation light source, specimen (sample) chamber, optical components, and sensitive fluorescent (emission light) detector.

Figure 1.16 shows the basic fluorescent instrumentation system with blue excitation light and green emission (fluorescent) light. A pair of light source and excitation filter is used to obtain the proper excitation light wavelength. Currently,

specific laser diode or light emitting diode (LED) are often used as excitation light generator. Dichroic mirror is used to direct the excitation light and filter the emission light. The emission filter is used to filtered out the light outside the fluorescent light wavelength before reached detector. If the sample is very small, additional lenses can be added in front of the sample (objective lens) or detector (ocular lens).

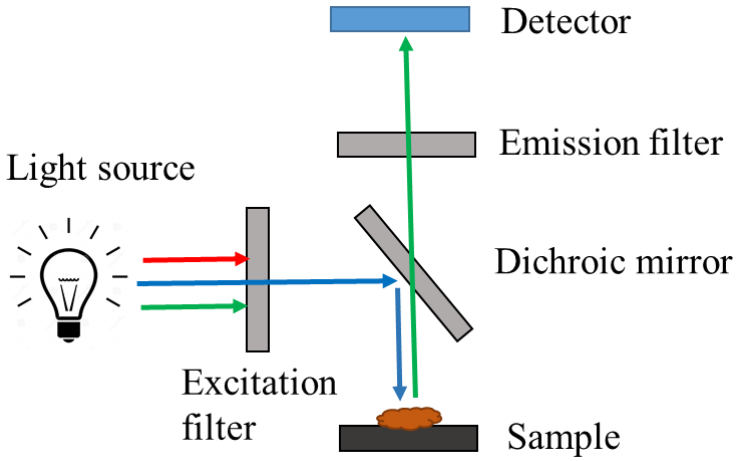

Figure 1.16. Schematic diagram of fluorescent instrumentation.

Fluorescent mechanism is found in many area of applications such as fluorescent lamp, mineralogy, sensor, biological detector, etc. A fluorescence-based artificial nose system that incorporates fiber-optic sensors as the vapor sensitive dyes had been developed [100]. Sensor responses are recorded during the vapor exposure using a CCD camera.

A material or chemical compound that can re-emit light upon light excitation and can be used as an indicator or reporter is called fluorophore. One of the common fluorophore in biological system is green fluorescent protein (GFP) as a reporter of an intracellular signal transduction pathway [101]. Signal transduction occurs when an extracellular signaling molecule activates a specific receptor located on the cell surface or inside the cell such as in the mechanism of olfaction which involved increasing calcium (Ca^{2+}) ion activities. By expressing the GFP and receptor, it is possible to use a fluorescent instrumentation to monitor the activity of calcium ion inside cell [102]. The optical fluorescent method is proven to be suitable for applications with high sensitivity and for further device miniaturization, especially when it is combined with a microfluidic system [103].

1.3.4 Ambient light and lock-in measurement technique

Typical emitted fluorescent light is very weak, therefore an image processing technique has to be developed to increase the signal to noise ratio. Another major problem is ambient light as a background of image signal since it has much higher intensity compared to the intensity of fluorescent light. Ambient light originating from the sun or indoor lighting has a component of its wavelength around the fluorescent light. The higher intensity of background, the less sensitivity of the sensor system. Although covering the instrumentation with black box is effective, it reduces the flexibility of measurement activities. Lock-in amplifier or lock-in measurement technique is a well-known technique to overcome the problem of finding a small signal buried under the noise [104]. De Marcellis et.al has applied the lock-in amplifier technique to accurate measurement of gas sensor down to ppb level [105]. Moreover, lock-in technique was used to improve the signal to noise ratio of the measurement [106].

Figure 1.17 shows the block diagram of typical lock-in amplifier technique. Sensor output is modulated by a signal (*m(t)*) with a known frequency (f_m) and resulted in *x(t)*. A bandpass filter (BPF) is used to remove the noise (unwanted, *n(t)*) contribution at all frequencies except for small frequency span around modulated signal f_m. The BPF output (*v(t)*) is then attenuated (optional) before it is input to phase sensitive detector (PSD). The next block is a mixer or PSD, which multiplies the *v(t)* by the reference signal (*r(t)*) to obtain the *w(t)*. Both multiplied signals *v(t)* and *r(t)* should be properly synchronized to have the same frequency and phase. Finally, the DC component of the processed signal (*w(t)*) is extracted by means of a low-pass filter (LPF) with a suitable cut-off frequency. The magnitude of output signal *y(t)* is attenuation of signal generated by the sensor.

Novak et al. had been implemented a fluorescent detection system with lock-in amplifier to enable measurement under ambient light conditions [107]. The LED excitation light was modulated to have a modulated fluorescent signal. Then, the modulated fluorescent signal was processed by a high pass filter (HPF), a demodulator, and LPF, respectively. In another application, an optical lock-in detection (OLID) method has been used to enhance the contrast of a living cell fluorescent image in the presence of a large background [108].

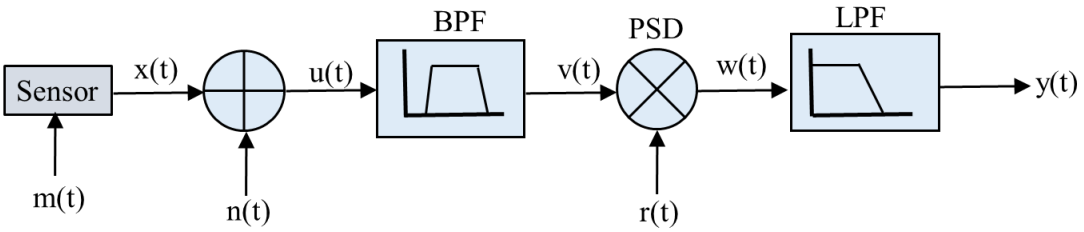

Figure 1.17. Schematic diagram of the lock-in amplifier

1.4 Field measurement of odorant and biosensor

Measurement (assessment) of odorant in ambient air is required in many areas of applications such as in environmental monitoring [109]. Among the methods of field measurements are field olfactometers, marker's chemical analysis, gas detector tube, and electronic nose. Table 1.8 shows some common methods in field measurement of odorant. Although the measurement process in field olfactometer method is a definable task, several factors related to individual inspector such as health status, alertness, and attention need to be considered. The examples of field olfactometer popular product are Nasal Ranger and Scentroid SM110 [110, 111].

In Markers' chemical analysis, the chemical marker of an odourous emission should be chosen based on its high concentration in the emission, representativeness of the emission, absence in the background air, and the ease of chemical analysis [112]. Ambient air is sampled on a special tube or bags through a vacuum pump and then analyzed using Gas Chromatograph/Mass Spectrometer to analyze the present of chemical marker. Measurement (assessment) of odorant in ambient air using a portable and robust e-nose, especially using biosensor, is a demanding task. One of the main obstacles in developing electronic nose for field measurements is the presence of many odorant backgrounds with significant intensities [113].

Another method of field measurement for odor (gas) is gas detector tube, a glass tube filled with a chemical reagent that produces a color change when exposed to the gas [114]. It is used with a hand pump that will draw a sample into the tube. Detector tubes are available for hundreds of compounds, and have been around in a practical format since the 1930s. It is easy to use, relatively inexpensive, intrinsically safe, and allowing it to be used in almost all occupancies. However, its accuracy is not high since the color change is checked by manual inspection.

Biosensor with very high selectivity such as immunosensors seems to be suitable for specific applications of detecting chemical substances in ambient air because of its selectivity and sensitivity. A surface plasmon resonance immunosensor using Au nanoparticle has successfully used for detection of trinitrotoluen (TNT) [115].

Table 1.9. Several methods in field measurement of odorant

Methods	**Principles**	**Notes**
Field olfactometer	A dilution-to-threshold dilution (D/T) factors is obtained by dynamically dilutes the ambient air with carbon-filtered air in distinct dilution ratio.	A trained inspector is needed to run the instrumentation and do measurements.
Markers' chemical analysis	Ambient air is sampled on a special tube or bags through a vacuum pump and then analyzed for the present of chemical marker using GC/MS.	A chemical marker represent odourous emission on ambient air should be chosen.
Gas detector tube	A glass tube filled with a chemical reagent that will produce a color change, when exposed to the gas	Easy to use, safe, and cheap.
Electronic nose	Odor sensing system is applied directly on the field.	Continue of developing.

1.5 Research purpose

The main purpose of this research is to develop a portable fluorescent instrumentation system robust against ambient light using lock-in measurement technique and to achieve a lower detection limit of sensing. The more detail research purposes are:

1. To develop a compact fluorescent instrumentation system.

There are many advantages of developing a portable odor sensing system instead of the fixed one. Mostly, the needs or applications of odor sensing system is outside room or laboratory. Thus, having a compact and robust sensing system is demanding.

2. To apply the lock-in measurement technique on the instrumentation system.

The developed fluorescent instrumentation system intended to be used in many areas, not only inside laboratory where the external condition can be adjusted. Ambient light condition dominated the fluorescent light. To handle that problem, a lock-in measurement technique is applied to the system. Lock-in measurement technique is used when signal information buried in the noise. The performance of the developed instrumentation system should be analyzed in terms of how much the ambient condition affect the measurement results before and after the application of lock-in measurement technique

3. To achieve lower detection limit of sensing.

In ambient light condition the background light from the sun or lightning is dominant, thus deteriorate measurement results and decreasing the detection limit. Application of lock-in measurement technique in fluorescent instrumentation system should be lower the

detection limit compare to without application of lock-in technique in any conditions of ambient light.

1.6 Organization of the Thesis

The block diagram of the research strategy is shown in Figure 1.18. A biosensor is used since typically it has more selective characteristics than artificial sensor. In the biosensor an olfactory receptor (OR) based sensor is taken because it is more flexible than other biosensor such as immuno-sensor. In terms of its olfaction mechanism, insect OR is simpler than mammal's one. Biosensor using OR can be classified into tissue-based sensor, cell-based sensor, and receptor-based sensor. The cell-based sensor is expected to have characteristic close to that of living body. Moreover, this sensor uses fluorescence since it is a non-invasive technique and is easy to extent to array of sensors. The sensor system uses lock-in technique which provides robustness against ambient light.

The thesis covers background, motivations, related works, research instrumentations, experimental set-up, system development, experimental results and their discussion. The thesis is made up of 9 chapters,

- Chapter 1 presents in brief about background and motivation of the research, olfaction mechanism, and some related works.
- Chapter 2 presents the instrumentation development and experimental setup.
- Chapter 3 presents an experiment on static measurement system.
- Chapter 4 presents a development of flow measurement system.
- Chapter 5 presents an experiment of flow measurement system.
- Chapter 6 presents a development of lock-in measurement system for fluorescent instrumentation.
- Chapter 7 presents an experiment on lock-in measurement system.
- Chapter 8 presents discussion on performance of developed instrumentation system.
- Chapter 9 presents a conclusion of the research.

The block diagram of the thesis organization is given in Figure 1.19.

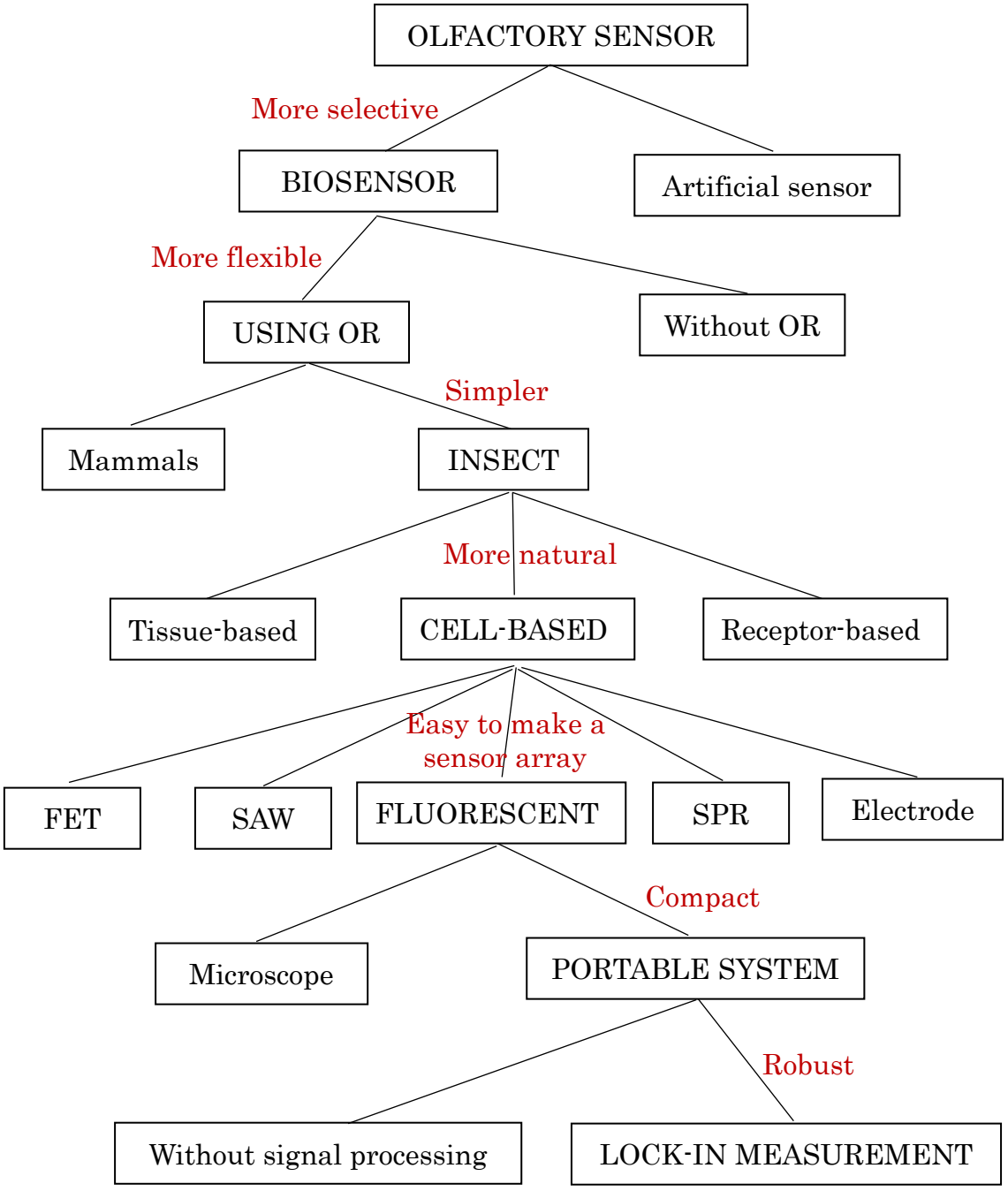

Figure 1.18. Block diagram of research strategy.

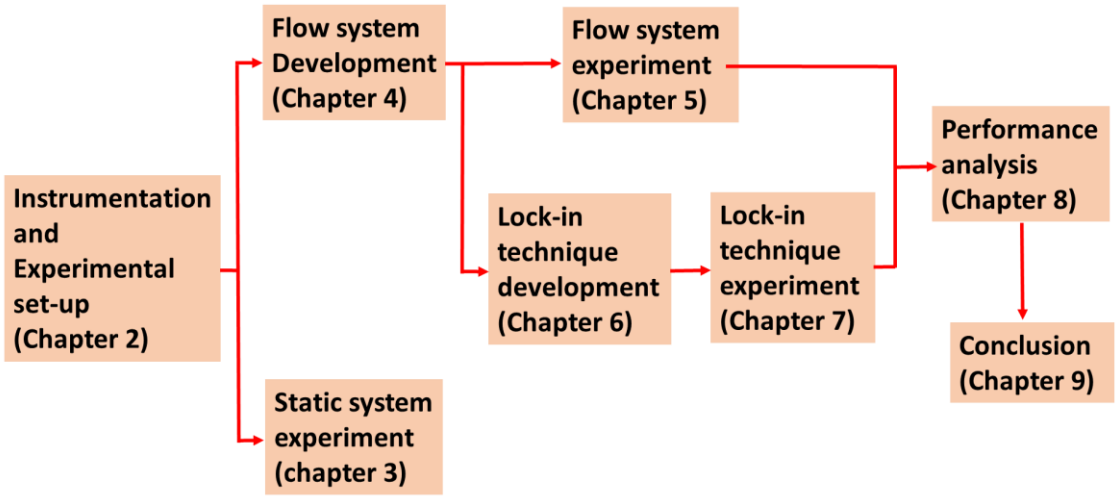

Figure 1.19. Block diagram of thesis organization.

Chapter 2.
Instrumentation Development and Experimental Set-up

This chapter discusses the experimental set-up for observing the response of the cell to the odorant. It consists of the topics about fluorescent microscopy instrumentation system, chamber, fluidic system, cells preparation and odorant preparation. Figure 2.1 shows the basic schematic of instrumentation set-up for experiment on odorant exposure. The cells as a sensor are put on the pool of the chamber. Then, the liquid with specific concentration of odorant is introduced to the cell by the flow. Several types of odorant liquids are available on the reservoirs and are flowed out with specific flow rate by syringe pump. The solenoid valve is used to select the type of odorant flow to the cell. The optical fluorescent instrumentation system is used to observe the cells response to the odorant. A light of 488 nm wavelength (blue) generated by a laser diode is directed towards the cells to excite them (thus it is called excitation light) followed by the fluorescent light (515 nm wavelength, green). The fluorescent image of the cell is capture by a camera and is send to the computer for further processing. Thus, the fluorescent instrumentation basically consists of a laser system to generate the excitation light, an optical system to direct the excitation and emission lights, a camera to capture the fluorescent image, and a computer for process the obtained images. Basic experiments for the purposes of setting-up the measurement system such as using fluorescent instrumentation system and microfluidic are also discussed in this chapter.

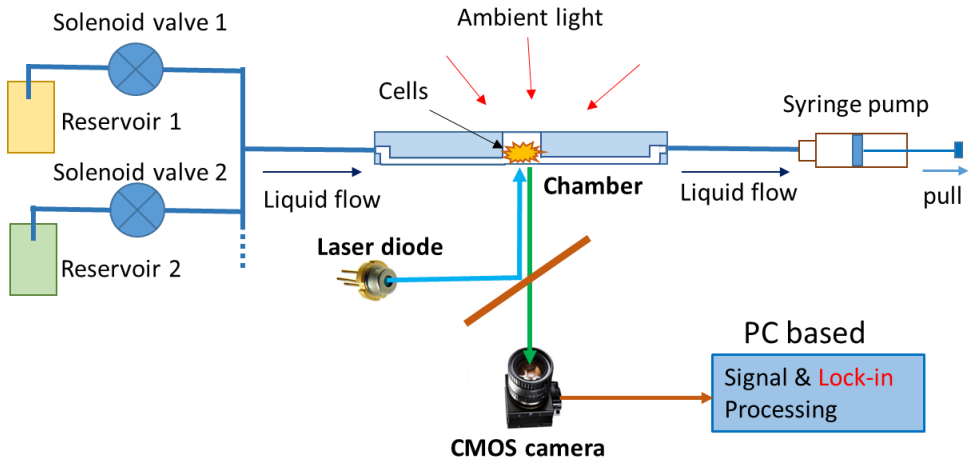

Figure 2.1 Basic schematic of instrumentation set-up.

2.1 Fluorescent instrumentation construction.

Basic diagram of fluorescent instrumentation is shown in Figure 2.2. A blue excitation light produced by a laser system (discussed in section 2.1.1 in detailed) is concentrated using collimator lens (all wavelength, US-Laser Inc.) and is filtered (MIL-C-48497A) to only allow, the light with blue wavelength to pass through it. The focal length of the collimator (f_{col}) lens is 3.41mm. Through the blue optical filter, the blue light is reflected by a dichroic mirror (MIL-STD-810F) and is directed toward objective lens to be concentrated on the cells. The dichroic mirror is placed so that it can guide the blue light from the laser system to the chamber and pass only the green fluorescent light from the cell to the camera. An objective lens (MPlanFL N 10/20, Olympus) is placed in front of the cells. Its magnification (M) of the objective lens and the focal length (f_{obj}) of the objective lens are 10 or 20 and 18 mm, respectively. An objective lens with proper magnification is needed since the cell size is tiny (20 μm). The green optical filter (MIL-C-48497A) is placed for fluorescent light before captured by the CMOS (Complementary Metal Oxide Semiconductor) camera (Bitran, CS-52C). A CMOS camera is cooled down to 0°C using a peltier device to enhance signal to noise ratio. The cooling function was implemented into the camera.

In designing the fluorescent instrumentation with construction shown in Figure 2.2, the distances of focal lengths of both objective lens (f_{obj}) and collimator lens (f_{col}) should be precisely determined. Thus both distances need adjustments. f_{col} needs to be adjusted for proper laser beam while f_{obj} needs to be adjusted to obtain clear image. f_{col} is the distance between laser diode and collimator lens while f_{obj} is the distance between object (cell) and objective lens.

The collimator lens and the laser diode are located at the laser housing. The position of laser diode is fixed while the position of collimator lens toward laser diode can be adjusted backward and forward, thus the f_{col} can be adjust in that way. The cells are placed at the chamber located at the chamber holder. The position of the chamber holder toward objective lens can be adjusted up and down, thus f_{obj} can be adjust by adjusting chamber holder. The other distances such as x and y are freely determined and can be optimized to have a compact system. In this thesis, we made 14 cm and 18 cm for x and y, respectively.

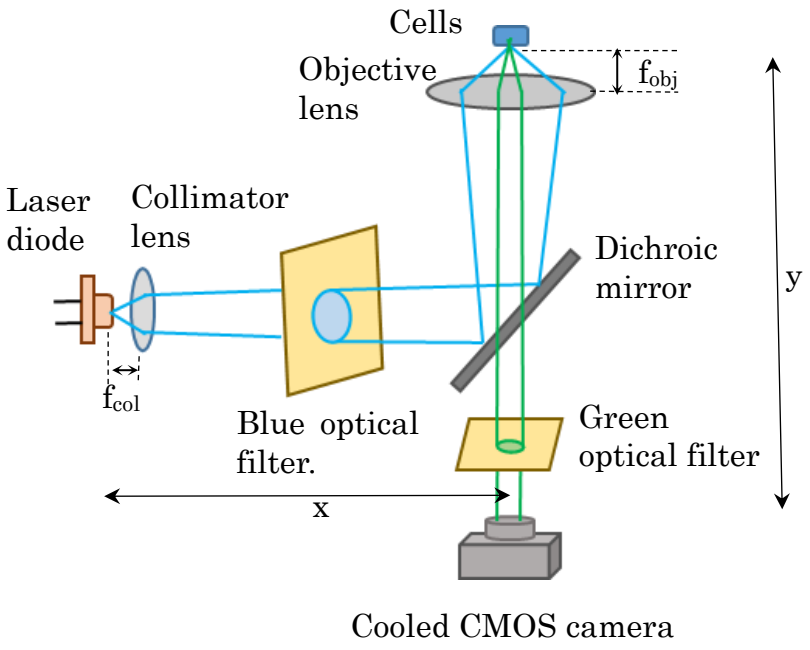

Figure 2.2 Basic schematic of instrumentation set-up for flow system experiment

2.2 Design of laser system

Laser (Light Amplification by Stimulated Emission of Radiation) diode is a device that produces monochromatic, coherent and highly collimated light beam. The laser diode has been chosen as excitation source since it has characteristics of low power in spite of small size, thus it the best excitation light source in this study. The replacement of the heavy lamp house in fluorescent microscope with laser diode enables a compact system. The beam emitted from a semiconductor laser typically has an elliptical spatial profile caused by diffraction. The output of laser diode fluctuating both in its wavelength and amplitude. The sources of fluctuation are vibration, stress, and temperature change. A laser diode driver typically consists of a slow starter circuit, current regulation, transient suppression, and automatic optical power control (APC). Laser driver circuit is used as both to drive and to control the laser diode.

Laser system consists of Sky blue laser diode and its driver. Two types of laser diodes from NICHIA were prepared, NDS1316E and NDS4116E. Both NDS1316E and NDS4116E are 4-pin laser diodes with 488 nm peak wavelength. The optical output power of NDS1316E and NDS4116E are 25mW and 60mW, respectively [116, 117]. The photo of the laser diode and its schematic diagram is shown in Figure 2.3. It can be seen from Figure 2.3(c) that the laser diode includes diode (PD). Since photo diode also receives the light generated by laser diode, it can be used to monitor the optical power

generated by laser diode. With some additional external component such as resistors and capacitors, it is possible to develop automatic optical power control. Typical operating voltage (V_{op}) and operating current (I_{op}) for NDS1316E is 6.2V and 80mA respectively, while the typical operating voltage (V_{op}) and operating current (I_{op}) for NDS4116E is 5.9V and 100mA respectively.

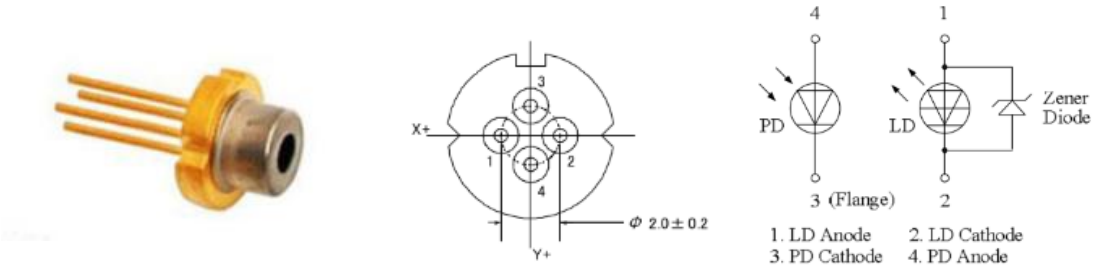

(a) (b) (c)

Figure 2.3 NDS1316E and NDS4116E [116, 117]. (a) Picture. (b) pin-out. (c) Schematic symbol.

The main component of laser driver is an integrated circuit (IC) for specific application, ELM185BB Laser Diode Driver from ELM Technology [118]. This device was chosen mainly because of its low operation voltage (2 volt) and thus its power dissipation and its size are small (SOT-026 package), and is easy to use. Figures 2.4 (a) and (b) show the functional block diagram of the ELM185BB and its pin description, respectively. Moreover, some important electrical characteristics of the ELM185BB is shown in Figure 2.4 (c).

The driver circuit based on ELM185BB is shown on Figure 2.5 (a) while its printed circuit board (PCB) layout is shown in Figure 2.5 (b). The driver can be used for both continuous mode (CM) and pulse mode (PM). In the continuous mode the laser is always on, while in the pulse mode the laser is on-off in specified frequency. Pulse mode operation is obtained by applying the square wave to *pulse in* node. Operation in pulse mode can be used to decrease the power of the laser and to implement the lock-in measurement technique described later into the system.

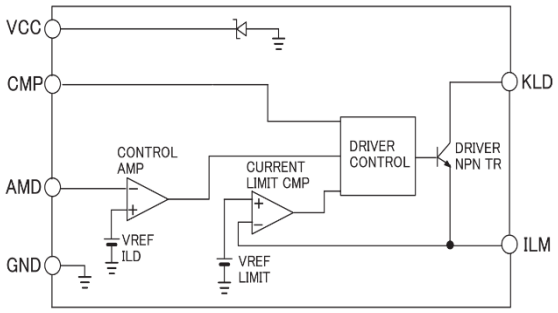

(a)

Pin description

Pin	Name
AMD	LD monitor input
CMP	phase compensation
ILM	LD current limit
KLD	LD drive output
VCC	power output
GND	ground

(b)

Parameter	Symbol	Condition	Min.	Typ.	Max.	Unit
Operation voltage	VCC		2.0		6.5	V
Current consumption	ICC	VCC=3.6V		1	3	mA
AMDreference voltage	Vamd	VCC=3.6V	0.285	0.300	0.315	V
Vamd temperature characteristics	$\frac{\Delta Vamd}{\Delta Top}$	VCC=3.6V		±200		ppm/°C
KLD current	IDkld	VCC=2.7V, Vkld=1.0V	400			mA
KLD leak current	ILkld	VCC=5.5V			1.0	µA
ILM current limit voltage	Vilm	VCC=3.6V	0.13	0.15	0.17	V
Max. external clock frequency	Fext	VCC=3.6V			20	kHz
AMD input current	Iamd	VCC=5.5V, Vamd=1.0V	-0.5		0.5	µA
Zener diode avalanche voltage	ZDBV		6.8		8.0	V

(c)

Figure 2.4 ELM185BB Laser Diode Driver [118] (a) Functional block diagram. (b) Pin description. (c) Electrical characteristics.

There are three (3) electrical parameters of laser diode needed to design the laser driver. They are operating current I_{op} (max), monitor current mirror I_m (min and max) and V_{cc}. Minimum and/or maximum values of those electrical parameters given in the data sheet. Several equations are provided for calculating the components which are:

$$R_1 = \frac{Vamd}{I_m(\max)}$$

$$V_{R1} = \frac{Vamd}{I_m(\min)} \text{ - R1}$$

$$R_2 = \frac{0.15}{I_{op}(max)}$$

$$R_3 = R_1 \frac{V_{CC} - V_{amd}}{V_{amd}}$$

Monitoring diode voltage V_{amd} = 0.3 volt (from data sheet) and V_{cc} is set to 6 volt. The

calculation of the components needed for both laser diode NDS1316E and NDS4116E summarized in Table 2.1. Capacitors C1 and C2 were set to 3300pF (ceramics) and 47μF respectively. The resistor R = 3.3 kΩ is used to reduce the V_{cc} while 7 volt applied at V_p. V_p = 7 volt or higher is needed to make laser diode in its operating condition. The ELM185BB is easy to be broken if V_{cc} is 6 volt or higher. A 7 volt zener diode Z is used for overvoltage protection.

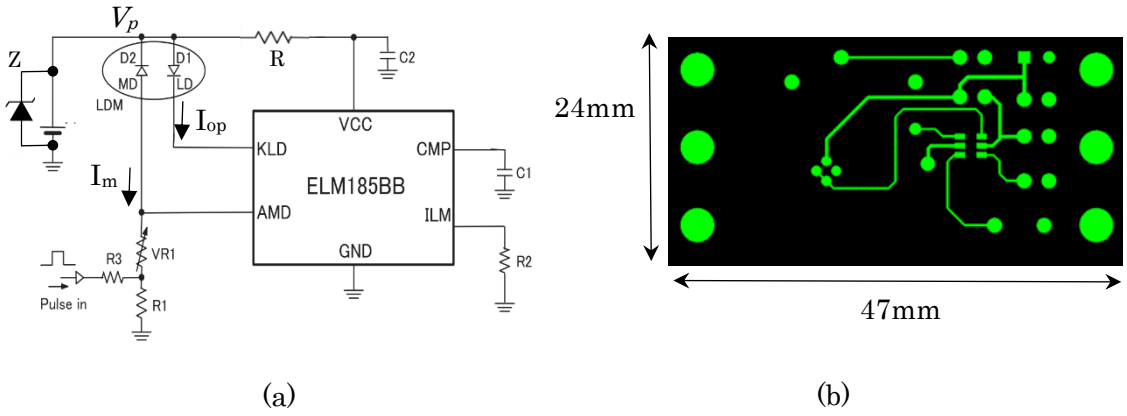

Figure 2.5 Driver for laser diode, (a) Schematic diagram [118] (b) PCB

Table 2.1. Components for NDS1316E and NDS1316E.

Device	I_m (mA)		I_{op} (mA)	R1	VR1	R2	R3
	min	max	max	(ohm)	(ohm)	(ohm)	(ohm)
NDS1316E(25 mW)	0.8	4.0	100	75	300	1.5	1500
NDS4116E(60 mW)	0.2	1.8	130	200	1500	1	3800

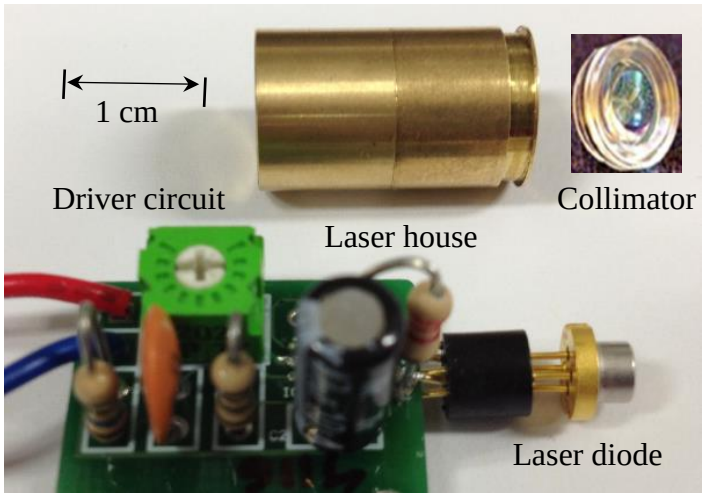

Figure 2.6 Picture of the driver for laser diode.

The driver for both 25mW and 60mW laser diode has been implemented for laser system. Laser diode is a sensitive component and suffer from electrostatic damage. Manual handling should be minimized and direct soldering should be avoided. A socket (S8060, thorlab) is used for that purpose. The picture of the laser system composed of laser diode, collimator lens and driver circuit is shown in Figure 2.6. At the operation, laser diode is covered with the laser house. Collimator lens is installed at one side of the laser house. There is an adjuster at that side, thus the distance between laser diode and collimator lens can be adjusted. Laser house is made of metal, thus it has another important function as a heat sink since the performance of the laser diode is influenced a lot by temperature. The dimension of the laser diode system is 3cm x 1cm x 2cm.

Both 25mW and 60mW laser diode systems have been tested as excitation light source for cell based odor sensor. Both types of laser diodes show possibilities of being used. However, 25mW laser diode dissipates less power than to 60mW one. Moreover, the optical power generated by 60mW laser diode is too high for the cells, resulted in higher photo bleaching effect than 25mW laser diode. Photo bleaching reduces capability of cell to emit the fluorescent light.

2.3 Laser system testing

Several experiments were done for the purpose of laser system testing. The experiment includes: voltage and current of the laser system at operation condition, effect of using heat sink (laser housing), optical power emitted by the laser system, the effect of temperature to the current of the laser driver. A 60 mW (NDS4116E) laser diode system was used in the experiments. The schematic diagram of the circuit is shown in Figure 2.7(a). The voltage at V_P was set to 7 volt. A photodiode for visible light detection (GaAsP photodiode, Hamamatsu) was used to observe the optical power stability of the blue laser [119]. Figure2.7 (b) shows the circuit diagram of the photodiode [120].

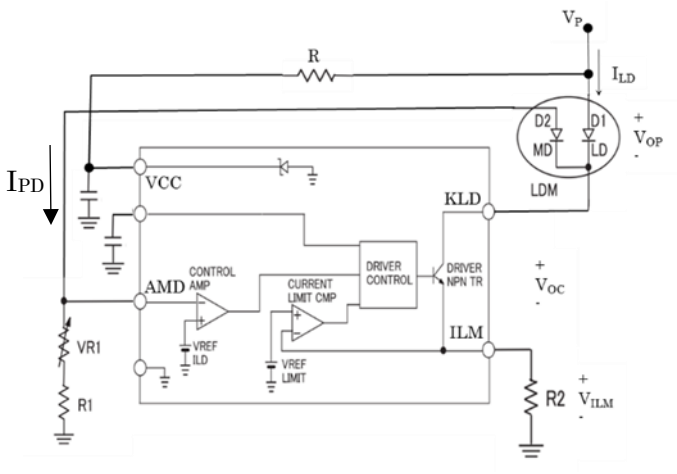

(a)

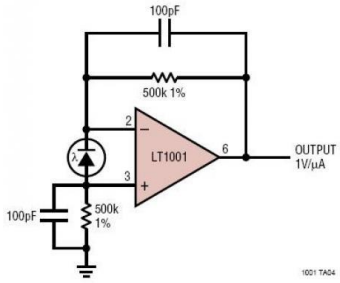

(b)

Figure 2.7 Schematic circuit for testing the laser diode. (a) Laser driver circuit [118], (b) Photodiode circuit [119].

2.3.1 Voltage and current of the laser system at operation condition.

The experiment was intended to measure the voltages and currents of the laser system at operation condition. The laser housing (heat sink) was not applied to laser diode and the measurement was done 10 minutes after the circuit was turned on. Several measurement results are shown in Table 2.2. The power dissipated by laser diode is V_{OP} x I_{LD} = 5.6 volt x 66.7 mA = 373.52 mW. This power was mainly converted to laser beam and heat produced by the laser diode. For the purpose of pulse mode application, V_{AMD} should be less than (VCC*R1)/(R1+R3).

Table 2.2 Measurement result of driver circuit at operating condition.

VCC (volt)	V_{AMD} (volt)	V_{OP} (volt)	V_{OC} (volt)	V_{ILM} (volt)	I_{LD} (mA)	I_{ILM} (mA)
2.7	0.15	5.6	1.3	0.15	66.7	66.8

2.3.2 The effect of heat sink.

The experiment was intended to observe the effect of heat sink laser diode current (I_{LD}). There were two experiments here. In the first experiment, laser house was removed from the system before the laser system was turned on. After 4 minutes, the laser house was put on the laser diode and experiment continued for the next 3 minutes. The results are shown in Figure 2.8 (a). Without heat sink (laser house), laser diode easily became hotter and then the generated optical power was decreasing. After the current increased up to around 65mA, the heat sink was used at t = 240 s (4 minutes), the laser diode current decreased immediately down to around 50mA. This is because the heat at the body of the laser diode transferred to the laser house and then it was cooled by the air.

Both heat sink and automatic power control (APC) are important for laser diode. Heat sink dissipates the heat generated by laser diode thus its temperature is kept low while APC is used to control the optical power generated by the laser diode. When the temperature of the laser diode increased, the optical laser power decrease. The APC help to control optical power to become constant by increasing the diode current.

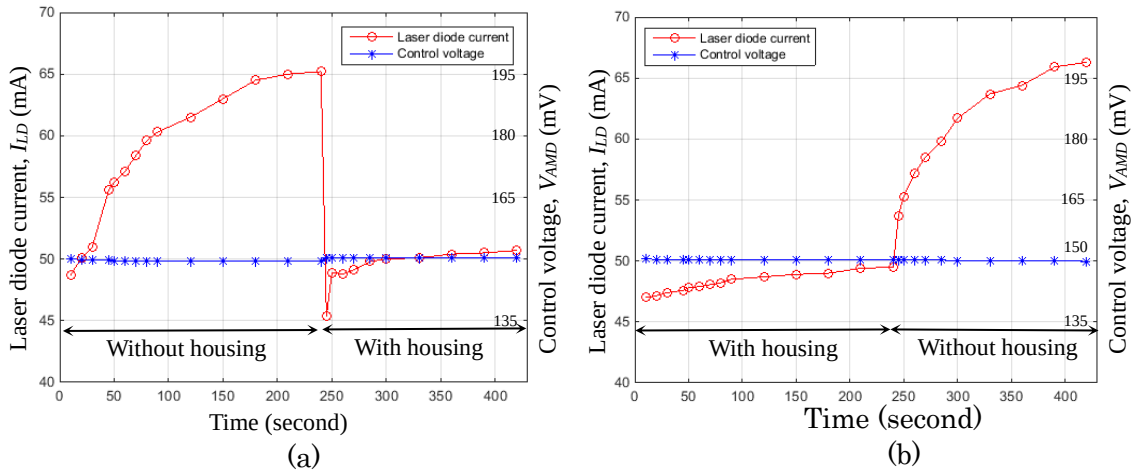

Figure 2.8 Effect of heat-sink to laser diode current. (a) Start without laser house followed by with laser house and (b) Start without laser house followed by with laser house.

The opposite treatment was performed in the second experiment. First, the laser house was put on the laser diode. After the laser diode current settled at around 50 mA (4 minutes) the house was removed from the laser diode. It was found that heat-sink removal made the temperature at laser diode body increase suddenly. To compensate for the temperature, laser diode current became higher. The plot of laser diode current in this experiment is shown in Figure 2.8(b).

There are several effects of using heat-sink (laser housing):

1. Reduce the laser diode current I_{LD} from 65mA to 50mA. This reduces the power dissipation.
2. Reduce the settling time of the laser diode current I_{LD} from around 4 minutes to around 2 minutes.
3. Reduce the temperature of the laser diode, thus it can prolong its lifetime.

2.3.3 Optical power emitted by laser diode

The purpose of the experiment is to observe response stability of the laser. A photodiode was placed in front of the laser diode with the distance 5 cm. Both laser diode and photodiode circuit are shown in Figure 2.9. In this experiment, laser house was put on the laser diode. Both laser diode (I_{LD}) and photodiode currents (I_{PD}) were recorded for 30 minutes just after the circuit was turn on. It can be seen that the laser diode current started from 48.5mA and settled at around 50mA. This current behavior indicates that once the driver was turned on, the temperature of laser diode increased. The current of laser diode was increased to compensate for the increase in its temperature until it reach the equilibrium after around 4 minutes.

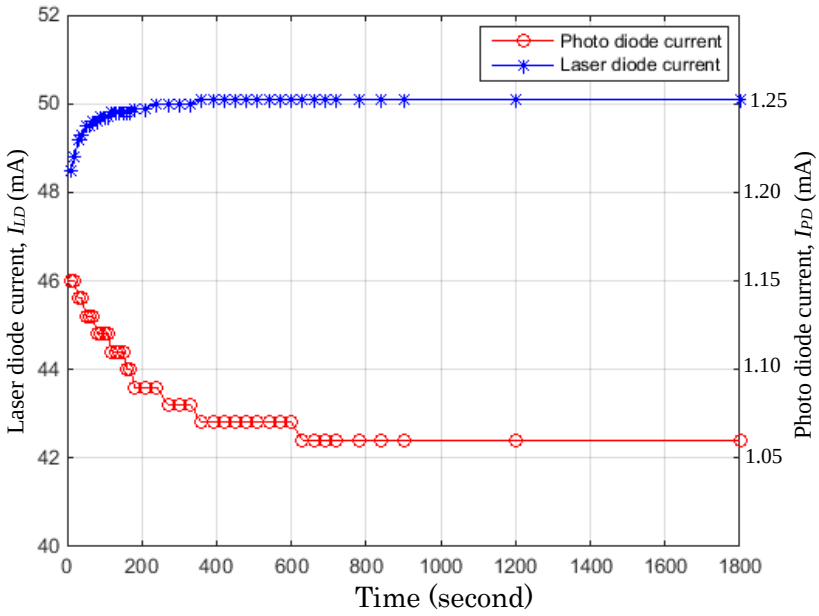

Figure 2.9 Effect of heat-sink to laser diode current.

In case of photodiode current (red curve), indicating the optical power of the laser beam, its value was decreasing before the equilibrium. This power decrease indicates that the temperature of the laser diode increases, whereas the laser diode current increases. The power of the laser beam (optical power) becomes stable after around ten minutes. Settling time of the laser diode current (blue curve) was around twice faster than its beam power (red curve).

2.3.4 Effect of ambient temperature

The purpose of this experiment was to observe the influence of ambient temperature upon the laser diode current. A blower of the hot air was used to increase the ambient temperature around the area of laser diode. After the laser system settled, four minutes (240s) after it was turned on, hot air from the blower was applied to surrounding the laser system for about 1500s (25 minutes) before it was turned off. The thermometer of laser diode surrounding was monitored by commercial digital temperature (see Figure 2.10). Laser diode current (I_{LD}) and ambient temperature were recorded for about 1 hour (3600s). The experiment results are shown in Figure 2.10. The blue curve shows the ambient temperature. After four minutes, the temperature increased slowly until it reached 50°C and constant for several minutes. The ambient temperature measured by thermometer decreased when the blower was turned off.

The laser diode current (I_{LD}), indicated as red curve, increased with the ambient room temperature. It seems that I_{LD} reaches the saturation at temperature around 40°C while the ambient temperature was still increasing. When the ambient temperature started decreasing, after about 30 minutes (1800s), I_{LD} also started decreasing. Automatic power control (APC) worked in the case of ambient temperature change. It seems that there is hysteresis relationship between the laser diode current and its ambient temperature.

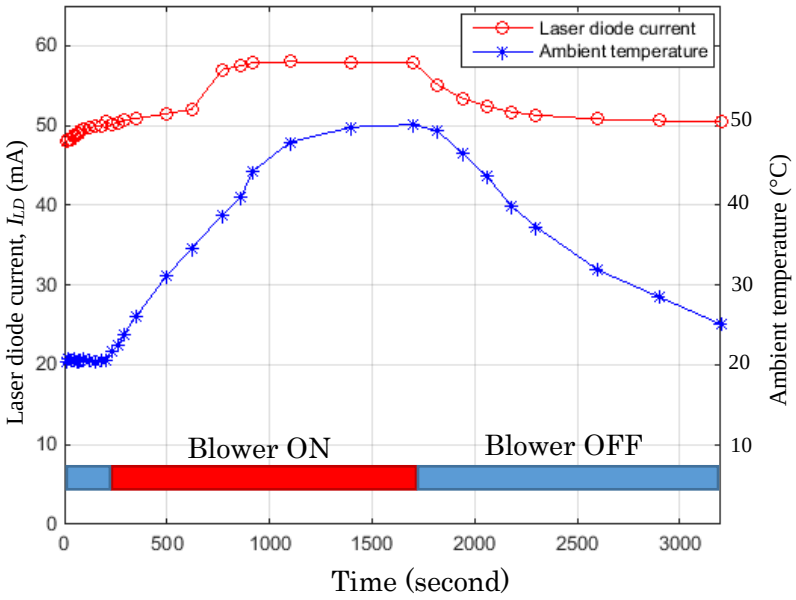

Figure 2.10 Effect of heat-sink to laser diode current.

2.3.5 Laser diode on pulse wave setting.

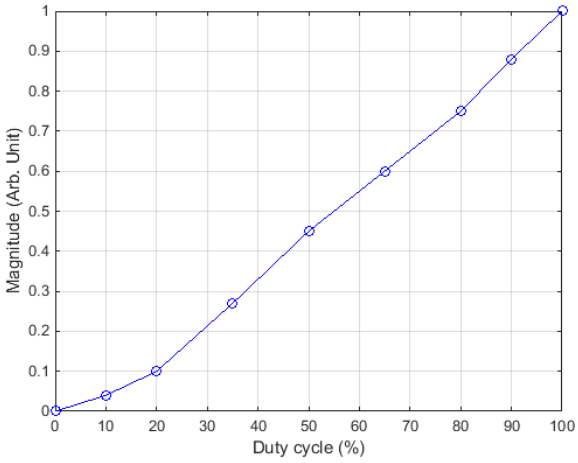

Figure 2.11 shows the magnitude change as the change of duty cycle.

The purpose of this experiment was to observe the optical power when the pulse mode (PM) was applied to the laser system. A square wave signal is applied to *pulse in* node (see Figure 2.5 (a)) to control the on-off state of laser beam output. A photodiode was placed in front of the laser diode with the distance of 5 cm to observe the optical power of laser beam. Both laser diode and photodiode circuits are shown in Figure 2.7. In this experiment, laser house was put on. Normalized photodiode currents (I_{PD}) was recorded

to obtain the optical powers as a function of square wave control signal duty cycle.

In the experiment, a square wave signal (0 – 3.3 volt) with frequency of 1kHz was applied to the *pulse in* node. The duty cycle of the signal were changed during the photodiode current measurement. The measurement results were normalized by the current at 100% duty cycle (continuous mode). Figure 2.11 shows the magnitude change versus duty cycle. The relationship between duty cycle and output optical power is linear. For example, at 50% duty cycle, the output will be around 45% of that one in continuous mode.

2.4 Chambers and microfluidic

Microfluidic system (MFS) is used to immobilize the cells, to provide the cells with odorant, and it works as sensing chamber. Based on its liquid flow, MFS can be categorized into discrete and continuous one. The discrete microfluidic system is based on droplet, while the continuous microfluidic system is based on continuous flow of liquid (odorant). Both types of fluidic systems were used in this research. Discrete system was used on static chamber to observe the sensor response to the odorant through optical fluorescence instrumentation system. Continuous system on flow chamber was used to observe the sensor response before/after the application of lock-in measurement technique on the optical fluorescent instrumentation system. Open chamber was applied to both static and flow chamber to optimize the number of cells involved for observation. Some considerations in designing the chambers are:

- Transparent base for excitation and emission light.
- Easy to control the cells on the chamber.
- Easy to handle the experiment variables (odorant concentration, flowrate, etc.)
- Easy to clean up.

Two types of chambers suc as static chamber and flow chamber were prepared for experiments, as shown in Figures 2.12 (a) and (b) respectively. The pictures of both chambers are shown in Figures 2.13 (a) and (b) respectively.The bottom plates of both type of chambers were transparent, thus the laser beam can pass throuh it and the fluorescent light can be observed from bottom side of the chamber. The cell was put on the pools of the chamber. In the static chamber, the odorant liquid does not move once it is introduced (static) to the cell. In the flow chamber, the odorant liquid flows from the inlet, through the cells and out to the outlet.

Static chamber is made of acrylic plate. In this type of chamber, the liquid is kept in the pool without flow. The cells are adsorbed at the bottom of the pool. The maximum volume of the pool is 21.21μl. During the experiment, first 18μl cell within ringer solution cells

are injected using micro pipet into the pool. After about 20 minutes, the cells are attached to the bottom of the pool and are ready for odorant exposure. The odorant liquid is introduced to the cell by dropping it onto the pool. The 2µl liquid with known concentration of odorant is introduced to the cells inside the pool using micro pipet. Using this volume, concentration of odorant is known. For example, if the concentration of the odorant introduced to the cells is 10µM, then the concentration of the odorant is diluted according to the following equation

$$10\mu M \text{ x } \frac{2\mu l}{2\mu l+18ul} = 1uM$$

The intensity change of fluorescent light caused by odorant introduction is measured using the optical instrumentation.

The flow chamber is made of Polydimethylsiloxane (PDMS) material and the glass plate for the base. There are two holes in both ends of the chamber as either odorant liquid inlet or outlet. A large hole in the middle of the chamber is used to put the cells into the pool at the beginning of the experiment. Around 20 minutes was needed for the cells to go down and to be attached to the base of the chamber. A thin flow path along the glass plate between inlet and outlet was used to flow the odorant liquid with known concentration, followed by the passage through the cell area at the middle of the chamber. In order to flow the liquid from inlet to outlet, the top hole of the pool had to be closed. A pump was used to allow the liquid to flow from inlet through the path and out to outlet. Micro-pump (mp6, Bartels) and syringe pump were used on the experiment. The flow rate should be kept low enough to avoid cell removal from the chamber. The fluorescent observation of cell in the flow chamber was done using the optical instrumentation.

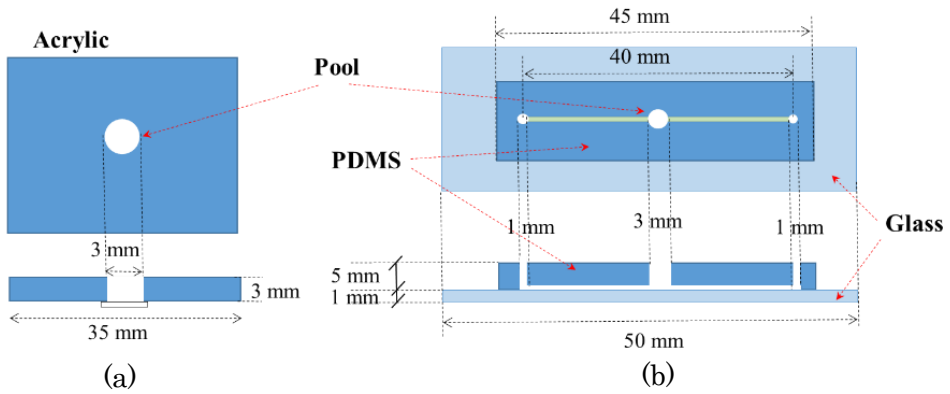

Figure 2.12. The cells chambers. (a) Static chamber and (b) Flow chamber.

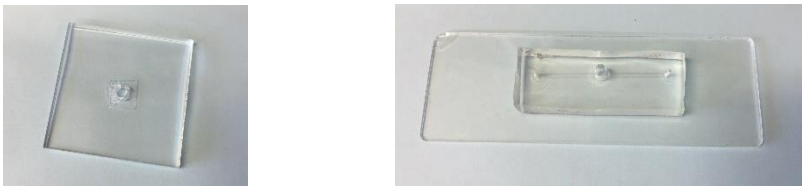

(a) (b)

Figure 2.13. Photos of the chambers. (a) Static chamber. (b) Flow chamber.

2.5 Fluorescent beads observation

Two samples were prepared for the observations. Each sample was a 4um fluorescent beads (T7283, TetraSpeck) on slide glass. Observation was performed at both 20 objective lens magnification microscope (BX43, Olympus) and assembled fluorescent instrumentation. Both samples are shown on Figures 2.14(a) and (b), respectively. It was confirmed that assembled instrumentation can be used to observe florescent phenomena in the same as that of the fluorescent microscope.

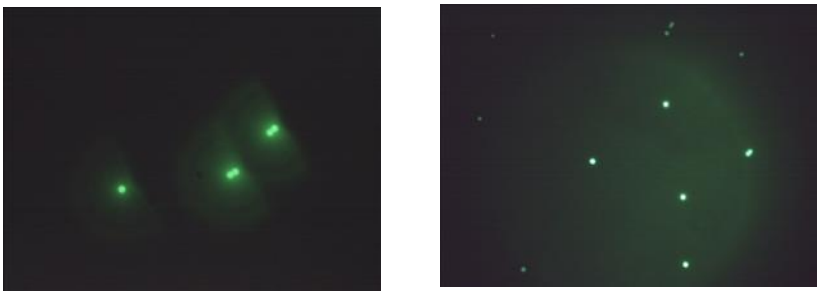

(a) (b)

Figure 2.14. 4 μm fluorescent beads image. (a) From developed fluorescent instrumentation. (b) Using fluorescent microscope.

2.6 Cells: types, preservation and preparation

2.6.1 Type of cell

Sf21 cells expressing BmOR3, Or56a and Or13a were used in this study. BmOR3 is a type of ORs which responds to bombykal, a pheromone of silkworm moth. OR56a is a fruit fly (*Drosophila melanogaster*) OR which responds specifically to geosmin. OR13a is also fruit fly OR which responds mainly to 1-octen-3-ol.

2.6.2 Cell preservation

The cells maintained inside the 70ml flask (353082, Falcon) with 5 mL grace medium

with additional 3 antibiotics zeocin (invitrogen), blasticidin (gibco), and gentamicin (gibco). Each of them is 5µl. The grace medium consist of 90% SBF (11605-09, gibco) and 10% FBS (10082-139, gibco). The life time of the cell is around 8 days. The cells tend to live and grows on the bottom of the flask. The life time of the cell is around 10 days and it is cultured every 4 days. The cell gives maximum response at 3-4 days after culturing. In the experiment, the cell of 3-4 days after culturing were mostly used. Since the cells are sensitive to ambient temperature, the cells are preserved in the incubator with the temperature of 27°C.

2.5.3 Cell Preparation

Prior to the experiment, the cells were prepared replacing the grace medium with the ringer solution. Since the cells were attached to the base of the flask, a cell scraper was used to detach the cell. Then, a small volume of cell solution (for example 18ul) was put into the chamber and was settle for a while. After several minutes, the cells were ready for odorant exposure.

2.7 Odorant preparation

Several type of odorants were used in the experiment including ionomycin, bombykal, geosmin, and 1-octen-3-ol. Ionomycin is an ionophore to induce Ca^{2+} influx into the cell forcibly. Bombykal is a pheromone component of silkworm moth. Geosmin is an organic compound produced by a type of *Actinobacteria*. Geosmin has a typical smell of mold. 1-octen-3-ol is a type odorant produced by most mycotoxigenic fungi, and can be used as an indicator of fungal contamination in grain. To obtain the proper concentration all odorants were dissolved in dimethyl sulfoxide (DMSO) since it is not possible to dissolve them directly into water. The concentration of the DMSO was kept less than 0.1%.

2.8 Observation of cell response

There are two types of images provided by Bitran Camera, full mode and VGA mode [121]. Figure 2.15 shows the illustration of area covered by both types of images. The camera resolution for full mode is 2048 x 1536 pixels. The length or width of full mode image is 4 times bigger than VGA mode. Since VGA mode covers smaller area, it needs smaller memory thus can be operated faster than in full-mode. When the capture time is set to 500ms, in VGA-mode it can be used for sampling time 1s while in full-mode minimum sampling time around 2s or more. Using the same setting 500ms capture time, for tif file, using VGA-mode it takes around 1.8kbyte while using full-mode it takes around 18kbyte memory.

Typical fluorescent images captured by the camera are shown in in Figures 2.16(a) and (b). Each small circle in the image is a Sf21 cell expressing olfactory receptors (ORs) such as BmOR3, Or56a, or Or13a. The diameter of a cell is around 20μm. Image taken in full mode have wider view area compared to VGA mode. However, image taken in VGA mode has a smaller view (part of full mode area) area but faster in capturing and smaller in data size. Thus, VGA mode offers a higher sampling rate than full mode.

Photos taken at static chamber and flow chamber are almost the same. When the more ringer solution mixed with the cell is used, the density of the cell becomes lower (Figure 2.16 (a)) while Figure 2.16 (b) show the image with denser cells. When the odorant liquid is introduced to the cell, the fluorescent intensity changes with time. It increases, reaches the maximum and then decreases. The intensity calculation is performed using Matlab.

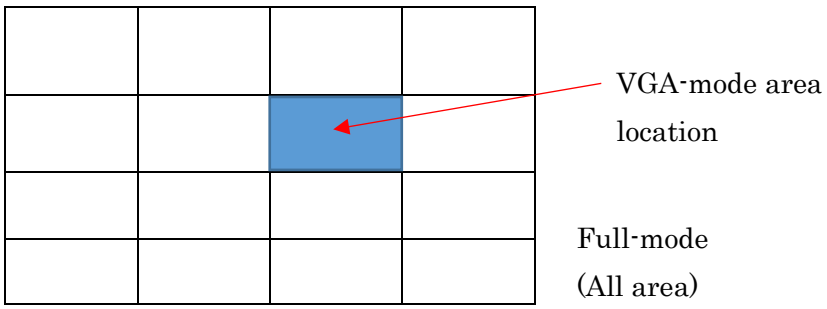

Figure 2.15 Image on Bitran Camera: Full-mode (All area) and VGA-mode (blue rectangle are)

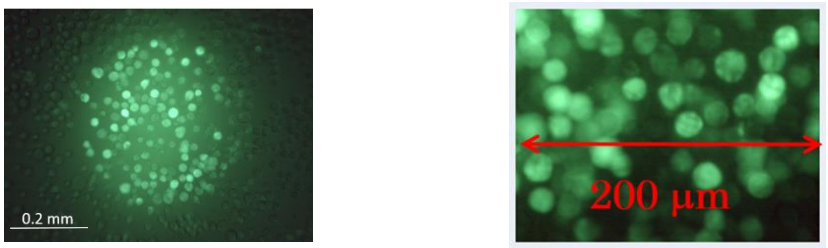

Figure 2.16. Typical fluorescent image. (a) Full mode and (b) VGA mode.

As shown in the previous figures, many cells are involved in the image. However, not all cells responded to the odorant. Moreover, the responses were different from cell to cell. These characteristics are shown in Figure 2.17(a) which shows the responses of five Or56a cells to 10μM geosmin. It can be seen that the response varies in terms of intensity and transient behavior. Thus it is essential to use a group of cells as a sensor to increase the response stability and decrease the variance among sensors. This is shown in Figure

2.17(b). The upper line shows the sum of the intensities of all pixels in the image while the lower lines show the individual five cells responses.

Since the brightness (intensities) are varies from one experiment to another, normalization (standardization) is needed to bring all the data into proportion with one another. In this thesis, the response is normalize by the data before odorant exposure, for example by the first measurement data. The normalized response curve is shown in Figure 2.18. Sensor response to the odorant is defined as the maximum brightness change of fluorescent intensity while the response time is defined as the time needed to increase the response from 10% to 90% of maximum intensity. Figure 2.16 shown a measurement results of Or56a cell to 10μM geosmin which has response 12% and response time 20 second.

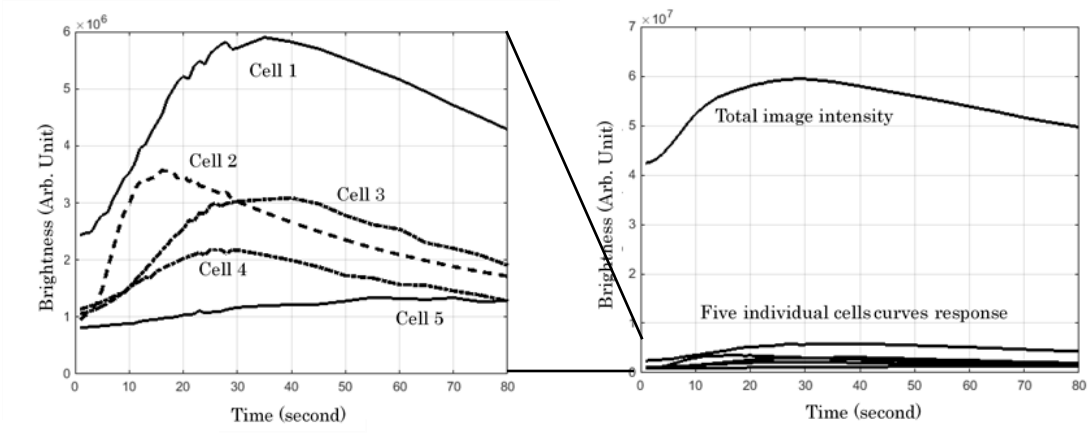

(a) (b)

Figure 2.17. Cells response. (a) Individual cell. (b) Total cell.

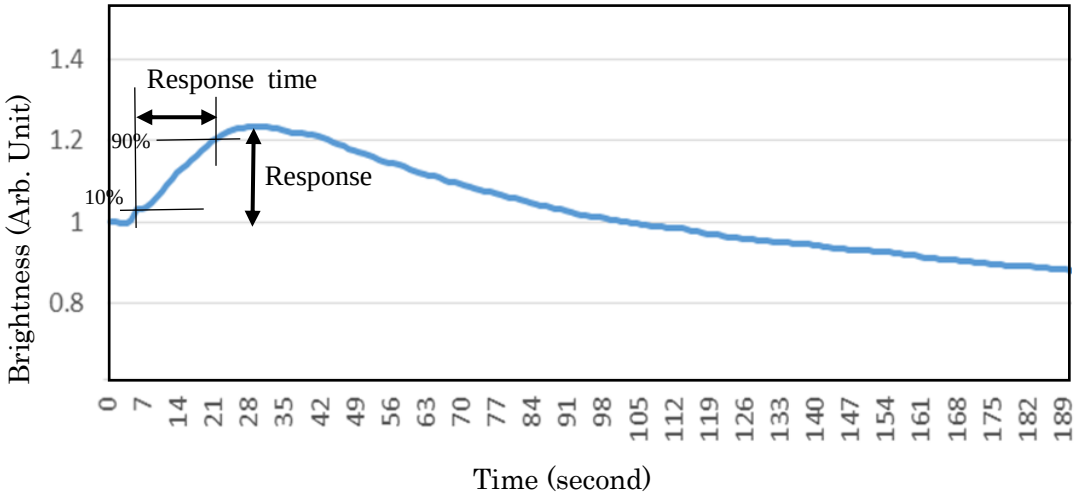

Figure 2.18. Normalized cells response to the certain odorant and some measurement definition.

2.9 Summary

In this chapter, experimental set-up for observing the response of the cell to the odorant was discussed. The related topics includes fluorescent instrumentation system, cells and their related odorants, and observing the cells responses. Fluorescent instrumentation system consists of the laser system. Some experiments have been done to observe the behavior of laser system especially its APC (automatic power control) since it is very important to have stable optical power of laser beam. Experiment results shows that the automatic power control works properly. The fluorescent bead image taken using developed instrumentation system shows the image comparable with fluorescent microscope. The next topic is related to the cells and their related odorant preparation for experiments using both static chamber and flow chamber. The materials of the experiment were discussed in this chapter. The last topics were related to observation and measurement of cell responses to odorant.

Chapter 3
Experiment on measuring sensor response using static system

Chapter 3 discusses experiment on observing the responses of the cells using a static system, where the odorant remains in the pool together with cells without flow. Detailed explanation about static chamber was given in Chapter 2. The Sf21 cells expressing two types or OR, BmOr3 and OR56a were used. BmOr3 responds specifically to bombykal while Or56a responds specifically to geosmin. The experiment using static chamber consists of several steps. The first step is to put the cells on the pool of the chamber. After several minutes, the cells are adsorbed on to the bottom of the pool and are ready for odorant exposure. The next step is to drop the odorant liquid to the cells using 10μl micro-syringe. Dropping the odorant should be done carefully in order to minimize the artifact. The last step is the observe the cell responses using the fluorescent instrumentation. Observation of the fluorescent intensity emitted by cells starts from the time before the odorant exposure and stops at the time several minutes after the exposure.

3.1 Purpose

The main purpose of the experiment was to investigate the odorant detection by the cell under the static condition. The specific purpose of the experiments includes:

1. To investigate the fluorescent intensity emitted by the cells under continuous exposure of excitation light.
2. To investigate the influence of dropping odorant liquid on the cell response.
3. To investigate the influence of DMSO solvent on the cell response.
4. To investigate whether the Calcium ion (ionomycin) is able to influx into the cell.
5. To investigate the response of the cell to the odorant with different concentration.

3.2 Experimental set-up.

3.2.1 Preparing the odorant

There are many liquids involving in experiments including ringer solution, dimethyl sulfoxide (DMSO), ionomycin, bombykal, and geosmin. Ringer solution is used as isotonic solution for the cell and also used to prepare for the proper concentration of odorant liquids. DMSO was used to dissolve geosmin and bombykal into the ringer solution and then the ringer solution was added to adjust the concentration.

3.2.1.1 Ringer solution

Ringer's solution is a solution of several salts dissolved in water for the purpose of creating an isotonic solution for establishing the environment fluids of a cells. Ringer's solution with PH 7.2 contains of 140nM NaCl, 5.6nM $CaCl_2$, 11.26nM $MgCl_2$, 19nM HEPES, and 9.4nM D-glucose. Ringer solution is used as isotonic solution for the cells and as solvent to dilute odorant. Ringer solution is provided by University of Tokyo. For the use as concentration adjustment, ringer's solution with 0.1% dimethyl sulfoxide (DMSO) was used. To make ringer's solution with 0.1% DMSO, 50mL ringer's solution was mixed with 50ul DMSO.

3.2.1.2 Dimethyl sulfoxide (DMSO)

DMSO ($(CH_3)_2SO$) is a colorless solvent widely used as chemical solvent composed of many kind of compounds and is miscible in a wide range of organic solvents as well as water. In this research, DMSO (99%, Wako) is used as solvent for geosmin and 1-octen-3-ol.

3.2.1.3 Ionomycin (Sigma-Aldrich)

Ionomycin is an ionophore to induce Ca^{2+} influx into the cell forcibly. It is used in research to raise the intracellular level of calcium (Ca^{2+}) and as a research tool to understand Ca^{2+} transport across biological membranes. To prepare for several concentration (10 μM and 100 μM), Ionomycin was dissolved to ringer solution with dimethyl sulfoxide (DMSO) concentration less than 1%.

3.2.1.4 Bombykal

A 1 mM Bombykal odorant dissolved in DMSO (1mM, 100% DMSO) was obtained from University of Tokyo. To prepare for the others concentration, bombykal dissolved to the ringer solution. Mixing between 1 part of bombykal and 999 parts of ringer solution resulted in a bombykal odorant with concentration 1μM with 0.1% DMSO. The concentration can be obtained in the similar way. For example, to get 100nM bombykal, 1 part of 1μM bombykal is mixed with 9 parts of 0.1% ringer solution.

3.2.1.5 Geosmin (Wako)

Geosmin is commercially available in many types of packing. One of them is Geosmin Standard 20mg in a bottle from Wako. Geosmin odorant with 100mM concentration was obtained by mixing 1 bottle of this package with 1075 μl of DMSO. Thus, a stock of 100mM geosmin with 100% DMSO was created. Mixing 1 part of 100mM geosmin with

999 parts of ringer solution resulted in 100μM, 0.1% DMSO.

3.2.1.6 1-octen-3-ol (Sigma-Aldrich, China)

Two types of solvents, DMSO and ringer solution, were used for the purpose of preparing the proper concentration of odorant liquids. DMSO was used to dissolve 1-octen-3-ol into the ringer solution and then some ringer solution was added to adjust the concentration.

3.2.2 Preparing and immobilized the cell

The cells are preserved inside the flask with 5 ml grace medium as explained in chapter 2. Normally, the cells are attached to the surface of the bottom of the flask. The cells are cultured every 4 days since the life time of the cells is at most 2 weeks. A 3 to 4 days cells (after culturing) is usually used for experiment. The procedure for preparing for the cells for experiment includes:

1. Remove the grace medium from the flask.
2. Wash the cells with ringer solution. Using the syringe, put 1 mL ringer solution into the flask and then take it out.
3. Using the syringe, put 4 ml ringer solution into the flask.
4. Using the cell scrappers, scrap the cells to remove them from the surface of the bottom parts of the flask.
5. Using the syringe, take 18 ul solution with cells from the flask and put at the pool of static chamber.
6. Wait for several minutes to let the cell attached firmly to the base of the chamber before odorant exposure

3.2.3 Preparing for the instrumentation for measurement.

Preparation for the instrumentation for measurements includes,

1. Turn on the laser system, set the supply voltage 7 volt. Wait for 10 minutes to let the power of the laser beam stable.
2. Turn on the CMOS camera and open its software application. Set the cooling temperature at 0°C. While waiting for the temperature becoming 0°C (shown in the menu) for 1 minute, several options such as camera mode (full mode), capture time (1 second), optical attenuation (50%), and number of image to be taken should be set.
3. Put the chamber on the holder so that the laser beam illuminate the cells. Set the image capture on. Adjust the distance between the cells and the objective lens (objective length focal point) to have the appropriate image.
4. It is ready for experiment. Before starting the experiment, set the file type of image

to save. In this experiment, two types of image tiff and jpg files are used. The tiff files is used for further processing by matlab while jpg files is used for observing the image since it is shown in computer display.

3.3 Experimental results and discussion

3.3.1 Exposing the odorant

In the experiment to observe the effect of odorant, the cells were exposed to the odorant for several seconds after experiment started. Thus, the transient response of the cells can be observed. The odorant liquid is introduced to the cells by dropping the odorant with known both in its concentration and volume onto the pool. Illustration of the odorant exposure is shown in Figure 3-1. Normally, during the experiments, the odorant volume is one-tenth of total volume of odorant and cell liquids. Thus final concentration of the odorant applied to the cells is one-tenth of odorant concentrations. In most of the experiment, the volume of cells and odorant liquids were 18µl and 2µl, respectively. If the concentration of odorant is 100µM, the final concentration of odorant becomes 10µM. The dropping should be done carefully and the tip of the needle should be approached as close as possible to the liquid surface to avoid the artifact. Liquid was dropped to the cell several seconds after observation started.

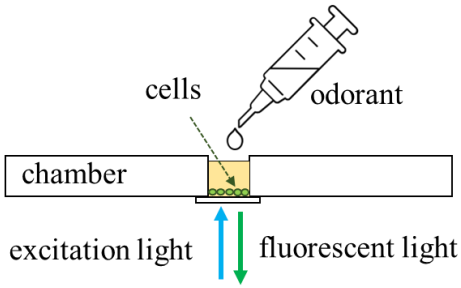

Figure 3-1. Introduction of odorant to the cells by dropping.

3.3.2 Image of the cells

Figure 3-2 shows the image of the cells captured by the camera. In this experiment, BmOR3 was used. The density of the BmOr3 cells shown in Figure 3-2(a) is higher than that in Figure 3-2(b). The volume of the ringer's solution (section 3.2.2) for the experiment shown in Figure 3-2(b) is more than the one for experiment in Figure 3-2(a). The ringer's solution for the experiment was 4 ml and normally the cells image is more like in Figure 3-2(a) while 6 ml was used for image shown in Figure 3-2(b). The more cells density is, the more response is since more cells are involved in measurement. Around 18kbyte memory was used to save each tiff file image shown in Figure 3-2.

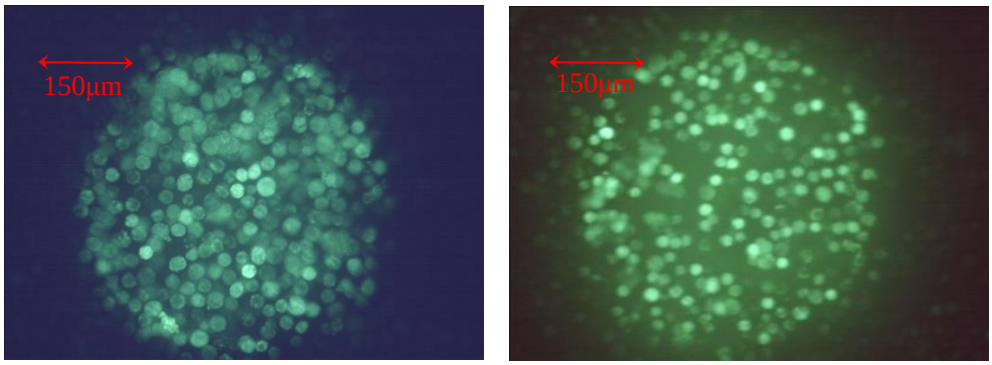

(a) (b)

Figure 3-2. Cell image. a) High density. b) low density.

3.3.3 Experiment without odorant

Figure 3-3 shows the response of the Or56a cells without odorant exposure. Fluorescent intensity of the cell decreases exponentially by the time. There was about 2% drop in fluorescent intensity brightness of the cell after continuous exposure for 120 second. This reduction in fluorescent intensity is due to decreasing cell capability of emitting the light after illumination of excitation light. The characteristics of cell itself change due to laser exposure (effect of photo bleaching), probably the brightness of the fluorescent even if the laser power is constant. Thus the optimum laser power should be optimized.

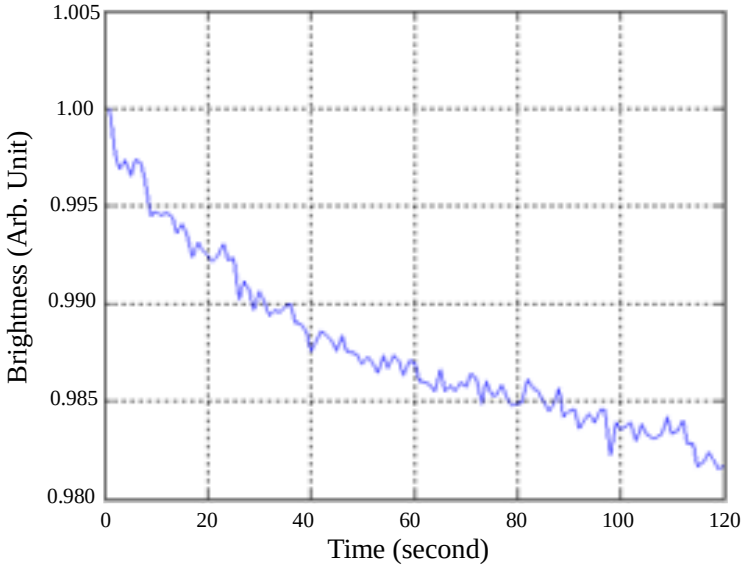

Figure 3-3. Typical Or56a cells responses without odorant applied.

3.3.4 Response to ionomycin

The experiment was performed for the purpose of investigating the ability of ion gate to influx the calcium ion into the cell. Another purpose was to investigate the responses of the cell to the odorant in static condition. The cells expressing Or56a and ionomycin odorant were used in this experiments.

The volume of the Or56a cells (with ringer's solution) put on the pool chamber was 18µl. 5 second after observation started, the odorant was introduced to the cells. This was done by dropping 2µl of ionomycin with concentration of 1mM to the cells. The final concentration of ionomycin introduced to the cells was 100µM. The results of the experiments are shown in Figure 3-4. Although there was an artifact at odorant introduction, the intensity of the cells increased sharply until it reached the maximum in the next 35 second. The maximum response reached around 100% (2x) of cells brightness change compared with brightness before ionomycin exposure. The 3 cell images, before ionomycin applied, with maximum brightness, and several tens of seconds after recovery, show the change of brightness.

From the Figure 3-4, the process of calcium ion influx into the cell has been confirmed by the response of the cell to the ionomycin 100uM. The response was large since ionomycin is an ionophore and its concentration (100uM) was high.

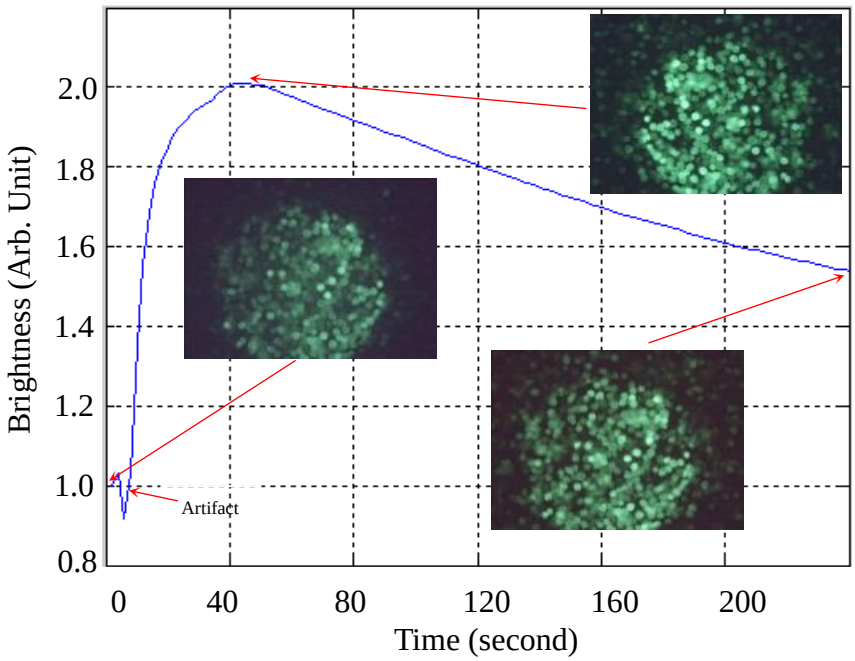

Figure 3-4. Responses of the Or56a to the 100µM ionomycin.

3.3.5 Influence of DMSO

Several experiments were performed to investigate the influence of DMSO on the cells. Three types of liquids were prepared, pure ringer solution (0% DMSO), ringer solution with 0.5% DMSO, and ringer' solution with 1% DMSO. Experiment without odorant was performed here for the purpose of response comparison among several concentration of DMSO. The odorants were introduced to the cells 5s after observation started by dropping it using micro syringe. The observation were performed for 120s. The results of the experiments are shown in Figure 3-5.

The cells response to pure ringer solution (0% DMSO), ringer solution with 0.5% DMSO, and ringer solution with 1% DMSO shown in green, red, and light blue, respectively. As a comparison, the cell response without any liquid exposure is given (dark blue curve). An artifact due to liquid dropping is very likely to happen to any odorant introduction including pure ringer solution even if it was done carefully. However, its peak did not exceed 4% as is shown in orange line Figure 3-5. If maximum 4% response is considered to be an artifact, the effect of 0.5% or even 1% DMSO solvent can be ignored since the response is almost the same that to solvent with 0% DMSO.

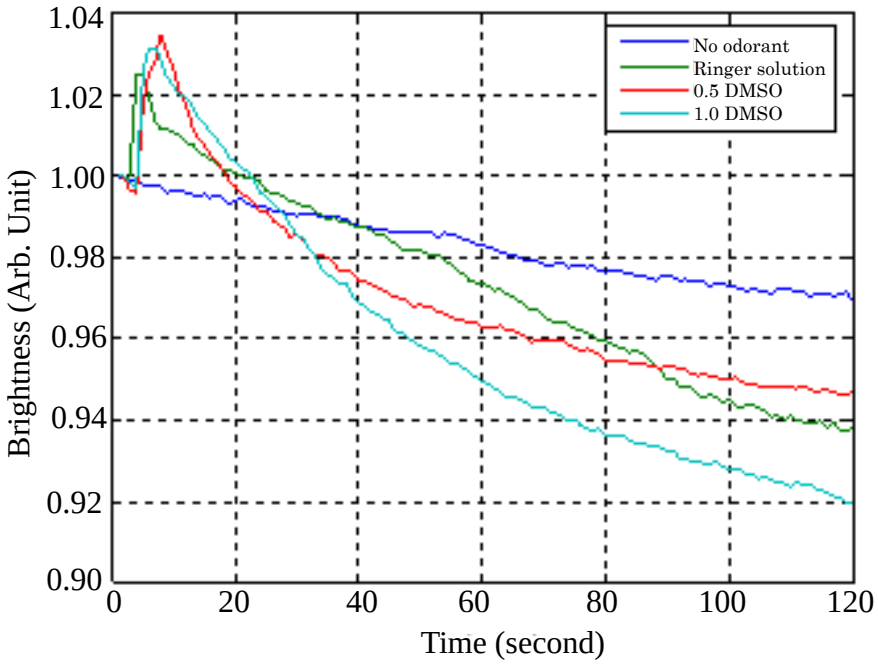

Figure 3-5. Responses of the BmOR3 to DMSO with several concentrations compared with the response of BmOR3 without any exposure.

3.3.6 Experiment results with Or56a cell line

In the experiments, 18µl ringer solution with OR56a cells was put on the pool of the chamber. After 20 minutes, the cells were ready for odorant exposure and the chamber was put on the experiment holder. A 2µl geosmin with concentration of 1mM was put into the pool using micro-syringe 5s after the observation started. In this case, the cells were exposed to 100 µM geosmin. Total concentration of DMSO on the cell was 1%. The observation was done for 240 seconds (4 minutes). The image was obtained every 1s. The brightness was integrated over the whole image and it was normalized by its value at 0s. The plot of brightness with the time is shown in Figure 3-6 (blue curve). Several experiment results using different final concentrations of geosmin, which were 1 µM, 5 µM, and 50 µM, respectively shown in Figure 3-6. The 2µl of geosmin solution with the concentration 10 times higher than the final concentration was added to the pool in each case. The cells for experiment is used only once, every experiment used different cells. From this experiment, several conclusions can be obtained:

- The OR56a cells responded to the geosmin odorant as its brightness increased, for example, the cell response to the 100µM geosmin reached maximum brightness change around 31%. The higher concentrations the higher maximum brightness change occurs. The responses to other concentrations 50µM, 5µM, and 1µM were around 18%, 6% and 3%, respectively.
- It can be seen that the higher concentration the faster response time (t_r). It was around 20s for the 100µM geosmin, whereas they were 23s and 25s for the concentrations 50µM and 5µM, respectively. The response time for 1µM was hardly observed.
- The dropping liquid contributed to the intensity change (at time about 5s). Even with the carefully handling, the artifact usually exists. A few percent change in brightness (intensity) was considered as an artifact.
- It can be observed that the OR56a cells were able to detect the odorant as low as 5 µM for about 15 second. The response to 1 µM geosmin can be considered as artifact since it reached the peak for short time with small (around artifact) brightness change.

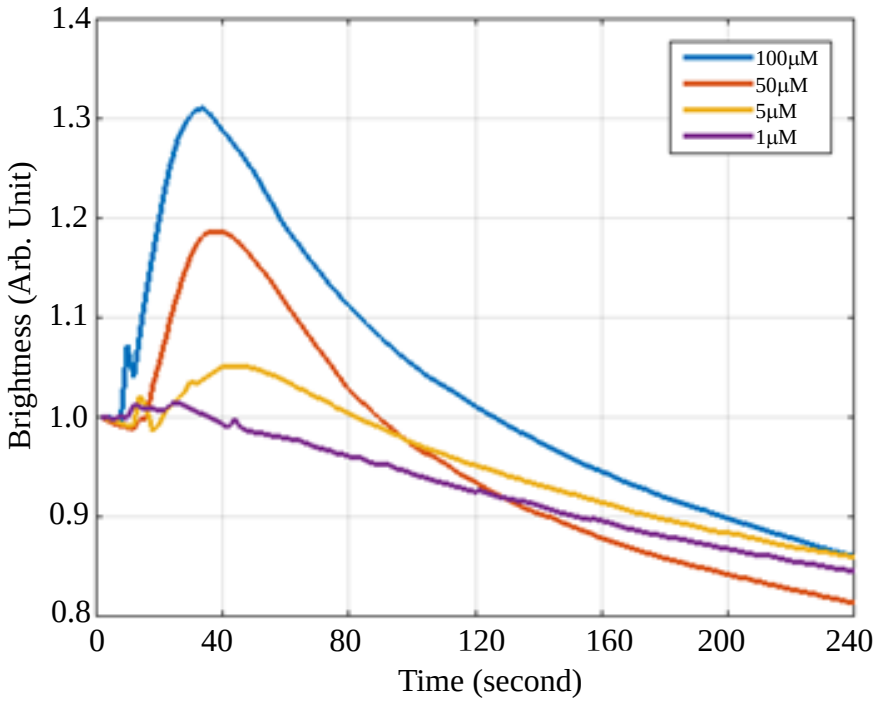

Figure 3-6. Typical responses of the OR56a to geosmin with several concentrations

3.3.7 Experiment results with BmOR3 cell line

Several experiments were performed for BmOR3 cell line in responses to several concentrations of bombykal odorant, 1μM, 5μM and 10μM, respectively. Different cells were used in different experiments. In every experiment, the volume of the cells were 18μL while the odorant volume is 2μl. Thus, the final odorant concentration was 10% of odorant concentration introduced since the volume of the odorant liquid is 10% of the total liquid on the chamber. The experiment results are shown in Figure 3-7. The response of the BmOr3 cell line to 10μM odorant was clearly observed (around 12%) while the response to 1μM was not clear since the response was as small as artifact. The response to 5μM odorant can be observed (around 6%) although it was not so clear. From this figure, it can be seen that BmOR3 cell line was able to detect the bombykal odorant with concentration as low as 5 μM.

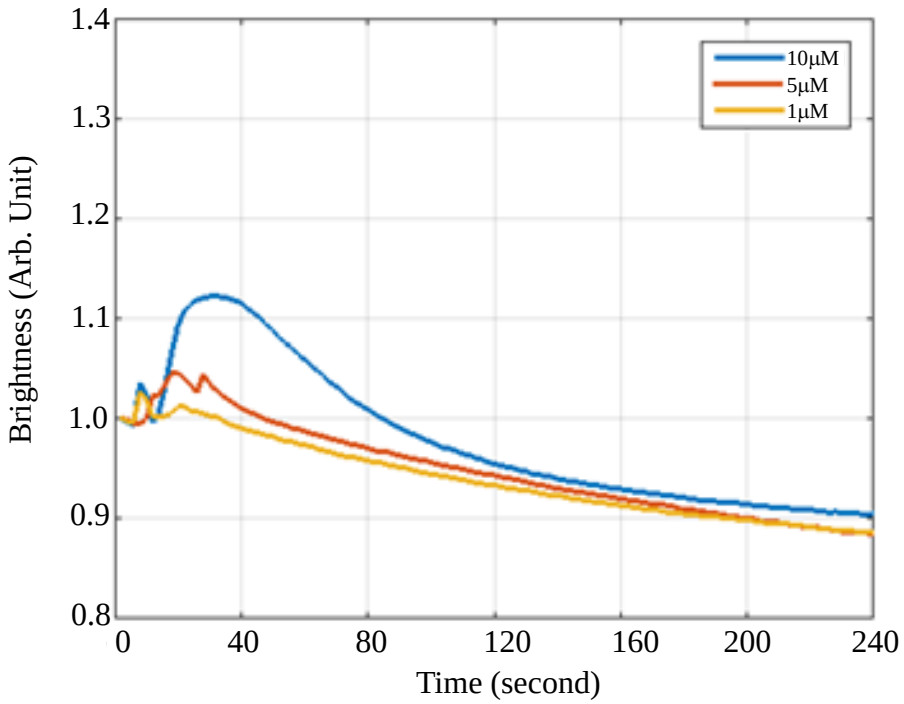

Figure 3-7. Typical responses of the BmOR3 to bombykal with several concentrations

3.3.8 Concentration dependencies

Several experiments for some concentrations using both Or56a and BmOR3 cell lines with geosmin and bombykal odorants, respectively were performed. Four experiments were done for each concentration. In case of Or56a, it was from geosmin concentration of 5μM, 50μM, and 100μM. 1μM concentration was not used since the results were closed to artifact. In case of BmOR3, the concentration dependencies to bombykal odorant was from 5μM to 10μM. 100μM and 1μM concentration were not used since for the first case the DMSO concentration was around 10% and for the second case since the results were almost artifact. These plot of cells responses to several concentration of odorant shown in Figure 3-8. The responses shows the dependencies to the odorant concentration.

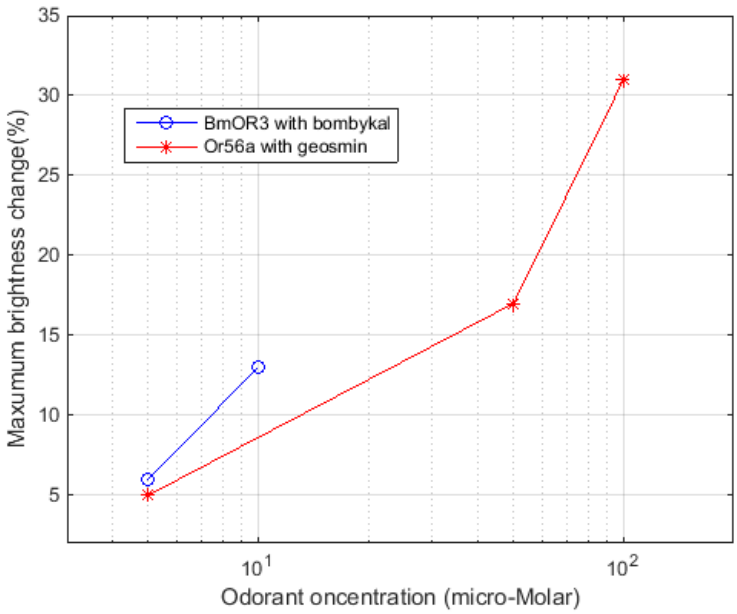

Figure 3-8. Concentration dependencies of cells responses to its associate odorant.

3.4 Summary

Chapter 3 discussed about experiment on observing the Or56a and BmOR3 cells response to its associates odorant, geosmin and bombykal, respectively using the static chamber. The odorant does not flow through the cells but of remains in the pool together with the cells. Sf21 cells expressing Or56a and BmOR3 were used in the experiments. Or56a is a type of OR which specifically respond to geosmin while BmOR3 is a type of ORs which specifically responds to bombykal. Before the cells exposed to their associated odorant, the experiment were done for:

- Without odorant exposure cells.
- BmOR3 cells exposed to DMSO with several concentration of DMSO.
- Or56a cells exposed to ionomycin.
- Or56a cells exposed to geosmin.
- BmOr3 cells exposed to bombykal.

Several conclusions can be obtained from the experiments including:

1. Without the odorant exposure, fluorescent intensity of the cells decreases exponentially by the time due to photo-bleaching effect.
2. DMSO concentration less than 1% does not affect the cells responses.
3. The dropping liquid contributed to the artifact, even with the carefully handling, the artifact usually present around 4% in brightness change.
4. The process of calcium ion influx into the cell has been confirmed by the response of

the cell to the ionomycin.

5. The Or56a cells respond to geosmin. The cells could not detect the geosmin concentration below 1μM since the artifact was dominant. The response dependency upon the concentration from 5μM to 100μM was obtained.
6. The BmOR3 cells respond to bomykal. The cells could not detect the bombykal concentration below 1μM since the artifact was dominant. The response concentration from 5μM to 10μM was observed.
7. For the reason of our stocks availability, the maximum concentration for Or56a and BmOR3 used were 100μM and 10μM, respectively since their DMSO concentration were 1% in both cases. Above that concentrations, the DMSO contains will be above 1%.

Chapter 4.

Development of flow measurement system.

The main purpose of experiment on odor detection system with static odorant is to verify that the cells can be used as a sensor and their responses can be detected using developed measurement system. Dependency of the sensor response upon odorant concentration can be obtained. Using static chamber for odor detection, the preparations and procedures were very simple. Moreover, the amount of materials such as cells and odorant were very small. However, the artifact due to odorant dropping often happens, even with carefully handling in dark condition. This is one of the disadvantages of static system. The odorant normally flows in the air or liquid. Thus, system such as flow system was investigated.

In this chapter, preparation for flow measurement system is discussed. It consists of materials, chamber preparation, simple fluidic system, and discussion of the experiment. The cell and its preparation were discussed in previous chapters.

4.1 Material

4.1.1 Flow Chamber

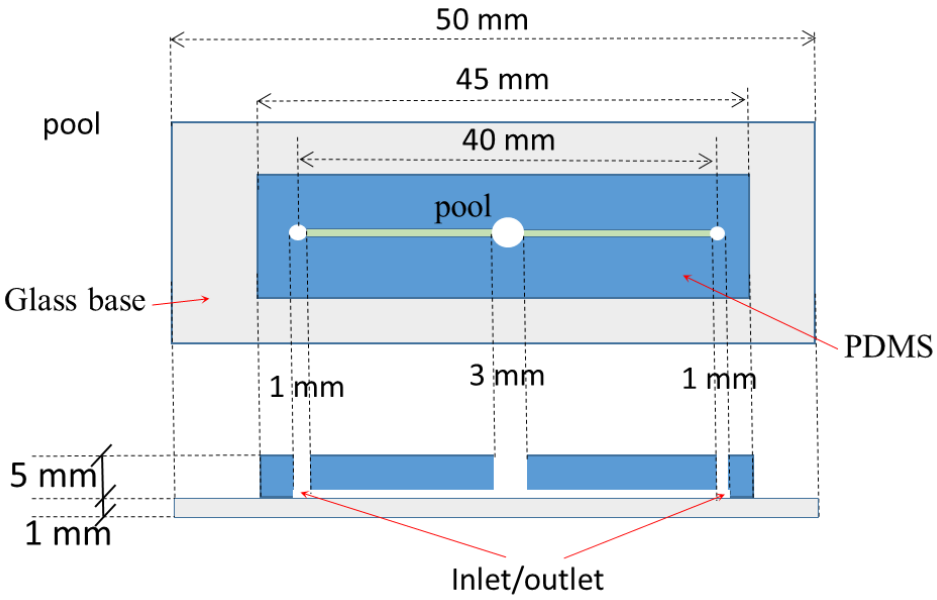

Figure 4-1 Flow chamber, Upper view (up) and side view (bottom).

The figures of both upper and side views of the chamber for flow system is shown in Figure 4-1. It has dimension of 5cm x 2cm x 0.5cm and made of Polydimethylsiloxane (PDMS) material (above) and glass (bottom) plate for the base. There are two holes at both ends of the chamber as odorant either liquid inlet or outlet. A large hole in the middle of the chamber is used to put the cells into the pool at the beginning of the experiment. A thin flow path along the glass plate between inlet and outlet is used to flow the odorant liquid which passes through the cell area at the middle of the chamber. In order to flow the liquid from inlet to outlet, the top hole of the pool has to be sealed by a tape covering the pool. Total volume of the chamber, composed of pool and two inlet/outlet, is around 50μl. During the experiment, the bubble inside the observation area should be avoided. Thus, the chamber should be fully filled with the liquids.

4.1.2 Pipette, disposable tip, and pipe

The main function of a pipette (with disposable tip) is to put the ringer's solution and the cells into the pool of the chamber prior to the experiment. A pipette, a tip, micro-pipes, a flow chamber, and a sink formed a simple fluidic system. A pipette is used to push the odorant liquid manually by hand. An odorant put at the tip of the pippette flows through the pipe and then passes the cells placed in the chamber before finally goes to the sink through the pipe. Pushing the pipette should be done carefully to avoid cells removal. The odorant flowrate should be in the order of several hundred microliter per-minutes or less. Figures 4-2.(a), (b) and (c) show the pictures of pipette (Discovery comfort, HTL Lab Solution), disposable pipette tips (200μL, AS ONE), and micro-pipe (R-3603, Tygon), respectively. A 20μL pipette (single channel, discovery comfort Inc.), tips and micro pipe, are used to connect the pipette with the chamber. The inner diameter of micro-pipe is 500um and the volume of 10cm pipe is around 0.008μL.

(a) (b) (c)

Figure 4-2. Apparatus for manual flow experiment. (a) Pipette, (b) Disposable tip, and (c) micro-pipe.

4.1.3 Micro pump.

Although using pipette to generate flow for fluidic system is very simple but it is very difficult to control or to have precise and stable liquid flowrate. Using micro pump (mp6-pp, Bartels Microtechnik GmbH.) has some advantages over pipette to generate the flow. Micro pump is a candidate for compact and portable system because of its small dimension (30mm x 15mm x 3.8 mm), very light weight (2 g), and low power consumption (<200mW). It can be used for liquid, gas, and their mixture. In case for liquid application, the pump can be operated at maximum flowrate around 5mL/min (at 100 Hz) and back pressure: 650 mbar (100 Hz) for liquid. Its principle is based on a piezoelectric diaphragm in combination with passive check valves. A piezo electric ceramic mounted on a coated brass membrane is deformed when voltage is applied. When the voltage decreases, deformation of the piezoelectric material causes an upstroke of the membrane. The medium is sucked in and the chamber is filled again. For every second, the pump can do several hundred pumping cycles.

Although there is a controller (mp-x controller or mp6-OEM) available for mp6-pp, our laboratory developed our own controller for the reason of flexibility. Basically the pump should be provided by a periodic signals in the form of either sinusoid, rectangular, or SRS (sounding reference signal). Beside the form of the signal, the other two parameters for driving the pump are frequency and amplitide of the signal. With available controller from bartels, the range of amplitude of the signal is between 0V and 250V while the range of frequency is between 0 to 300Hz. In our controller, the range of frequency can be set up to several kHz.

Figure 4-3. Micro pump (Bartels Microtechnik GmbH).

4.1.4 Syringe pump

Experiment with precise and stable flowrate was needed to observe the cells behavior under specific flowrate. To have a precise and stable flow-rate, a syringe pump should be used. For example, KDS (kd scientific) Legato 111 with Dual Syringe Infuse/Withdraw Programmable Syringe Pump is shown in Figure 4-4. It has flowrate between 0.5µl and 10 mL ±0.5% per minutes. The pump can be run based on time frame or total volume has been infuse/withdraw. Beside its advantages, the main disadvantage of syringe pump is its dimension and weight which are 22.6cm x 19.05cm x 15cm and 2.66 kg respectively. Thus, it is not possible to implement the compact system using syringe pump. It is shown in Figure 4-4 that two syringes can be used but only one was used for the current experiment.

Figure 4-4. Syringe pump (kd scientific).

4.1.5 Solenoid Valve

A solenoid valve is an electromechanically operated valve controlled by an electric current through a solenoid. In a two-way valve the flow is switched on or off to release or shut off fluids. Solenoids offer fast and safe switching, high reliability, long service life, low control power and compact design. A 2-way solenoid valve from Takasago electric ((2 ways, Clean Valve EXAK-2-NC, takas ago electric) was used. Since the valve is normally closed (NC), the valve is closed (off) when the solenoid is not energized, otherwise it is on. In this thesis, solenoid valve was used to control the liquid flows in automatic system.

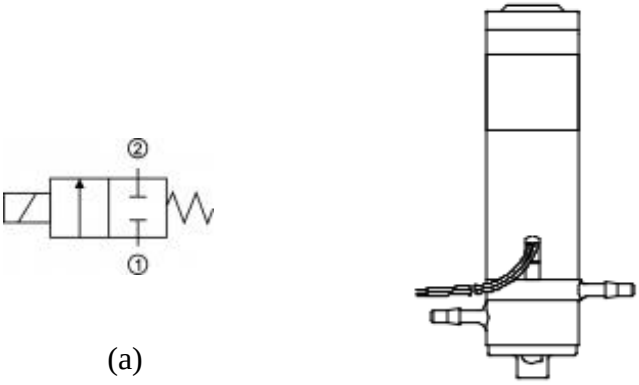

(a) (b)

Figure 4-5. Solenoid valve (a) Schematic symbol and (b) Illustration of solenoid valve.

4.2 Preparing for the cells in flow chamber. (Chamber preparation)

The cells need to be placed properly on the flow chamber. Two important things to be noticed before the experiment is that the cells should be firmly attached to the base of the chamber and that there is no bubble along the liquid path. The bubble does not affect the results in case of experiment in dark situation, but it does affect in the present of ambient light. The procedure for preparing the cells in flow chamber is as follows:

1. Using a 20µl-pipette get 20µl ringer solution (with 0.1% DMSO) and put it in the pool of flow chamber.
2. Using another 20µl-pipette take OR cells from the prepared flask (Cell preparations, explained in chapter 3) and put it in the pool drop by drop (little by little) until the chamber is full with the liquid as shown in Figure 4.6. Avoid the presence of the bubble in this step.
3. Seal the top area of the chamber by tape.
4. Wait for 20 minutes or more to let the cells go down and be attached to the bottom of the chamber (Figure 4-7)
5. Ready for experiment. Inlet and outlet is the place to enter and to release odorant.

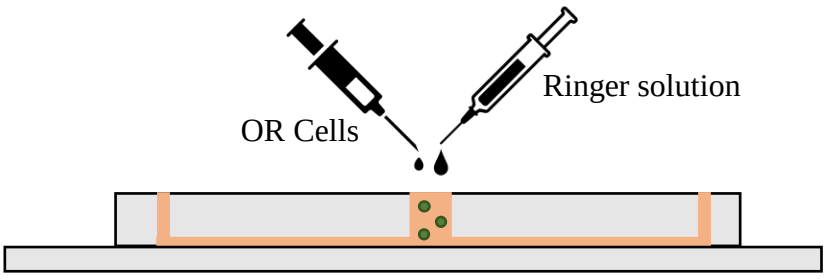

Figure 4-6. Introduction of ringer solution and cells in flow chamber

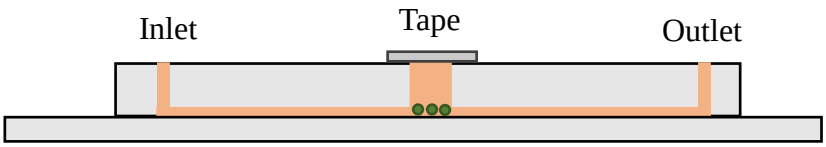

Figure 4-7. The chamber ready for experiment.

4.3 Experiment on microfluidic manual system.

Microfluidic system was developed from materials or parts explained above. There were two scenarios of creating the liquid flow and handling the measurement results, manual system and automatic system. In the manual system, the flow was created by pushing the plunger of the pipette, while in automatic system pump was used. Two types of electrical pumps were used here, micro pump and syringe pump. Manual system was used to observe in deep the fluidic system behavior, especially how to avoid the bubble inside the flow system. The presence of bubble in observation area affects the fluorescent light intensity under the ambient light. In automatic system, the flow operation (on and off) can be controlled automatically from the computer and it was combined with data handling. The automatic system will be discuss in chapter 5.

The micro pump is very light and small but it is not so easy to keep constant flowrate. However, it is suitable for implementing portable measurement system as long as the cells is not removed. The syringe pump is bulky, strong and heavy. Thus, it is not suitable for portable implementation. However, it can be used to generate precise and constant flowrate. The automatic syringe pump was used to the experiment where the precise flowrate is needed.

4.3.1 Experiment construction.

Figure 4.8(a) shows the schematic diagram of experiments on manual flow system. It consists of pipette, pipes, flow chamber, and waste. The prepared chamber previously discussed connected to the pipette and sink with pipes. Both pipe 1 and pipe 2 has inside diameters 1mm and length 5cm and 10cm respectively. Volume of both pipes can be ignored since they are very small compared with the volume of the chamber. A tip was used to connect the pipette to the pipe. 20µl odorant were placed on the pipette and flowed it through the pipe to the cell by pushing the pipette plunger carefully. A sink made of glass was used to collect the overflow liquid.

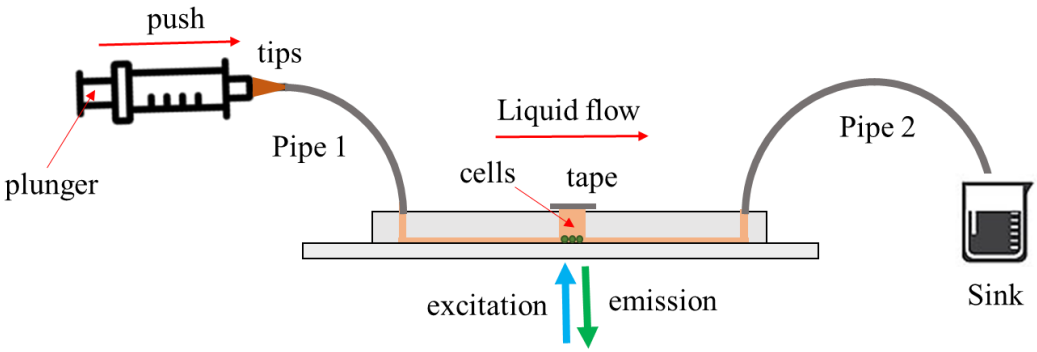

(a)

(b)

Figure 4-8. Manually flow system. (a) Schematic diagram of experiment using manual flow system and (b) Pipette plunger.

Figure 4-8(b) shows the length of the syringe plunger, which is 14mm. For example, If it was pushed by hand until it stopped for 10 second, it means that the average flowrate was 20µl/10s or 120µl/minute. Using the hand it was very difficult to make the flowrate constant, sometimes stop and another time faster than 120µl/minute.

Several cells images obtained from flow chamber are shown in Figures 4-9. Objective lens of 20 magnifications was used for those images. Figure 4.9 (a) shows an image out of focus. A typical image of dead cells is shown in Figures 4-9.(b). This image is normally obtained from the cells several days after preparation or the cells after exposed to the air for some time. Figure 4.9(c) shows the image with low cell density, prepared with 6.5 ml ringer solution. Figure 4.9(d) shows an image with normal density. The cells was prepared with 4.5 ml ringer solutions.

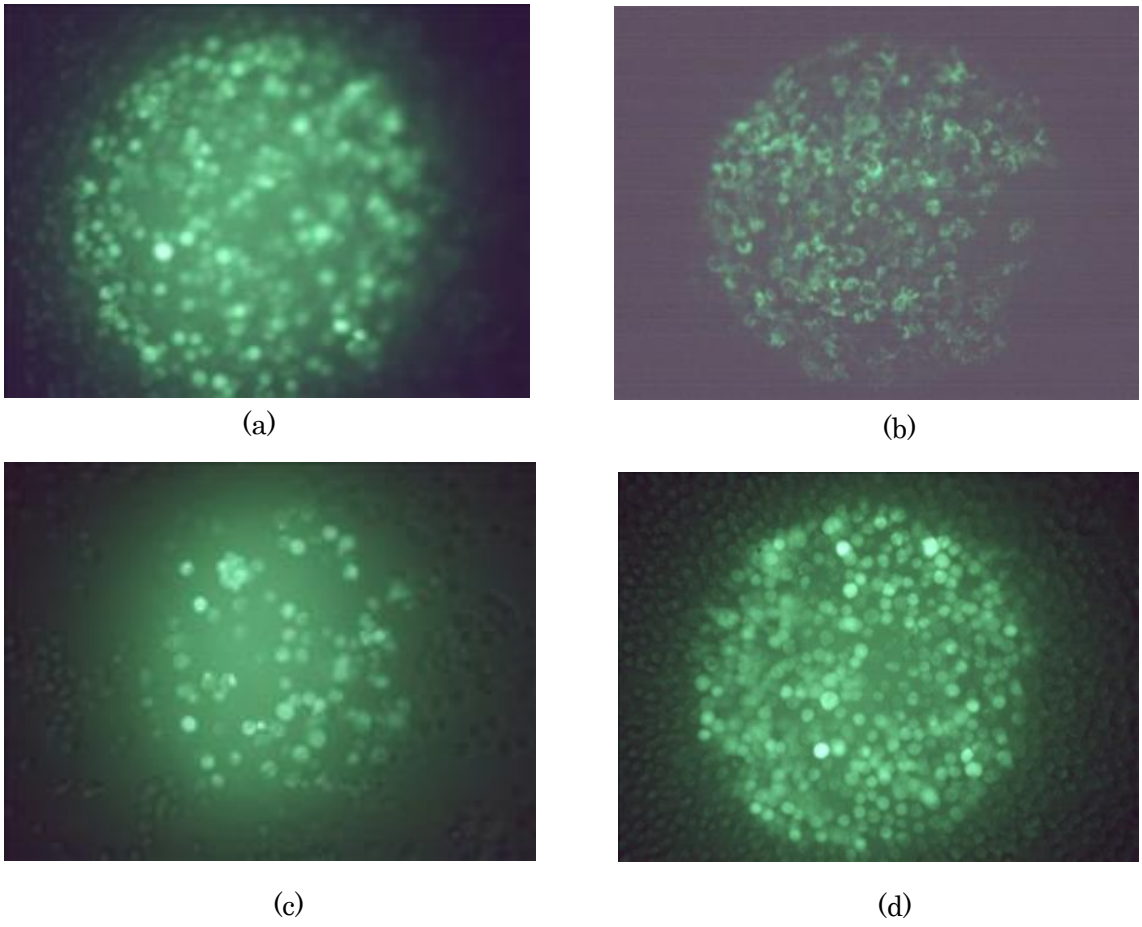

Figure 4-9. Typical cell images in full mode. (a) Out of focus, (b) Dead cells, (c) Low cell density and (d) Good images.

4.3.2 Experiment on the effect of flowrate.

The construction of the experiment is shown in Figure 4.8(a). The OR was Or56a and pure ringer solution was flowed. The experimental variable was odorant flowrate by means of the total time needed to push pipette plunger toward the end. The speed of pushing plunger tried to be as uniform as possible even if it was not so easy. Without skills, it was very difficult to flow the odorant without cells removed. Figures 4.10(a) and (b) shows one of the examples of image when cells were removed. Total time needed to push the pipette plunger was 5 second, thus the average of the odorant flowrate was around 3000μl/minute. Figure 4.10.(a) shows the image before odorant exposure, while Figure 4.10.(b) shows the image after pushing the plunger finished (5 second). About 75% of the cells were removed. This kind of experimental results cannot be used.

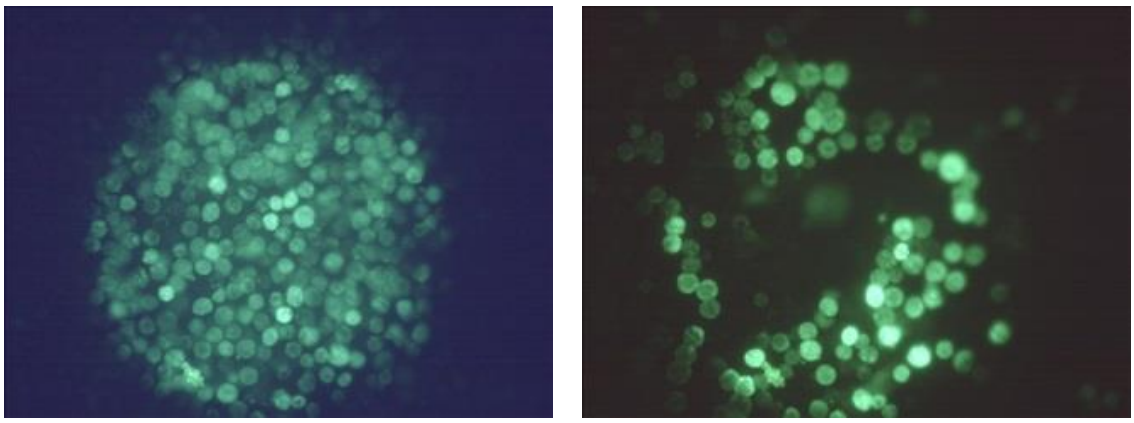

Figure 4.10. Cell image by manual flow (a) Before and (b) After the flow of ringer solution with average flowrate around 500µl/min.

4.3.3 Experiment on the response of cells to the odorant

In this experiment Or56a cells was used incorporated with ionomycin 10µM as an odorant. The odorant was introduced to the cells 10 second after observation started. The pipette plunger was pushed slowly and carefully. It took around 20 seconds to finish it. Thus the average flowrate was around 60µl/minute. After 20 second, the liquid flow was stopped and the odorant remain around cells. In this experiment, no cell was removed during the odorant introduction. The response of the cells to the inomaycin odorant is shown in Figure 4.11. The orange block (lower-left of the figure) indicates the time duration of introducing odorant to the cells. It can be seen that artifact was present during the odorant introduction. The artifact could not be ignored since it was quite significant. Although the response of the cells to the odorant can be obtained at t = 55 second with around 55% change in brightness, however, still not easy to quantify the cell response to the odorant using described method.

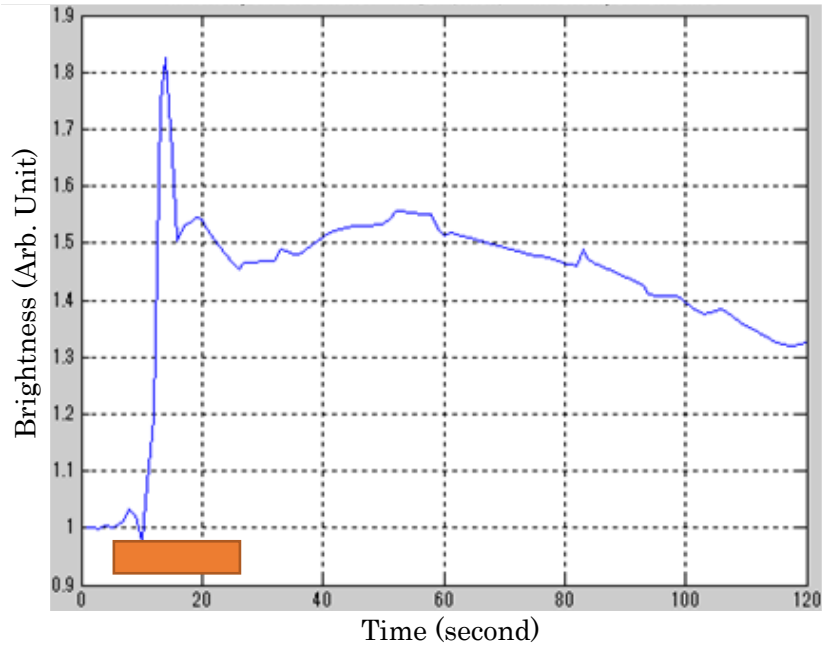

Figure 4-11. Or56a response to 10μM ionomycin odorant. Orange box represent time duration of pushing the pipette. The artifact is dominant since the manual system was used to introduce odorant to the cells.

4.4 Chapter summary

This chapter discussed about the development of flow system for introducing the odorant to the cells. The reason for this development is that in static system the artifact was dominant and static system was difficult to apply. Thus microfluidic flow system need be developed. The discussion started with material for flow system for both manual and automatic system. In this chapter, only manual system was discussed. In this system, liquid flow generated manually by pushing pipette plunger which, using pipe, flown the odorant to the cells before discarded to the sink. Since it was done manually, it was difficult to have a constant flowrate using this system. Flowrate is an important factor in a flow system. High flowrate resulted in cell removal. The odorant with flowrate around 500μl/min was made the cells removed. In manual system, repeatability was difficult to obtain and skill was needed to perform the experiment. Although the system was quite suitable for application, the artifact was still very significant to the results of the experiment.

Chapter 5.
Sensor Responses Using Flow System

In real conditions, odorant molecules are mixed with the air or liquid and flowed in certain direction. Previous chapter discussed about development of odorant detection in a liquid flow system. Basically it consists of a flow generator to generate liquid flow, a piping to transfer liquid flow and a chamber to facilitate odorant exposure to the cells as a sensor. Thus the responses of the cell to the odorant provided by instrumentation system take place at the chamber. A simple manual system using micro pipette was developed to mimic the real condition on micro fluidic system. Although it is possible to make a manual flow system, artifact is dominant. It was hard to obtain the constant flowrate at manual system and the flowrate should be low enough to prevent the cells from their removal.

In this chapter, measurement system on automatic flow condition is discussed. To generate the automatic flow system, two types of electric pumps such as micro-pump and syringe pump were used. Micro-pump was needed for portable system while syringe pump was used to observe the behavior of cell responses at flow system. Using the flow chamber, it is possible to flow the odorant to the cells, stop for a while or change to another odorant. The flow chamber is suitable for the most of the applications. The first step of the experiments was put the cells on the pool. Then, the condition for about 30 minutes was kept to let the cells be attached to base of the pool and the hole at the top of the pool was sealed. The exposure of the cell to odorant was done by flowing the odorant liquid for several seconds.

5.1 Purposes

The main purpose of the experiment is to establish microfluidic system for measuring the cell response to the odorant for confirming the possibility of portable implementation of odor sensing system. The next purpose is to observe the cells responses at relatively low concentration of odorant. Finally, to find the detection limit of the cells.

5.2 Microfluidic system with micro-pump

5.2.1 Hardware system

Figure 5.1 shows the diagram of the automatic flow system experiments using micro pump. It consists of bottles, micro-pipes, flow chamber and micro pump. The micro pump was used to generate liquid flow from odorant bottles (2 ml bottle), micro chamber, micro pump and finally the sink. As mentioned in Section 4.1.3, three (3) electrical parameters

available to control micro pump are wave form, amplitude and frequency. In this experiments the wave form and amplitude were fixed, that is, square wave and 250V, respectively. The signal frequency was set as variable. The length of pipe 1 was 10 cm, while both pipe 2, and pipe 3 were 5 cm in the length. The detail information about flow chamber was discussed in Chapter 4. Excitation light was applied to the cells from bottom part of the chamber. A serial communication interface circuit has been implemented in order to be able to control the micro-pump synchronized with image (camera) automatically from computer.

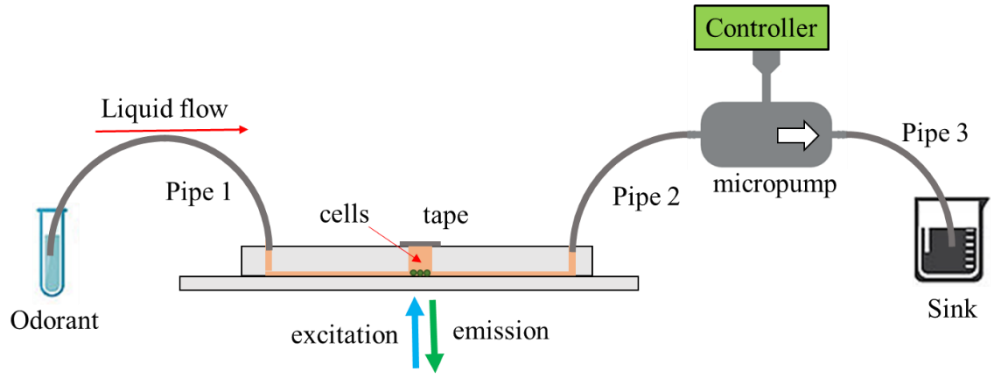

Figure 5.1. Diagram of automatic experiments with micro-pump

5.2.2 Software system

Together with interface circuit, a computer program based on Visual Basic was developed to implement the controller and its user interface for micro-pump. The frequency of the square wave signal applied to the micro-pump was the only variable to control the flowrate. The frequency range spans from dc (0 Hz) to several kHz. Several important menus for the micro pump are start, reset, and frequency setting. The driver can be automatically synchronized with the tools for collecting the image of the cells.

5.2.3 Flowrate measurement

There is no direct information about micro-pump flowrate on data sheet. However, the flowrate at specific frequency can be measured by the liquid volume collected during a specific time duration. The volume (liter) can be measured using liquid weight (gram) collected for certain range of time (minute) and then multiplied by liquid density (liter/gram). Most of liquids used in experiment were ringer solution and 98% of ringer solution was water. Thus, water was used as odorant liquid for calculating the flow rate. Moreover, cells were not used here and an excitation light was not applied.

Liquid weight can be converted to liquid volume (liter) by multiply it with liquid density. In case of drink water, its density is 0.9983ml/gr [117]. For example, at frequency

150 Hz, the weight of collected water for 10 second was 0.545 gr. The flowrate can be calculated as 0.545gr x 0.9983ml/gr = 0.544 ul/10sec or 3.264 ml/min..

The procedure of the experiment includes:

1. Using pipette and micro pump, fill the microfluidic system (Figure 5.1) with water. Avoid the presence of bubbles.
2. Set signal frequency of the driver.
3. Using "*start*" and "*reset*" menu, run the micro pump for 10 second and get the weight of the water.
4. Convert the weight of the water collected for 10 second to the flowrate.
5. Run the frequency from 0 to 300Hz with 25Hz step.

Figure 5.2 shows some weight for several frequencies from 0Hz to 300Hz. The different color means different sequence of experiment. There were 6 different sequences of experiments. There are some variances of the weight for each frequency. The maximum weight, which means the maximum flowrate, was obtained at frequency of 150 Hz. This is almost the same as that in micro pump data sheet, the data at 100Hz. The experiments were expanded in term of frequency. Figure 5.3 shows flowrate as a function of the frequency. Every flowrate value is the average of several measurements. The maximum flowrate (3 ml/min) reaches at frequency around 150Hz. Compared with data sheet, the flowrate and frequency are slightly different from data sheet, which is 5 ml/min at 100Hz. Probably this is because this measurement was done in a flow system while the data sheet the measurement was done without load or not in certain fluidic system.

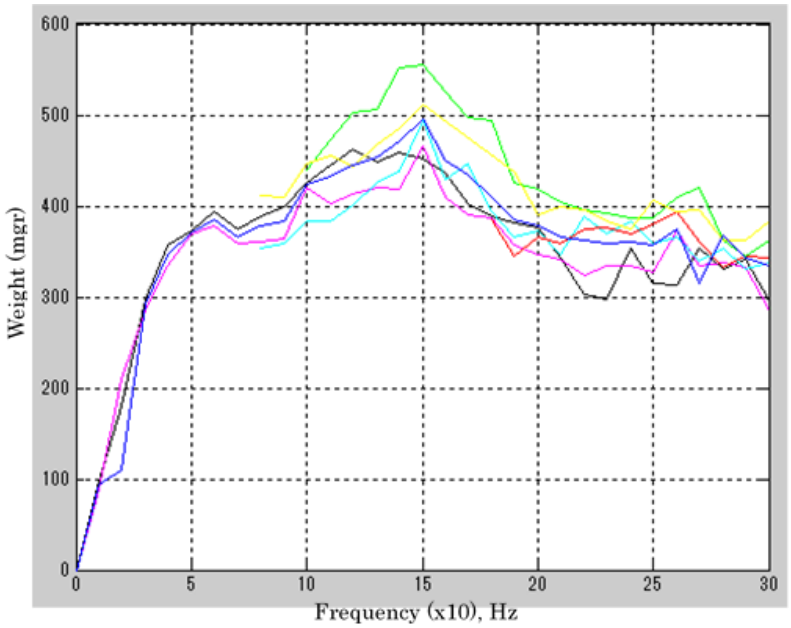

Figure 5.2. The weight of collected liquid as a function of frequency

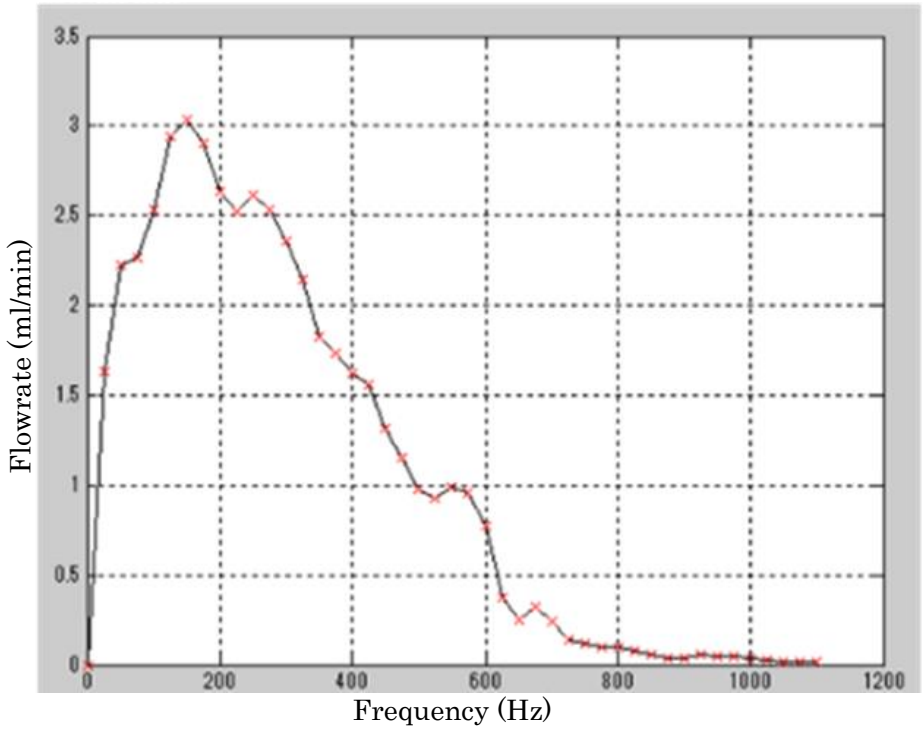

Figure 5.3 Micro pump flowrate as a function of frequency

5.2.4 Experiment for finding appropriate flowrate.

After the cells were attached firmly at the bottom of the chamber, the odorant can be introduced to the cells by flowing it from the inlet through the pool to the outlet. The flow rate should be regulated to prevent the cells from detachment during the odorant introduction. Using manual flow system, it was shown that the cells can be removed if the flowrate is too fast. However, using manual flow system it is difficult to find the exact flowrate that is not removed the cells. This experiment was intended to find an appropriate flowrate that the cells were kept in the chamber. The diagram of experimental set-up is shown in Figure 5-1. Either of ORs such as, Or56a or BmOr3, was used. Many different flowrates were applied for different experiments. The liquid flowrate controlled by frequency of input signal by the driver is shown in Figure 5.3. To check whether the cells removed or not, an image observation was used.

Figure 5.4(a)-(d) show a ringer solution with flowrate of 1ml/min applied to Or56a cells. This flowrate can be achieved by setting the frequency to 500Hz. Image of the cells before odorant introduction is shown in Figure5.4 (a). Several seconds later, the odorant was introduced, the cells was removed from the chamber as shown in Figure 5.4 (b), (c), and (d) respectively. Flowrate of 1 ml/min was too high for the cell application. The

smaller flowrate was used for the next experiment. From some experiments, it was found that maximum flowrate for both types of cells were around 400µl/minutes. This flowrate was achieved by setting the signal frequency to 600Hz. This flowrate was higher than that of the manual system where the cells were removed at around 300µl/minutes .

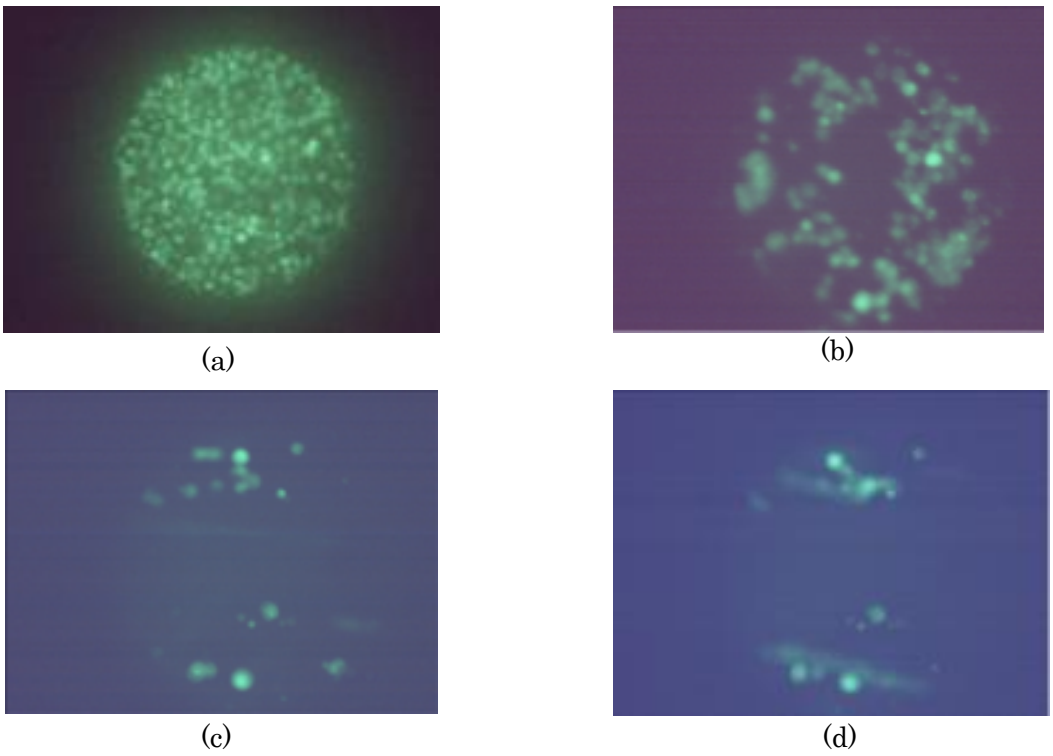

Figure 5.4 Cells removal because of odorant flowrate was too high (1ml/min). Or56a cells with ringer solution odorant were used in this experiments. Most of the cells removed withun 5 second. (a) Before, (b) 1 second after, (c) 3 second after, and (d) 5 second after odorant exposure.

5.2.5 Experiments on Or56a with Geosmin.

In the experiments, Or56a cells with geosmin odorant were used. The odorant flowrate was set to 400 µl/min and run for either 10s or 30s. Two geosmin concentrations were used, 10µM and 100µM. Thus, there were four experiments with results shown in Figure 5.5. They are:

- Experiment with 10µM geosmin odorant for 10 second (blue curve).
- Experiment with 10µM geosmin odorant for 30 second (orange curve).
- Experiment with 100µM geosmin odorant for 10 second (yellow curve).
- And experiment with 100µM geosmin odorant for 30 second (purple curve).

From these results, it can be seen that the odorant concentration affects the maximum brightness of the cell. These maximum brightness is considered as the response of the cells to certain concentration of odorant. Thus, responses of Or56a cells to 10μM and 100μM geosmin were 5% and 30%, respectively. The concentration, not flow duration, also affects the rise time. The rise time for 10μM and 100μM geosmin were around 20s and 30s respectively.

The time duration of flowing affects the recovery time. For the same concentration of odorant applied, the longer time duration applied the slower recovery time. Although it was not as big as in static system, flow system using micro pump still produced artifact. It can be seen in Figure 5.5. The small artifact still was produced at the beginning of micro pump operation (from off to on). At high concentration this artifact can be ignored. However in low concentration it cannot be ignored. Thus, micro pump was not suitable for measurement for small concentration which its small brightness change (4 % or less).

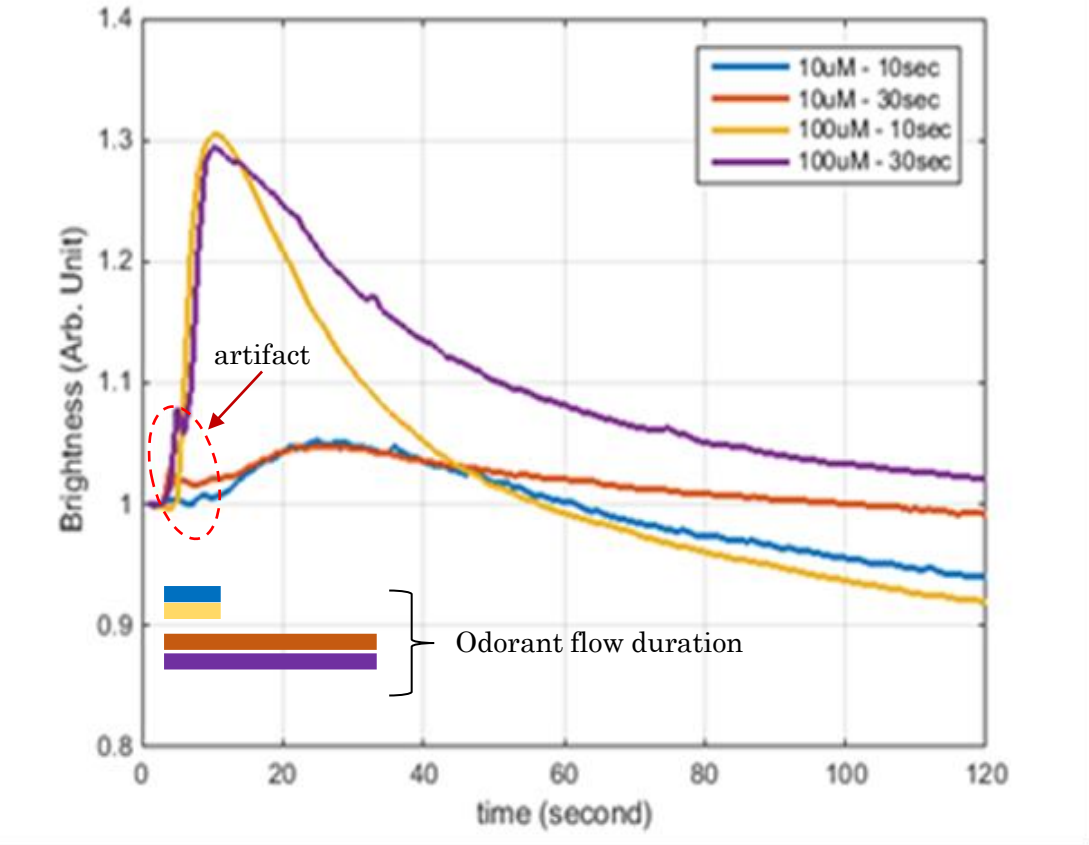

Figure 5.5 Curve responses of OR56a to two concentrations of geosmin and two time duration under 400μl/min flowrate

Further experiments were performed to obtain the concentration dependency of the cells responses. The geosmin concentrations for experiment were 5μM, 10μM, 50μM and 100μM and time duration 30s was used. Three experiment was performed for each concentration. The cell response to the odorant was calculated as the maximum brightness change compared to the brightness before odorant applied. Table 5.1 shows the experimental results while Figure 5.6 shows the plot of experiment results. It can be concluded that the concentration dependency of the response to geosmin was observed. The experiment for the concentration of 1μM or below was not performed since in that low concentration it was hard to distinguish between artifact and response.

Table 5.1. Some experiment results of Or56a with Geosmin

Concentration (μM)	**Exp. 1 (% change)**	**Exp. 2 (% change)**	**Exp.3 (% change)**	**Mean (% change)**	**SD (% change)**
5	5	4	8	5.3	2.08
10	6	11	9	8.7	2.5
50	13	23	17	17.7	5.3
100	45	30	23	32.3	11.4

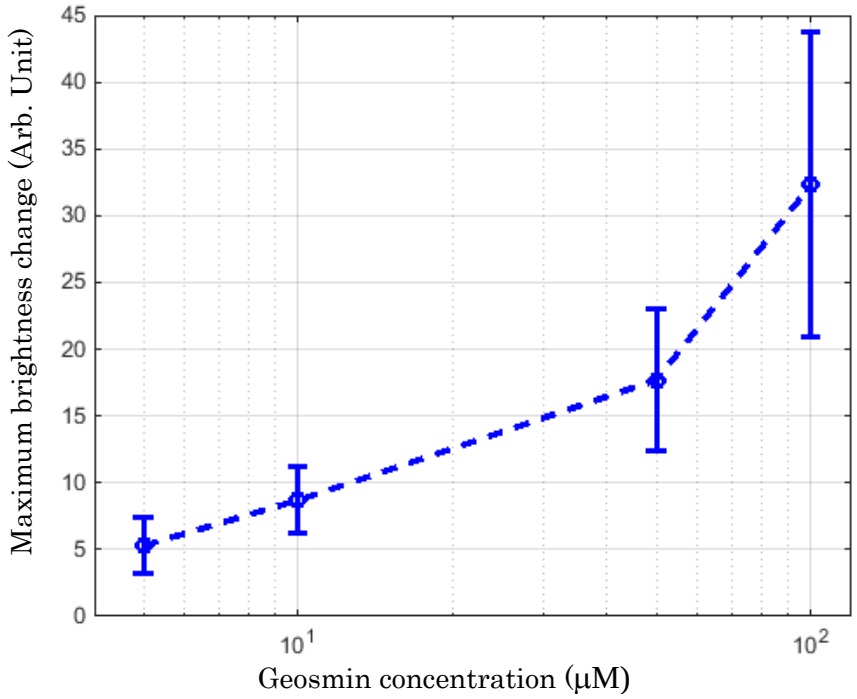

Figure 5.6 Dependency of maximum brightness change upon geosmin concentration.

5.2.6 Experiments on BmOR3 with bombykal

In this experiments, BmOR3 cells with bombykal were used. The bombykal was flown to the cells with flowrate of 400µl/min. Two bombykal concentrations (10µM and 100µM) and two time durations of the flow (10 second and 30 second) were used. The odorant liquid flow begined 5s after observation started and then stopped after 15s or 35s. The experimental result is shown in Figure 5.5. The results of cells response to 100µM odorant flown for 10 second shown in blue line, while 10µM odorant flown for 30 second shown in orange line. These experiment resluts support previous experiment results on Or56a cells with geosmin, including:

- 35% and 15% brightness change were obtained as a responses to 100µM and 10µM bombykal concentration respectively.
- Odorant exposure for 10 second was enough to get the cell response.
- Exposure time affected the recovery time of the cells.
- Exposure time did not affect the cell responses. However, more time needed to obtain the response to lower concentration.
- Artifact existed at the beginning of odorant introduction. This artifact caused by the switch of micro-pump power from off to on. The transition was not smooth enough in its liquid pressure causing some of the cells moving. At high odorant concentration this artifact can be ignored.
- The presence of the artifact limitted the application of micro-pump of the measurement for lower odorant concentration than 5µM since the response is almost the same with the artifact.

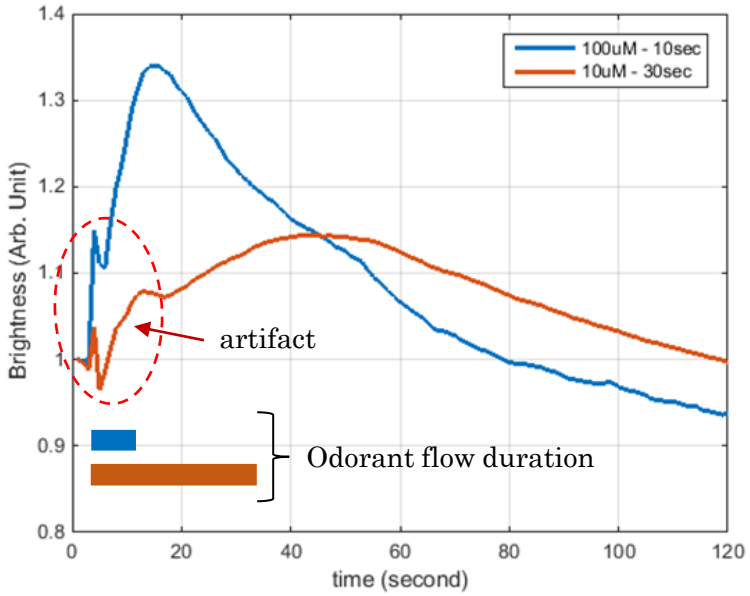

Figure 5.7 Sensor response of BmOR3 to several concentrations of bombykal under several condition using flow chamber

Further experiments were performed to obtain the concentration dependencies of the BmOR3 cell responses to the bombykal odorant. Similar to concentrations in the previous experiment, the bombykal concentrations were 5μM, 10μM, 50μM and 100μM. The time duration of introducing bombykal odorant to the cell was 30s. Three experiments were performed for each concentration. The cell response to the odorant calculated as the maximum brightness change compared to the brightness before odorant exposure. Table 5.2 shows the experimental results and Figure 5.8 shows the plot of experiment results. These experimental results show that there is concentration dependencies of bombykal between the range of 5μM and 100μM. The experiment for the concentration of 1μM or below was not performed since in that low concentration it was hard to distinguish between artifact and response.

Table 5.2. Some experiment results of BmOR3 with Bombykal

Concentration (μM)	**Exp. 1 (% change)**	**Exp. 2 (% change)**	**Exp.3 (% change)**	**Mean (% change)**	**SD (% change)**
5	2	5	6	4.3	2.08
10	7	15	9	10.3	4.16
50	12	18	22	17.3	5.03
100	35	27	21	27.7	7.02

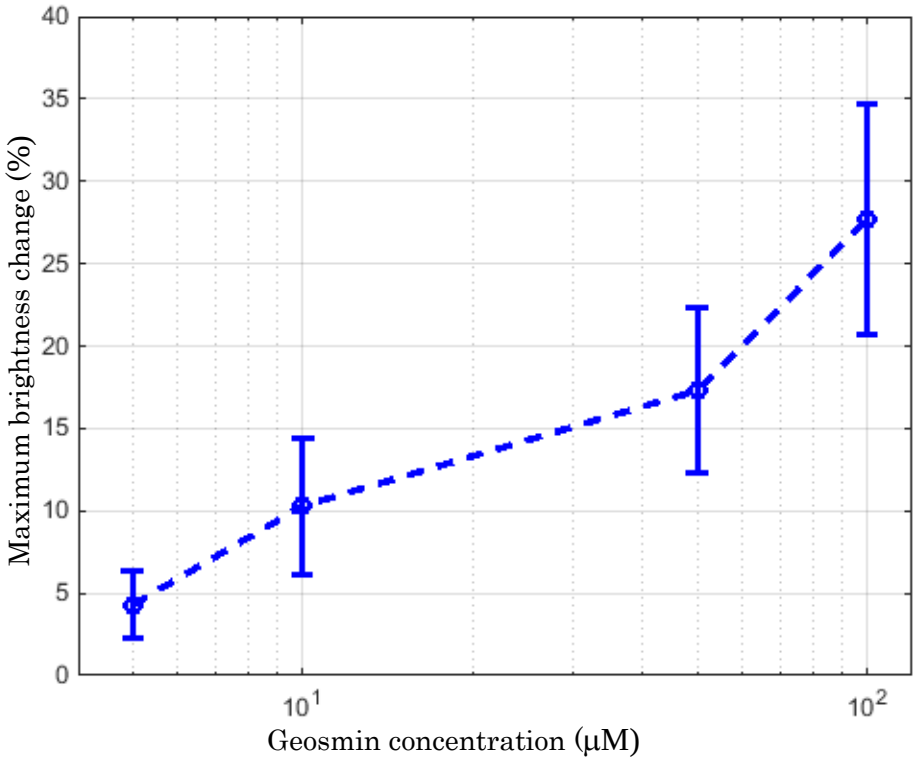

Figure 5.8 Dependency of maximum brightness change upon bombykal concentration.

5.3 Flow System with syringe pump (Or56a)

Application of micro-pump supports the portable system because of its small dimension and low power dissipation. It can be used for odorant measurement at relatively high concentration. However, micro-pump was not quite suitable for lower concentration since generated artifact became dominant. This phenomenon limited the measurement of the cell response to a lower odorant concentration to obtain its limit of detection. The limit of detection is important parameter in a sensor system since it reflects the sensing capability. Limit of detection is also important when it is compared with another technique in the instrumentation system. For example, measuring the improvement of incorporating lock-in measurement technique in the instrumentation. This was the main reason for using the syringe pump on the experiment. Lock-in measurement technique will be incorporated at the measurement system to overcome the effect ambient light during the experiment on ambient light condition. To make sure that the artifact was minimized, the liquid flowrate was set to 100μl/min.

5.3.1 Hardware system

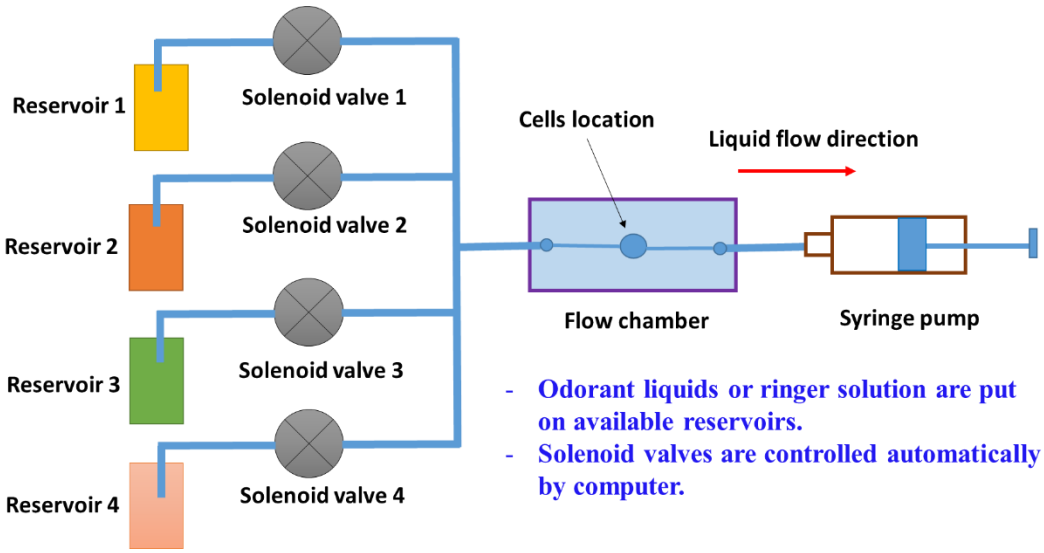

Figure 5.9 Diagram of automatic flow system using syringe pump.

Figure 5.9 shows the diagram of the automatic flow system experiment using syringe pump. The structure was more complex than previous system since the new system was prepared for more complex fluidic system. It consists of four reservoirs to store four different odorants, four solenoid valves, micro-pipes, flow chamber and syringe pump. The solenoid valves and syringe pump were connected to the computer to control the liquid flow automatically.

5.3.2 Software system

A visual basic program to control solenoid valve was developed to implement the controller and its user interface for four solenoid valves. Microfluidic system can be run standalone or synchronized with optical system (camera) for collecting the image of the cells.

5.3.3 Image mode.

For the experiments in flow system using syringe pump, the type of image was change to "*VGA mode*" instead of "*full mode*" in the previous experiments (terms from Bitrans Camera). As already discussed in chapter 2, VGA mode produces smaller image area and smaller file capacity, thus it make possible to fasten the sampling time. Figure 5.10 shows the image in "VGA mode". Another advantage of using "VGA mode" is more information area (cells) in the image compare to "full mode". In "VGA mode" 100% image area is information (cells) while in "full mode" only around 50% area is information (cells). Thus, measurement using "VGA mode" resulted in more precise compared to using "full mode".

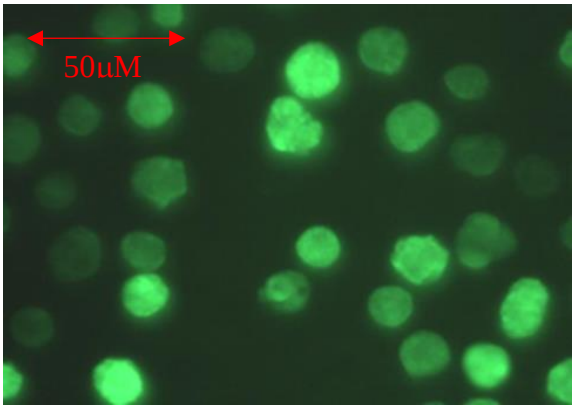

Figure 5.10. Image in VGA mode.

5.3.4 Experiment using syringe pump.

In this experiment, Or56a cells were used with two types of odorants, ringer solutions and geosmin 500nM. Ringer solution was prepared on reservoir 1 while geosmin 500nM was prepared on reservoir 2. The cells were exposed to the ringer solution for the first 30 minutes followed by geosmin 500nM for the next 30 minutes. Finally, after the geosmin, the cells were exposed again to ringer solution for the rest of time. Figure 5.11 show the timing diagram of exposing the cells to the odorants and its response. The flowrate of the liquid was kept at 100µl/minute.

From the first 40 second response curve, it can be seen that there is no response to the ringer solution. However, 10 seconds after odorant change (Time = 40 second), the response curve start raising until reach the maximum and soon recovery. This curve shown the cells respond to the geosmin 500nM. After the odorant switched to ringer solution at time = 60 second, the cells did not response to second exposure of ringer solution.

From the response curve, it can be seen that using syringe pump with low flowrate (100µl/minute), the artifact was minimized, even during odorant switching both from ringer solution to geosmin and from geosmin to ringer solution. Thus, it is possible to observe the response of the cells in very low concentration and then calculate the detection limit of ORs cells.

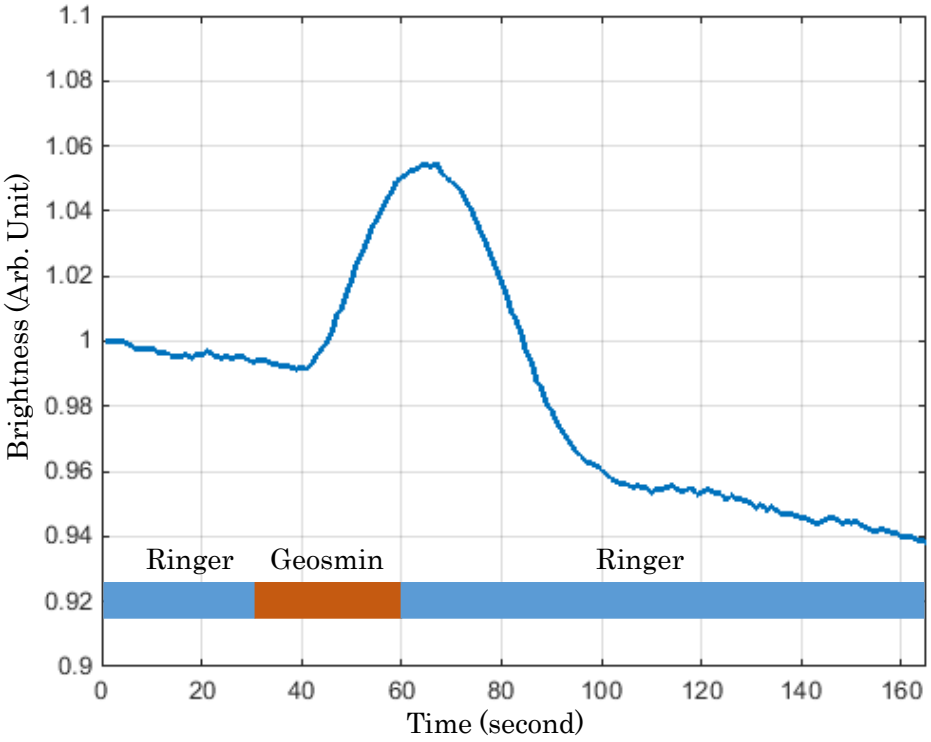

Figure 5.11. Or56a response to 500nM geosmin under automatic flow system using syringe pump. The first 30 minutes by ringer solution, followed by geosmin 500nM and finally ringer solution until finished. The artifact was minimized during the syringe pump.

5.3.5 Experiment for detection limit of the cells.

In the experiment, Or56a cells lines was used with several concentrations of geosmin odorant. The odorant exposure was performed by flowing the odorant with the flowrate 100µL/min. First, the geosmin odorant flowed for 60 second followed by ringer solution until observation was finished. There were several geosmin concentration used here, 0nM, 25nM, 50nM, 100nM, and 200nM. For every concentration, the experiments were performed 5 times. Figure 5.12 shows some typical response curves of the cells. Responses curves from several concentration were shown here. The blue line (Ringer) means the cells was expose to 0nM of geosmin concentration.

Table 5.3 shows the individual experiment results. Mean and standard deviation (SD) of every concentration were calculated. Moreover, Statistical analysis (t-test) for every concentration compared to 0nM geosmin (Ringer solution) were also performed. The analysis resulted in P value as is shown in the last column of Table 5.3. Geosmin odorant

concentration which has statistically significant differencewere 100nM and 200nM. Thus it can be concluded that the detection limit of the Or56a cells to odorant geosmin under developed instrumentation system is 100nM. One of the convenient way to describe the distribution of data is using a non-parametric statistical plot or Boxplot.

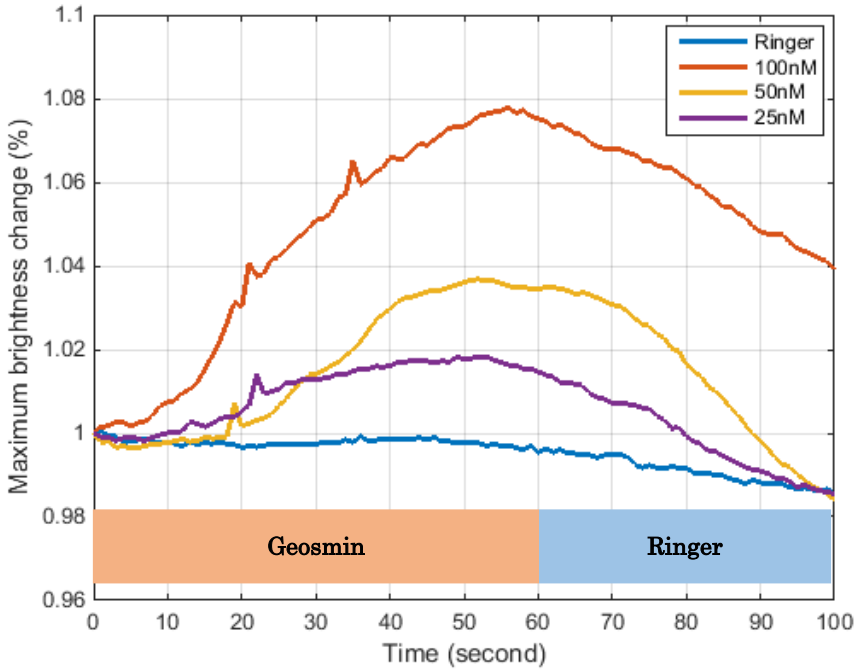

Figure 5.12. Typical Or56a response to 500nM geosmin

Table 5.3. Experiment Results

Conc (nM)	**Exp1 (%)**	**Exp2 (%)**	**Exp3 (%)**	**Exp4 (%)**	**Exp5 (%)**	**Mean (%)**	**SD[1)]**	**P value[2)]**
0	1.0	0	2.5	5.5	1.5	2.1	2.10	-
25	1.5	4	6	2.5	2	3.2	1.82	0.4027
50	5.5	6.5	1.5	4	2	3.9	2.16	0.2189
100	7	4	3.5	5	8	5.5	1.9	0.0288[*)]
200	8	5.5	6	3.5	9	6.4	2.16	0.0129[*)]

1) Standard Deviation (SD)

2) P value was calculated with online tool from Quick Calcs (Graph Pad software)

*) The difference from 0nM concentration is considered to be statistically significant.

A boxplot to show the distribution of the experimental results is shown in Figure 5.11. It consists of 5 information, minimum, first quartile, median, third quartile, and maximum data. The blue box (IQR or interquartile range) spans the first quartile to the third quartile. The red line indicate the median of the data. In case of 100nM, the response spans from 3.5 to 8 with median 5.

The stars (*) indicate that particular concentration has significant different statistically compare to 0M concentration.

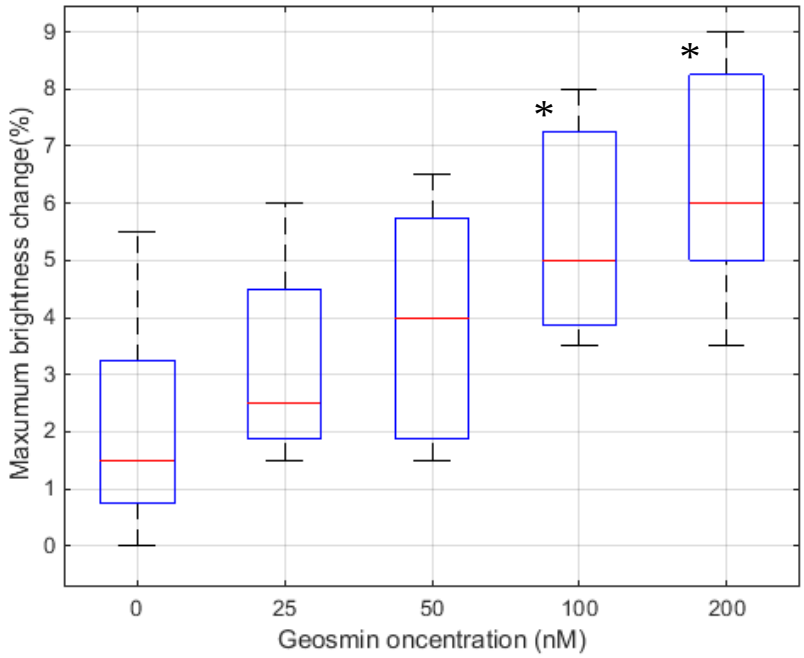

Figure 5.13 Boxplot of the experimental results of Or56a with geosmin odorant.

5.4 Chapter summary

In this chapter, sensor response on automatic flow system has been discussed. One of the main part of the system is a pump which is responsible for initiating the flow. Two types of pump were used here, micro-pump and syringe-pump. From the experimental results, the applied flowrate for OR cells should be low enough in order not to remove the cell. The odorant flowrate should be around 400µl/minutes or below.

The main characteristics of the micro-pump is small and low power, thus it is suitable for portable application. However, micro-pump cannot be used for small concentration since it produce the artifact. In small concentration the artifact from micro-pump was about the same as response of the odorant. Experimental results show that microfluidic system using micro-pump suitable for measuring odorant concentration between 5µM to 100µM (or above) for both Or56a and BmOR3 to geosmin and bombykal odorants, respectively.

On the other hand, syringe pump has main characteristics of precise and stable but it cannot be used for portable applications because of its weight and dimension. In low liquid flowrate (100µl/minute), almost no artifact was produced by syringe pump. Syringe-pump was used to investigate the detection limit of the cells response to the odorant. Experimental results show that the detection limit of Or56a cells lines to the geosmin odorant was 100nM.

Chapter 6

Design of measurement system using lock-in technique.

An image captured by the camera includes not only fluorescence but also noise, background and offset lights. Noise is randomly changing intensity regardless of fluorescence. Background is an intensity captured by camera in the absence of any cells. Background signal mainly comes from ambient light such as sun and room lighting. Offset is magnitude captured by camera without any light. Its value depends on camera setting. Noise, background and offset are unwanted intensity and deteriorate measurement sensitivity. In the previous chapters, the measurements were performed at dark condition where the background was minimized. However, noise and offset still existed in the image. Measurement in ambient light condition, background can be very dominant since its intensity is much higher than fluorescent light. The ambient light also increases the artifact and noise. Figures 6.1 (a) and (b) show images obtained under dark condition and image obtained under ambient light condition, respectively. It can be seen that at ambient light condition, the background becomes dominant.

This chapter discusses about incorporating lock-in measurement technique into the developed fluorescent instrumentation system to handle the influence of ambient light. It consists of lock-in measurement technique design and its implementation

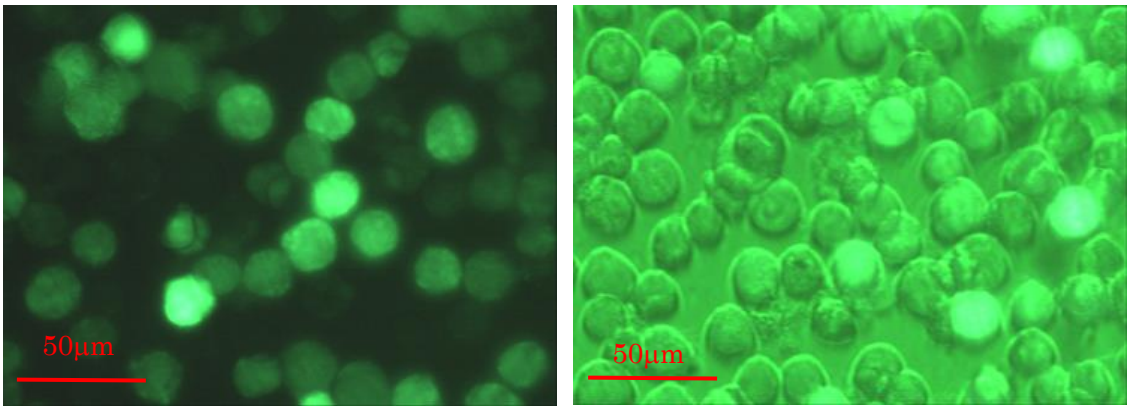

(a) (b)

Figure 6.1 Captured cell images. (a) Image obtained at dark condition. (b) Image obtained at ambient light condition.

6.1 Measurement in ambient light condition

In dark conditions, it is easy to monitor the brightness change of the cells when they are exposed to the odorant. This is not the case for cells in ambient light conditions since the fluorescent signal is very weak compared with that of the ambient light.

The total brightness intensity averaged over the entire image was used to measure the sensor response to the odorant. Plots of sensor responses as a function of time are shown in Fig. 6.2. Each curve was normalized by the brightness at t = 0 s. The blue and red lines plot the normalized brightness of OR56a cells without odorant exposure in dark and ambient light conditions, respectively. The brightness of the cells normally decreases without odorant exposure (blue line). In ambient light conditions, in spite of its high intensity, ambient light contains irregular noise (red line) although the phenomenon of decreasing intensity was not observed.

The yellow and purple lines show the response of Or56a to geosmin in dark and ambient conditions, respectively. The same odorant concentration (10 μM of geosmin) for both conditions were applied at t = 20 s. The fluorescence intensity has a peak corresponding to a sensor response. It can be seen that in ambient light conditions the response becomes smaller than that in dark conditions. We did not take the first purple line at t = 25 s since it was the artifact owing to water (liquid)-surface fluctuation caused by the liquid injection. Without normalization, the magnitude of the signal in ambient conditions is much larger than the magnitude of the signal in dark conditions. It was found from Fig. 6.2 that the ambient light deteriorates the sensor response unless we perform signal processing.

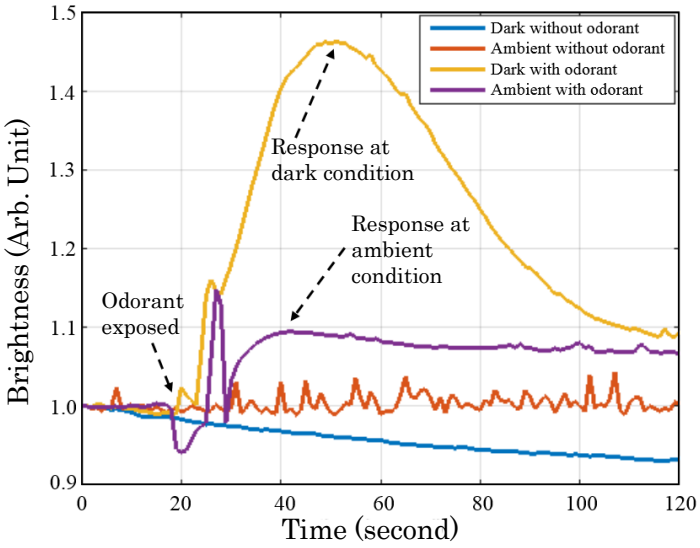

Figure 6.2 Comparison of experiment results between in dark condition and in ambient light condition.

6.2 Lock-in amplifier development

In fluorescent instrumentation system CMOS camera captures the fluorescent light *x(t)*, background *b(t)*, offset, and noise *n(t)*. Only fluorescent light *x(t)* is wanted signal, the others are unwanted. To suppress unwanted intensity, lock-in measurement technique has been added to the fluorescent instrumentation. Figure 6.3 shows the block diagram of lock-in measurement technique implementation used in this study. The fluorescent signal *x(t)* and its noise *n(t)* were modulated by setting the laser system at "pulse mode" or PM condition. Image captured by CMOS camera *u(t)* is composed of those modulated signals, background *b(t)* and offset. Since modulated signal *m(t)* is a 0 or 1, image captured by camera *u(t)* can be written as

$$u(t) = \begin{cases} b(t) + offset, & if\ m(t) = 0 \\ x(t) + n(t) + b(t) + offset, & if\ m(t) = 1 \end{cases}$$

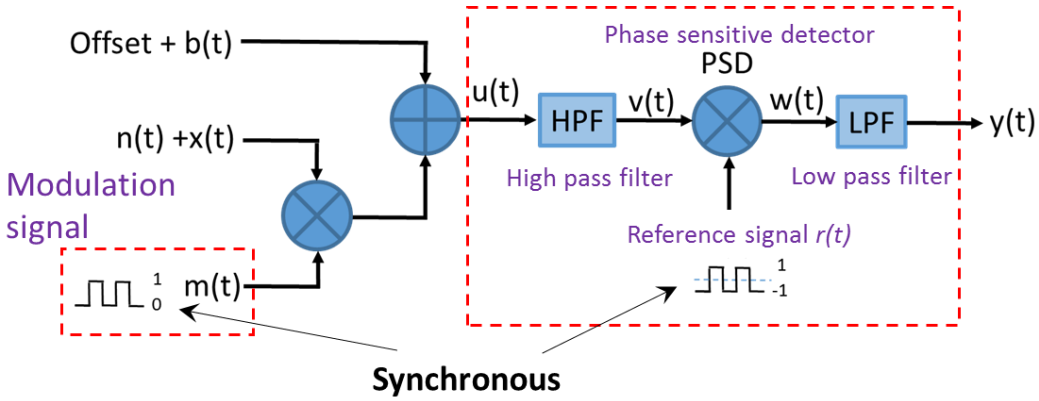

Figure 6.3 Block diagram of lock-in measurement technique.

Lock-in processing is performed by filtering (high-pass filter (HPF) and low-pass filter (LPF)) and synchronous detection of *u(t)* using phase sensitive detector (PSD). HPF is used to remove the low frequency contents of *u(t)* (background *b(t)* and offset) and outputs *v(t)*. Synchronous detection by multiplying *v(t)* with reference signal *r(t)* results in *w(t)*. The reference signal *r(t)* should be synchronous (in phase) with modulated signal *m(t)*. In this research, the reference signal *r(t)* is -1 or 1. A LPF is used to remove high frequency contents (noise *n(t)*). Thus the remaining output signal *y(t)* is fluorescent signal *x(t)*. Illustration of lock-in technique process is shown in Figure 6.4.

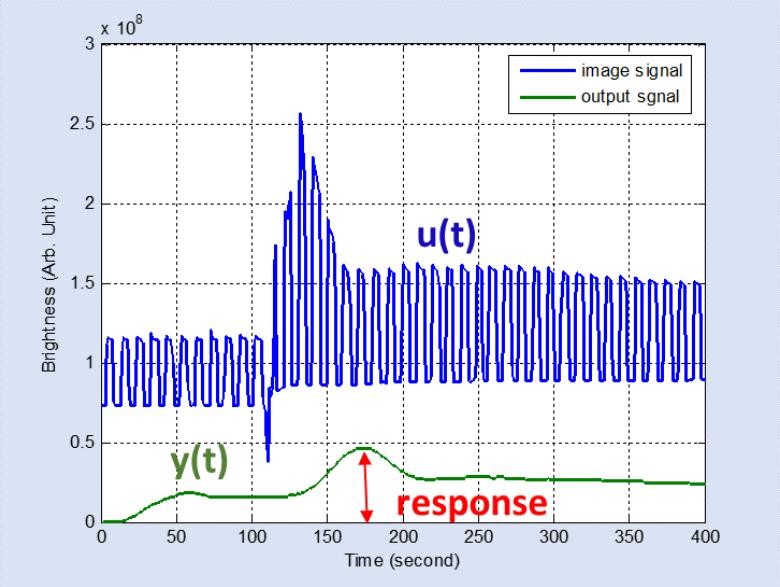

Figure 6.4 Lock-in measurement technique

6.3 Lock-in amplifier design.

The image of fluorescent light *x(t)* is sampled every second (f_s = 1Hz). According to sampling theorem, both modulated (f_m) and reference (f_r) frequencies should be 500mHz or less. In this research, both modulation and reference frequencies both were set to 100 mHz with 50% duty cycles generated from signal generator (1606 clock synthesizer, NF Electronics Instrumentation). The spectrum of the signal capture by CMOS camera *u(t)* (N = 1100) shown in Figure 6.4. The primary frequency is around 115 mHz with third order harmonics at 345 mHz. This is because the reference frequency is a square wave. From this figure, it was reasonable to choose cut-off frequency for high-pass filter (f_{CH}) = 60 mHz. A 5^{th} order Butterworth filter has been chosen to implement HPF. The filter coefficient was calculated using Matlab with following command,

[B,A] = butter(N, Wn, 'high')

with N is filter order (N=5) and Wn = $f_{CL}/0.5f_s$ = 0.06/0.5 = 0.12. B and A are numerator and denominator of the filter transfer function, respectively. Calculation using Matlab resulted in the coefficients of LPF as follows,

n_0 = 0.5409; n_1 = -2.7046; n_2 = 5.4091; n_3 = - 5.4091; n_4 = 2.7046; n_5 = -0.5409
d_0 = 1.0000; d_1 = -3.7821; d_2 = 5.8375; d_3 = -4.5777; d_4 = 1.8193; d_5 = -0.2926

The filter transfer function in z transform is

$$\mathrm{H(z)} = \frac{0.5409z^5 - 2.7046z^4 + 5.4091z^3 - 5.4091z^2 + 2.7046z - 0.5409z}{z^5 - 3.7821z^4 + 5.8375z^3 - 4.5777z^2 + 1.8193z - 0.5428}$$

High-pass filter removed low frequency component of the *u(t)* signal including dc component. The output of the HPF, *v(t)*, was a periodic signal with average 0. This signal was then multiplied by -1 or 1 as reference signal. Since the lock-in calculation was perform offline, *m(t)* and *r(t)* were assumed in-phase. A PSD with its reference frequency can be replaced by a full wave rectifier. If there is a phase difference between modulated signal and reference signal a PSD cannot be replaced with a full-wave rectifier. Rectifying *v(t)* resulted in *w(t).*

It can be seen from any curve response (fluorescent light) of the cells that the fluorescent signal *x(t)* has a low frequency characteristics. Figure 6.6 shows the spectrum of the fluorescent signal *x(t)* (N = 600). It was reasonable to have low pass filter (red curve) with cut-off frequency (f_{CL}) = 30 mHz. A 5th order Butterworth filter was chosen as LPF. The filter coefficient was calculated using Matlab with following command,

[B,A] = butter(N, Wn, 'low')

with N is filter order and Wn = $f_{CL}/0.5f_s$ = 0.03/0.5 = 0.06. B and A are numerator and denominator of the filter transfer function, respectively. Calculation using Matlab resulted in the coefficients of LPF as follows,

n_0=5.56x10^{-6}; n_1=2.78x10^{-5}; n_2=5.56x10^{-5}; n_3=5.56x10^{-5}; n_4=2.78x10^{-5}; n_5=5.56x10^{-6}
d_0 = 1.0000; d_1 = -4.3903; d_2 = 7.7429; d_3 = -6.8543; d_4 = 3.0447; d_5 = -0.5428

The filter transfer function is

$$\mathrm{H(z)} = \frac{5.6 \times 10^{-6}z^5 - 2.8 \times 10^{-5}z^4 + 5.6 \times 10^{-5}z^3 - 5.6 \times 10^{-5}z^2 + 2.8 \times 10^{-5}z - 5.6 \times 10^{-6}z}{z^5 - 4.3903z^4 + 7.7429z^3 - 6.8543z^2 + 3.0447z - 0.5428}$$

A low-pass filter removed the high frequency component of *w(t)* followed by output signal *y(t),* which is a recovered signal of fluorescent signal *x(t).*

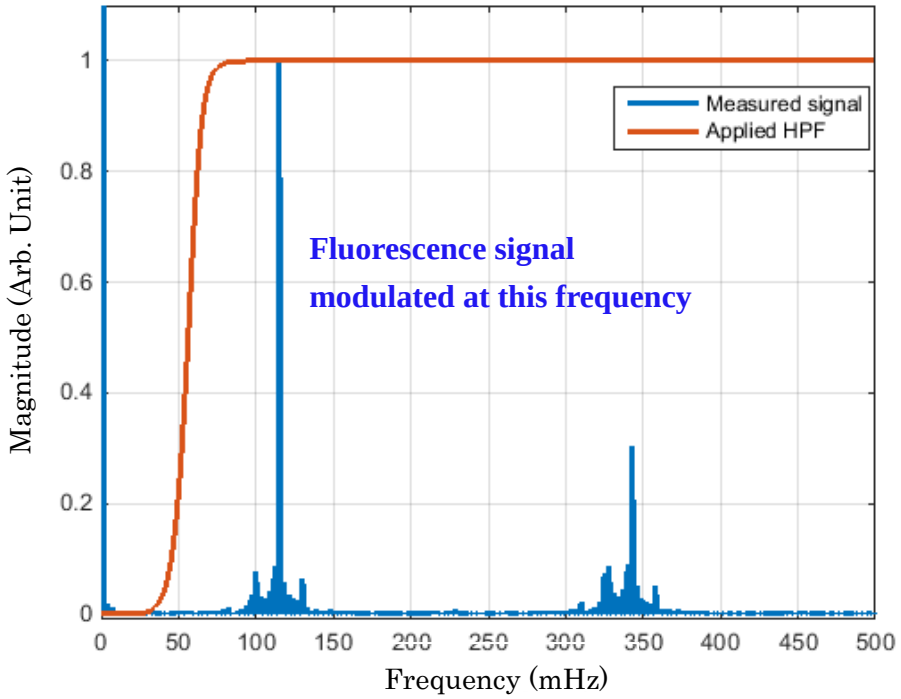

Figure 6.5. Spectrum of the signal capture by SMOS camera u(t).

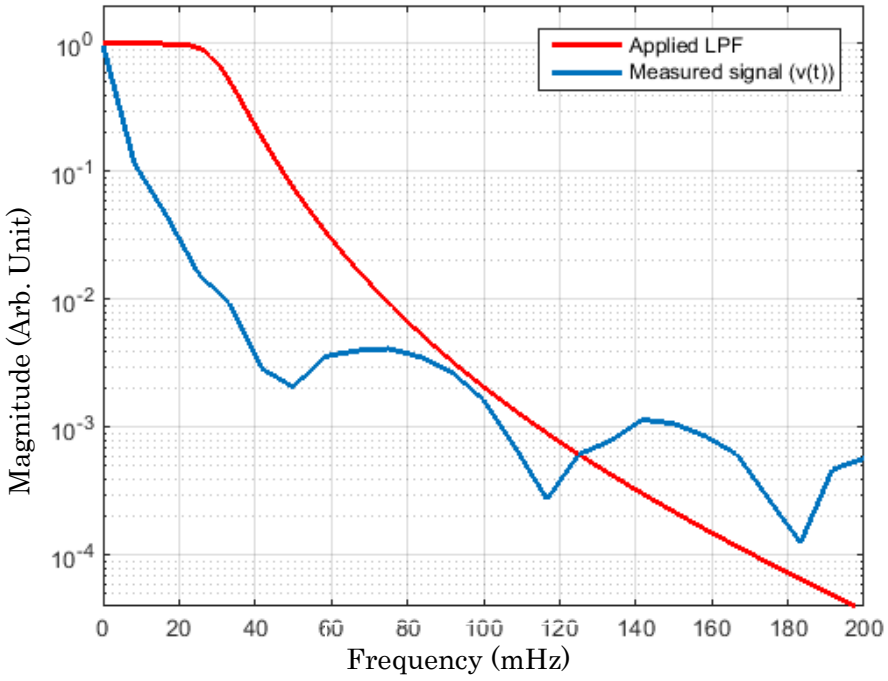

Figure 6.6. Typical spectrum of the fluorescent signal *x(t)* (blue line). The red line is transfer function of 5th order LPF with cut-off frequency 30 mHz..

6.4 Lock-in measurement technique implementation

Figure 6.7 shows the schematic diagram of fluorescent instrumentation system. Lock-in measurement system has a laser diode system to modulate the fluorescent light and personal computer (PC). A schematic circuit laser driver that facilitating a "pulse mode" operation shown in Figure 6.8(a). A pulse mode operation is possible by applying the square wave signal to "pulse in" terminal of driver circuit. When the "pulse in" is high, the laser diode is off and when the "pulse in" is low the laser diode is on. In this research, a pulse mode with its 3.3 V amplitude, 100 mHz frequency, and 50% duty cycle was used.

The lock-in measurement technique was implemented offline using Matlab on the computer. The functional blocks of lock-in measurement technique includes

1. 5^{th} order high pass filter with f_{CH} = 60mHz.
2. Full wave rectifier, to implement phase sensitive detector and -1 or 1 square wave reference frequency (*r(t)*).
3. 5^{th} order high pass filter with f_{CL} = 30mHz.

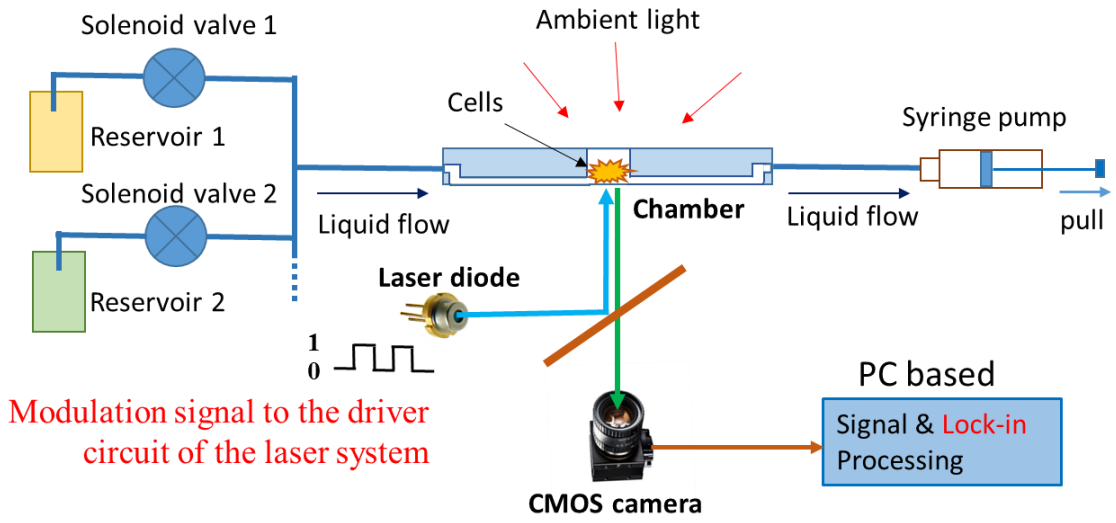

Figure 6.7. The schematic diagram of fluorescent instrumentation system. Lock-in technique is realized using laser diode driver and offline Matlab

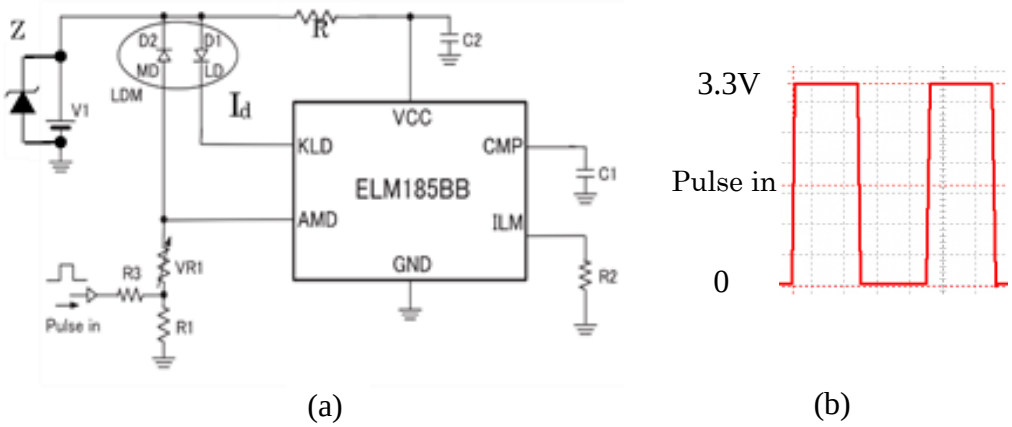

Figure 6.8. Laser diode driver. (a) Circuit diagram the pulse mode operation. (b) 100 mHz, 50% duty cycle, square wave signal to control pulse mode operation.

6.4 Chapter summary

Fluorescence-based instrumentation system suffers from ambient light condition which affects the sensitivity. Since the intensity of fluorescent light emitted by the cells is much weaker than the ambient light, the sensitivity deteriorates due to the ambient light. To deal with this problem, a lock-in measurement technique was incorporated into the fluorescent measurement system. Lock-in measurement technique basically consists of fluorescent signal modulator, high-pass filter, phase sensitive detector, reference signal, and low-pass filter. Based on the sampling signal used in the developed fluorescent instrumentation, requirements, specifications and implementation of each functional blocks of lock-in measurement technique were discussed.

The fluorescent signal modulation was performed by setting the “pulse mode” for the operation of laser diode system. The other blocks were implemented offline using Matlab. Since the modulation signal *m(t)* and reference signal *r(t)* are assumed to be in-phase, phase sensitive detector together with reference signal works as full-wave rectifier. The experiments using measurement system with lock-in technique is discussed in the next chapter.

Chapter 7
Experiment on lock-in measurement technique.

Chapter 6 discussed about development of fluorescent instrumentation system with incorporated lock-in measurement technique including its design and implementation. The incorporation of lock-in technique on fluorescent instrumentation system is important for instrumentation system applicable to ambient light conditions. This chapter discusses about the experiments on ambient light conditions.

7.1 Experimental set-up and procedures.

There is not so much difference between previous experiment (without lock-in) and current experiment (with lock-in). The slight differences are:

1. In the experiment in this chapter, the laser system was run on pulse mode (PM) instead of continuous mode (CM) which was applied in previous system. The pulse mode was for the purpose of fluorescent signal modulation.
2. A signal processing needed to further process the collected image intensities in experiments (lock-in processing). In the previous experiment, image intensity was calculated to get the cell response. The lock-in processing includes low-pass filtering, full-wave rectification and high-pass filtering.

There is no different procedures during experiment in terms of cells preparation and fluidic system. Flow system using syringe pump with flowrate of 100µl/min was used in the experiments.

7.2 Experiment using Or56a cells line without odorant in several ambient light conditions.

The purpose of this experiment is to observe both signals captured by camera *u(t)* and output *y(t)* at three conditions:

1. Dark condition. The chamber is covered with the black box (0 lux).
2. Low intensity of ambient light (ambient 1). The ambient light comes from day light outside laboratory and some laboratory lamps (500 lux).
3. High intensity of ambient light (ambient 2). The ambient light comes from day light outside laboratory and all lamps in the laboratory (1000 lux).

In the experiments, the cell was Or56a cell line and the cell was not exposed to the odorant. The three experiments used exactly the same prepared cells. The experiments at all conditions were performed for 250 s. The experiment results are shown in Fig. 7.1. Since the plots were not normalized, the absolute magnitude of measured brightness at every condition is given here.

The three upper square wave signals were the measured signals *u(t)*s at 3 different conditions before further process of lock-in technique was applied. Square wave signals appeared in *u(t).* In each curve, low signal indicates the laser diode in "off" condition while high signal indicates the laser diode in "on" conditions. It can be seen that the DC (direct current) level of *u(t)* at ambient 2 (green line) was approximately 2-3 times higher than at ambient 1 (blue line) and dark condition (red line). Although the intensity of the ambient light at those three conditions were different, those three output signals had similar AC (alternating current) level.

Further process (lock-in processing) was applied to each of *u(t)*s using Matlab. The processes include:

1. High-pass filtering. 5th order butterworth with f_{CH} = 60mHz, resulted in *v(t)*.
2. Full-wave rectifying of *v(t)*, resulted in *w(t)*.
3. High-pass filtering, 5th order butterworth with f_{CL} = 30mHz, resulted in *v(t)*.

The results shows that the outputs from any condition were similar except its dc level. In other words, the same fluorescent AC signal was obtained regardless of ambient light condition.

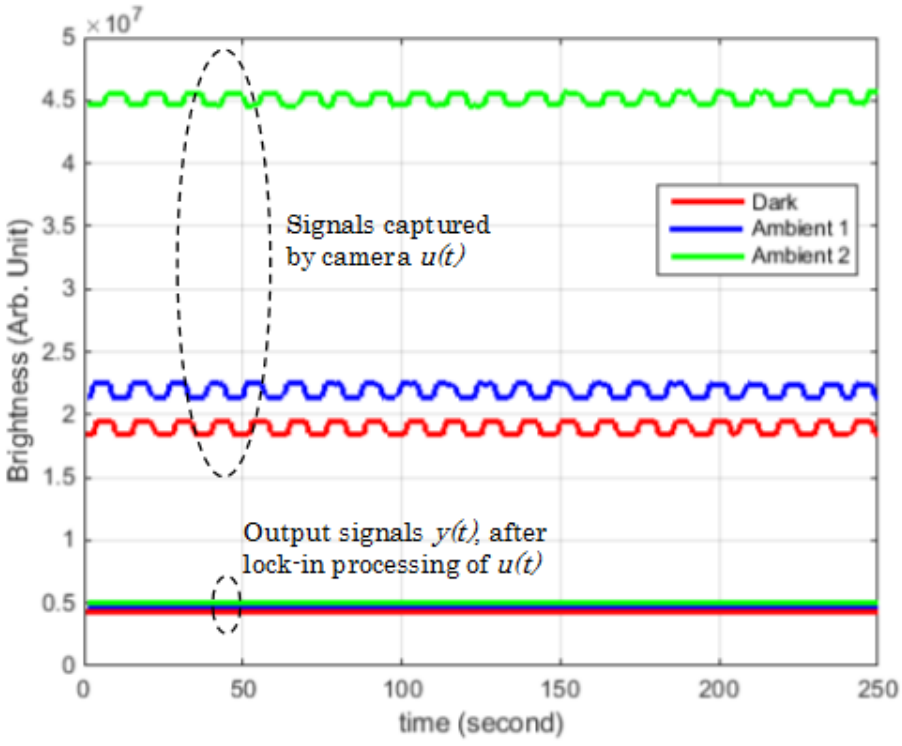

Figure 7.1. Captured and output signals of Or56a cells without odorant exposure under three different conditions.

7.3 Experiment using Or56a cells line with Ringer solution and odorant

The purpose of the experiments was to observe the effect of incorporating lock in measurement technique in fluorescent instrumentation system. For that purpose, comparison to the measurement without lock-in technique was also performed. Flow system with micro-pump was used for experiment. In the experiment the odorant (500nM geosmin or ringer solution) was flown to the cell at flowrate 100 μL/min for 20 s, followed by ringer solution. Three experiments were performed using OR56a cells with ringer solution and 500 nM geosmin. They were:

1. Experiment with ringer solution at ambient light condition (1000 lux) with lock-in measurement technique (blue line).
2. Experiment with 500nM geosmin odorant at dark condition without lock-in technique (orange line)
3. Experiment with 500nM geosmin odorant at ambient light condition (1000 lux) with lock-in technique (yellow line).

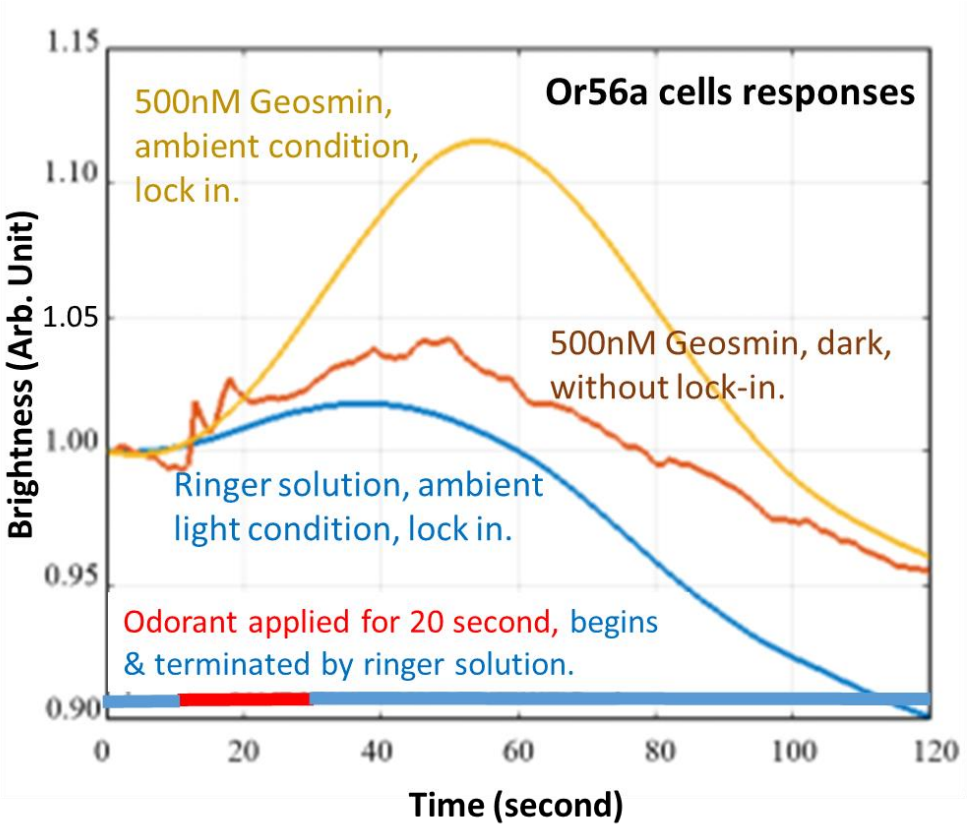

Figure 7.2. Or56a response to ringer solution and 500 nM geosmin at several conditions with and without lock-in technique.

Figures 7.2 shows the experiment results. The plots were normalized using their own values at t = 0 s and thus the responses to the odorant at both conditions were observed. The results of the experiments are as follows:

1. The blue line shows the result of the first experiment. Small change in brightness after the exposure indicates as an influence of ringer solution.
2. The arange line shows the results of second experiment. The response was hardly detected even under dark condition without lock-in measurement
3. The yellow line shows the results of third experiment. The response was clearly detect (12%) even under ambient light condition using lock-in measurement technique

It can be concluded that the lock-in measurement technique enables the detection of odorant with relatively low concentration even under the ambient light condition, whereas the response without lock-in technique was almost the noise level. Related to the response time, it took longer time to obtain the response from the measurement using lock-in technique compared with the response without lock-in technique. This is due to time constants of the filters used incorporating lock-in technique.

7.4 Experiment using Or56a cell line with low geosmin odorant concentrations.

The purpose of these experiments were to find the detection limit of Or56a cells to geosmin odorant under three conditions. The flow system with syringe pump was used for the experiments. In the experiments, the odorant exposure was performed by flowing the odorant liquid with specific concentration to the chambers for 60 second followed by the ringer solution with the flowrate 100μL/min.

There were three ambient light conditions of experiments, dark (no ambient light), low intensity (around 500 lux), and high intensity (around 1000 lux) of ambient lights. In every experiment the cells were exposed to many concentrations of odorant from 0nM to at most 100μM. For every concentration in any conditions, the experiments were performed several times to obtain the valid data. These data were used for statistical test (t-test) to check whether there was significant difference between condition with 0nM odorant concentration and that with specified sample concentration.

7.4.1 Experiment in dark conditions.

The experiment was done in dark conditions (0 lux). Several concentrations of geosmin odorant were prepared: 0nM (ringer solutions), 25nM, 50nM, 100nM, 500nM, and 1μM. Experiment on each concentration was done 6 times. Figure 7.3(a) shows the typical response curves of Or56a cells to several concentration of geosmin odorant. Figure

7.3(b) shows the Boxplot distributions of cells responses under various concentration of geosmin odorant. Statistical analysis (t-test) was performed to each concentration in pair with 0M concentration. Cells responses to 50nM concentration and above has statistically significantly different from the response to 0M. Thus the detection limit of Or56a cells at dark conditions was around 50nM.

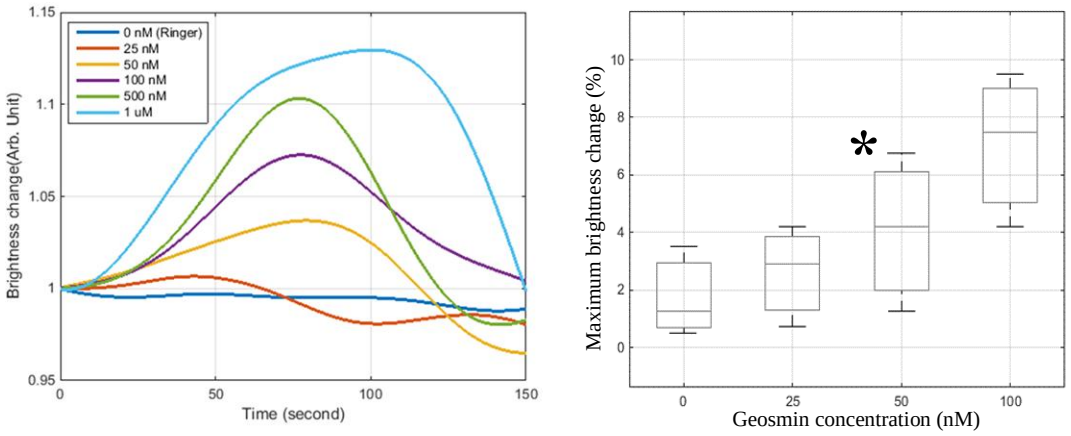

(a) (b)

Figure 7.3. Or56a response curves to geosmin at dark conditions. (a) Typical response curve. (b) Response distribution on Boxplot under various concentration. Response with (*) indicates the limit of detection.

7.4.2 Experiment in low intensity of ambient light condition.

The experiment was done at low intensity of ambient light conditions (around 500 lux). Several concentrations of geosmin odorant were prepared: 0nM (ringer solutions), 25nM, 50nM, 100nM, 500nM, and 1μM. Experiment on each concentration was done 6 times. Figure 7.4(a) shows the typical response curves of Or56a cells to several concentrations of geosmin odorant while Figure 7.4(b) shows the Boxplot distributions of cells responses under various concentration of geosmin odorant. Statistical analysis (t-test) was performed to each concentration in pair with 0M concentration. Cell responses to 100nM concentration and above has statistically significant difference from the response of 0M. Thus the detection limit of Or56a cells at dark conditions is 100nM.

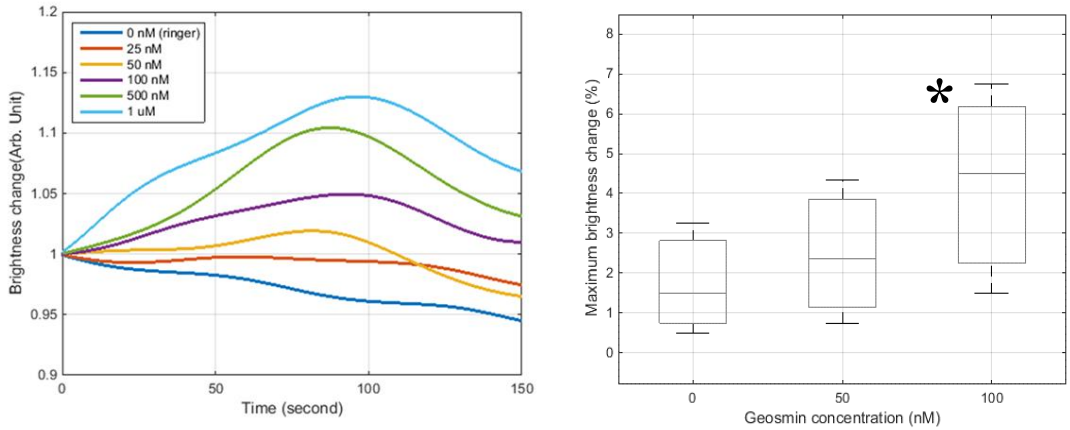

(a) (b)

Figure 7.4. Or56a response to geosmin at low intensity of ambient light conditions. (a) Typical response curve. (b) Response distribution on Boxplot under various concentration. Response with (*) indicate the limit of detection.

7.4.3 Experiment in high intensity of ambient light condition.

The experiment was done at high intensity of ambient light conditions (around 1000 lux). Several concentrations of geosmin odorant were prepared: 0nM (ringer solutions), 25nM, 50nM, 100nM, and 500nM. Experiment on each concentration was done 6 times. Figure 7.5(a) shows the typical response curves of Or56a cells to several concentrations of geosmin odorant while Figure 7.5(b) shows the Boxplot distributions of cell responses under various concentration of geosmin odorant. Statistical analysis (t-test) was performed to each concentration in pair with 0M concentration. Cell responses to 100nM concentration and above has statistically significant different to the response of 0M. Thus the detection limit of Or56a cells at dark conditions is 100nM.

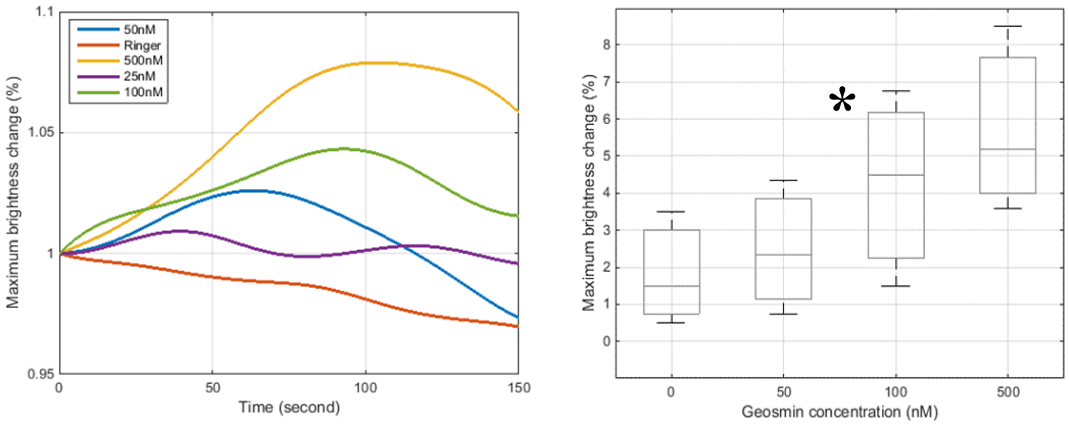

(a) (b)

Figure 7.5. Or56a response to geosmin at high intensity of ambient light conditions. (a) Typical response curve. (b) Response distribution on Boxplot under various concentration. Response with (*) indicate the limit of detection.

7.5 Experiment using Or13a cell line with low 1-octen-3-ol odorant concentration

The purpose of these experiments were to find the detection limit of Or13a cells to 1-octen-3-ol odorant under three conditions. Flow system with syringe pump was used for experiments. In the experiments, the odorant exposure was performed by flowing the odorant liquid with specific concentration to the chambers for 60second followed by the ringer solution with the flowrate 100µL/min.

There were three ambient light conditions of experiments, dark (no ambient light), low intensity (around 500 lux), and high intensity (around 1000 lux) of ambient lights. In every condition of experiments, the cells were exposed to many concentrations of odorant from 0nM to at most 100µM. For every concentration in any condition, the experiments were performed several times to obtain the valid data. These data were used for statistical test (t-test) to check whether there was significant difference between condition with 0nM odorant concentration and that with specified sample concentration.

7.5.1 Experiment in dark conditions.

The experiment was done at dark conditions (around 0 lux). Several concentration of 1-octen-3-ol odorant were prepared: 0nM (ringer solutions), 25nM, and 50nM. Experiment on each concentration was done 5 times. Figure 7.6(a) shows the typical response curves of Or13a cells to several concentration of 1-octen-3-ol odorant while Figure 7.6(b) shows the Boxplot distributions of cell responses under various concentration of 1-octen-3-ol odorant. Statistical analysis (t-test) was performed to each

concentration in pair with 0M concentration. Cell responses to 25nM concentration and above has statistically significant different from the response of 0M. Thus the detection limit of Or13a cells at dark conditions is around 25nM

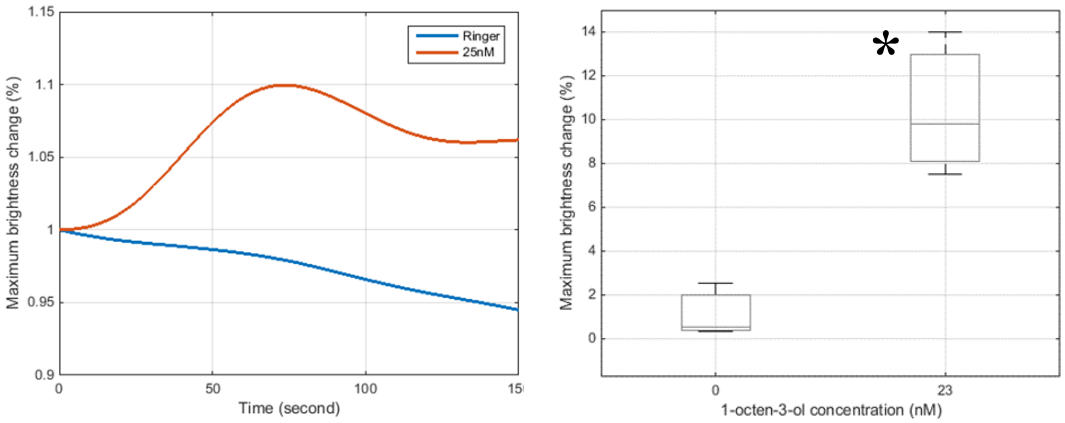

(a) (b)

Figure 7.6. Or13a response to 1-octen-3-ol at dark conditions. (a) Typical response curve. (b) Response distribution on Boxplot under various concentration. Response with (*) indicate the limit of detection.

7.5.2 Experiment in low intensity of ambient light condition

The experiment was done at low intensity of ambient light conditions (around 500 lux). Several concentration of 1-octen-3-ol odorant were prepared: 0nM (ringer solutions), 25nM, and 50nM. Experiment on each concentration was done 5 times. Figure 7.7(a) shows the typical response curves of Or13a cells to several concentration of 1-octen-3-ol odorant while Figure 7.7(b) shows the Boxplot distributions of cell responses under various concentration of 1-octen-3-ol odorant. Statistical analysis (t-test) was performed to each concentration in pair with 0M concentration. Cells responses to 25nM concentration and above has statistically significant difference from the response of 0M. Thus the detection limit of Or13a cells at dark conditions is around 25nM

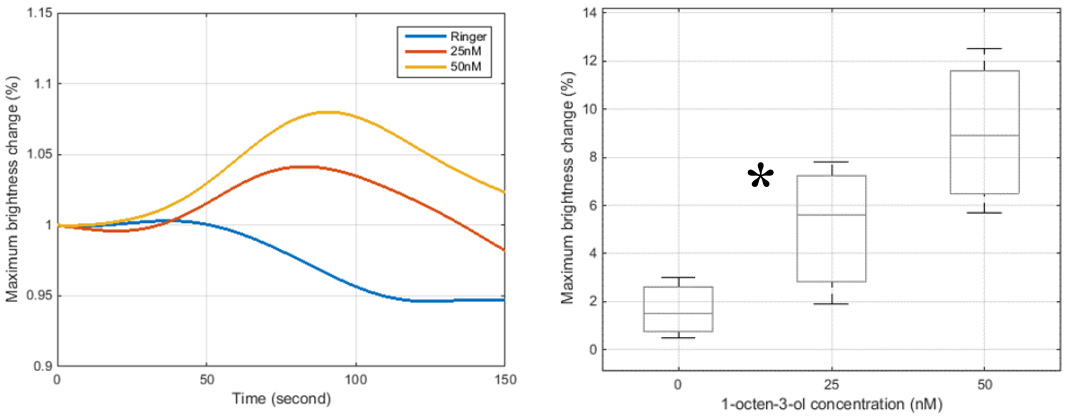

(a) (b)

Figure 7.7. Or13a response to 1-octen-3-ol at low intensity of ambient light conditions. (a) Typical response curve. (b) Response distribution on Boxplot under various concentration. Response with (*) indicate the limit of detection.

7.5.3 Experiment in high intensity ambient light condition

The experiment was done at high intensity of ambient light conditions (around 1000 lux). Several concentrations of 1-octen-3-ol odorant were prepared: 0nM (ringer solutions), 25nM, and 50nM. Experiment on each concentration was done 5 times. Figure 7.7(a) shows the typical response curves of Or13a cells to several concentration of 1-octen-3-ol odorant while Figure 7.7(b) shows the Boxplot distributions of cell responses under various concentration of 1-octen-3-ol odorant. Statistical analysis (t-test) was performed to each concentration in pair with 0M concentration. Cells responses to 50nM concentration and above has statistically significant difference from the response of 0M. Thus the detection limit of Or13a cells at dark conditions is around 50nM.

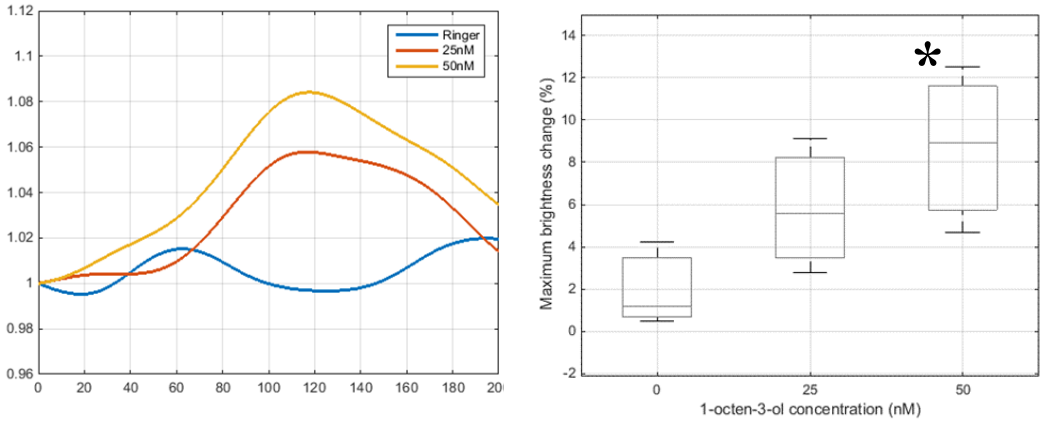

(a) (b)

Figure 7.8. Or13a response to 1-octen-3-ol at high intensity of ambient light conditions. (a) Typical response curve. (b) Response distribution on Boxplot under various concentration. Response with (*) indicate the limit of detection.

7.6 Chapter summary

In this chapter, some experiments using lock-in measurement technique on fluorescent instrumentation were performed. The purposes of the experiments were:

1. To observe the ability of lock-in measurement technique to extract the low intensity fluorescent light under ambient light conditions.
2. To do experiment on three different ambient light conditions (dark, low intensity, high intensity) and comparing the results among them.
3. To obtain the detection limit of the developed instrumentation with lock-in measurement technique incorporated.

Experiment using Or56a cells line without odorant in several ambient light conditions (section 7.2), shows that the outputs waveform obtained from three different conditions were similar except its dc level. In other words, the same fluorescent signal was obtained regardless of ambient light condition when we used lock-in amplifier technique. The dc level of the captured signal reflect the ambient light and it is not constant.

Experiment using Or56a cells line with Ringer solution and odorant (section 7.3) shows that the lock-in technique has ability to extract the low intensity fluorescent light under ambient light conditions. A lock-in technique shows the effectiveness in fluorescent measurement. Lock-in technique also improve the sensitivity of the instrumentation, thus a relatively low concentration of odorant can be detected at ambient light condition.

Experiment using two cell lines (Or56a and Or13a) with low concentration of their associate odorants (geosmin and 1-octen-3-ol) summarize in Table 7.1. The table shows that lock-in technique can be used at relatively low odorant concentration. It is also shown that the limit of detection at various conditions were relatively the same.

Table 7.1 Detection limit of Or56a (geosmin) and Or13a (1-octen-3-ol) under several conditions.

	Dark (0 lux)	**Low intensity (500 lux)**	**High intensity (1000 lux)**
Or56a	50nM	100nM	100nM
Or13a	25nM	25nM	50nM

Chapter 8

Performance of fluorescent instrumentation system with lock-in technique.

This chapter discussed improvement achieved by applying lock-in technique on fluorescent instrumentation system. The analysis was done by comparing experimental results in chapter 7 and chapter 5. Experiments in both chapters were conduct using flow system with syringe pump. In chapter 7, lock-in measurement technique was applied, while in chapter 5 was not. Previous experiment results from both static chamber and flow system with micro-pump showed a concentration dependency of the cell response. This dependency is expected to appear on experiment using flow system with syringe pump since it has better accuracy compared with micro-pump.

8.1 Analysis of the output signal of lock-in measurement technique.

The signals came from the experiment using Or13a cell line exposed to 50nM 1-octen-3-ol odorant at high intensity of ambient light condition. This concentration was impossible to be detected using developed measurement system without lock-in technique.

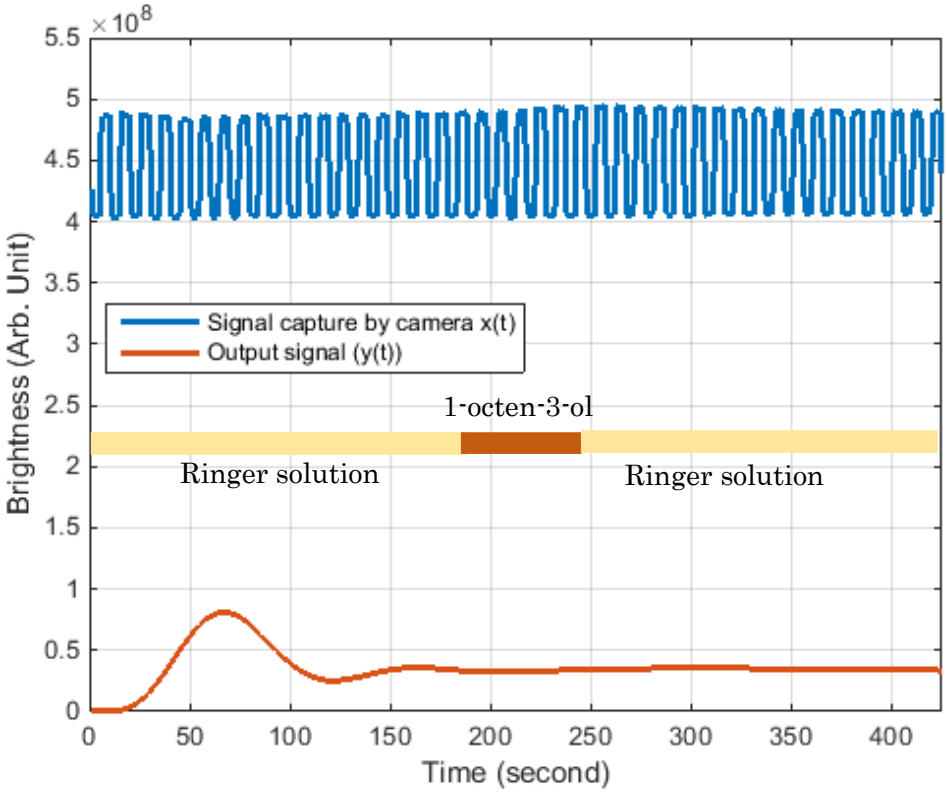

Figure 8.1 Plots of signal captured by camera u(t) and output signal y(t) from experiment using Or13a cell line and 50nM 1-octen-3-ol.

The cells were exposed to the ringer solution for the first 3 minutes followed by exposure to 50nM 1-octen-3-ol for 1 minute. Then, the solution was switched to the ringer one until the measurement was finished. Thus, the odorant was exposed at t = 180 second for about 60 second. Figure 8.1 shows the plot of signal *u(t)* captured by camera. The plot was not normalized, thus the value came from the image intensity calculated by camera. The width of *u(t)* was considered as fluorescent signal *x(t)*. Processing of u(t) by high-pass filter, phase sensitive detector, and low-pass filter resulted in output signal *y(t)*. From *y(t)* response (orange line), it can be seen that it took around 200 second for the system to be settled.

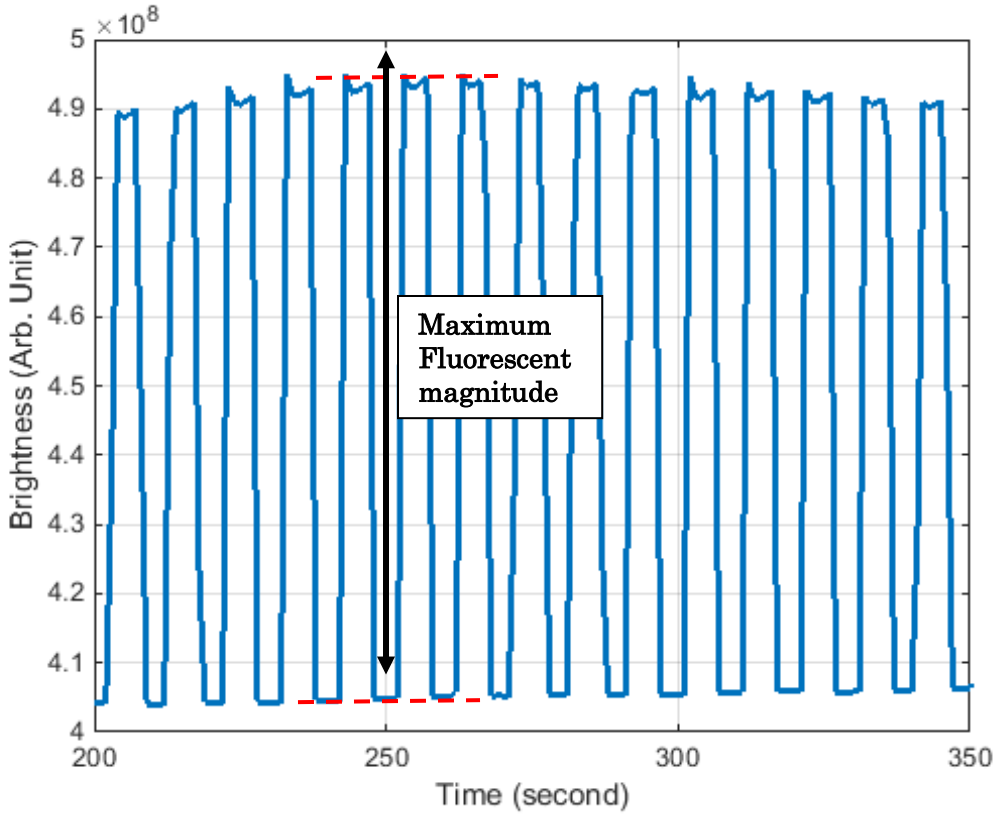

Figure 8.2 Magnification of *u(t)* in Fig. 8.1

The cell response to the odorant appeared at around t = 250 second, as it can be clearly seen in Figure 8.2. At t = 250 second, the magnitude of fluorescent signal was maximum which was around $9x10^7$ (arb. unit). The maximum value of *y(t)* achieved at around t = 300 second as shown in Figure 8.3. The constant time of lock-in measurement technique, combinations of its three blocks, was 50 second. At t = 300 second the magnitude of *y(t)* = $3.55x10^7$. In this section, the process of the analysis using lock-in technique was shown.

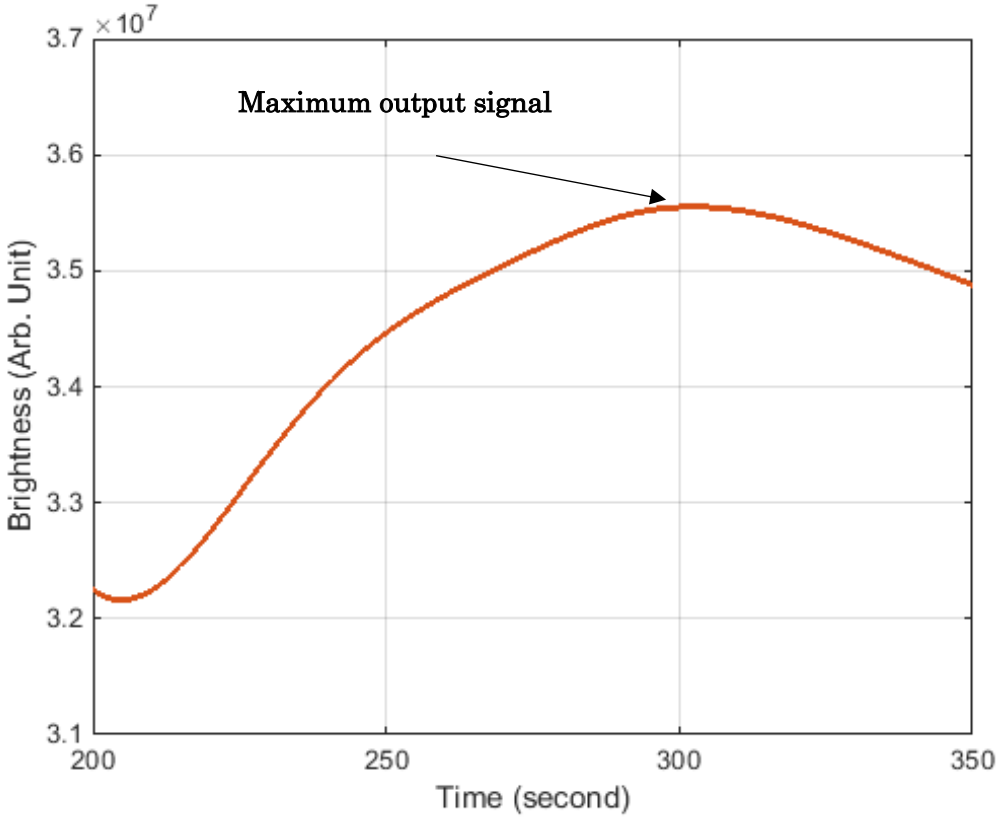

Figure 8.3 Magnification of *y(t)* in Fig. 8.1

8. 2 Improvement of detection limit.

Comparison of the detection limit in several conditions of ambient light both without and with lock-in technique applied shown in Tables 8.1 and 8.2 respectively. Table 8.1 is for Or56a cell with geosmin odorant while Table 8.2 is for Or13a with 1-ocnten-3-ol. The data for both tables obtained from chapter 5, for without lock-in, and chapter 7, with lock-in. The plots of data in tables 8.1 and 8.2 are shown in Figure 8.4 (a) and (b) respectively.

Table 8.1 Comparison of detection limit for Or56a with geosmin odorant

	Dark (0 lux)	**Low intensity (500 lux)**	**High intensity (1000 lux)**
Without lock-in (chapter 5)	200nM	10μM	100μM
With lock-in (chapter 7)	50nM	100nM	100nM
improvement	4x	100x	1000x

Table 8.2 Comparison of detection limit for Or13a with 1-octen-3-ol odorant

	Dark (0 lux)	**Low intensity (500 lux)**	**High intensity (1000 lux)**
Without lock-in (chapter 5)	50nM	10μM	100μM
With lock-in (chapter 7)	25nM	25nM	50nM
improvement	2x	400x	2000x

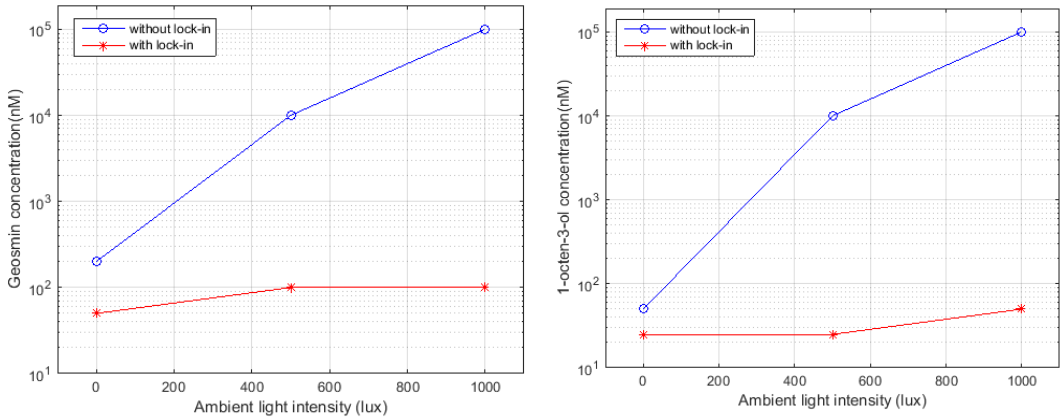

Figure 8.4 Plot of odorant detection limit of cells as a function of ambient light intensity. (a) Or56a cells with geosmin odorant and (b) Or13a cells with 1-octen-3-ol odorant.

From tables and figures, it was clear that application of lock-in technique improves sensitivity of the instrumentation system, especially when the intensity of ambient light becomes higher. Moreover, the fluorescent instrumentation with lock-in technique has stable detection limit. In this case either detection limits were around 50nM to 100nM for both Or56a and Or13a to geosmin and 1-octen-3-ol odorants respectively.

8.5 Summary

Fluorescent instrumentation system with incorporated lock-in measurement technique has been developed. Around 200 second was needed for the system to settle while the response time was around 50 second. This is due to very low sampling time (1 second). However, the developed instrumentation system has low and stable detection limit over the wide range of ambient light intensity compared to the system without lock-in technique. Moreover, the developed system has higher and more stable dynamic range compared to the system which does not have lock-in technique.

Chapter 9

9.1 Conclusions

The topic of the research is compact odor sensing system based on insect olfactory receptor fluorescent instrumentation system robust against disturbance. Fluorescent instrumentation system allows olfactory receptor based odor sensor to be realized. Development of small size and low power laser system contributed to the compact system. Moreover, small size chamber and micro-pump were also has contribution to compact system. Incorporating lock-in measurement technique in fluorescent system allows the system to be robust against disturbance such as the ambient light. Experimental results show that the system has low level stable detection limit under wide range of ambient light intensity. Moreover, the system has wide-stable dynamic range over various ambient light conditions. The conclusions from the development of odor sensing system and its experimental activities were:

- Using static chamber, the cells respond to the odorant and show a response dependence upon odorant concentration. However artifact occurs especially at odorant introduction.
- Using flow chamber with micro-pump the cells respond to the odorant and show a response dependence to odorant concentration. Although small artifact occurs, it is possible to realize a portable system using micro-pump.
- Using flow chamber with syringe-pump, the artifact can be minimized, thus it was possible to do measurement at low concentration of odorant and to find the detection limit.
- The presence of ambient light reduces the accuracy of measurement. However, by applying the lock-in measurement technique, the influence of ambient light can be reduced.
- A lock-in technique shows the effectiveness in fluorescent measurement. Experimental results show that the fluorescent signal can be extracted even under strong ambient light condition.
- The system has low-level & stable detection limit over wide range of ambient light intensity.
- The system has wide-stable dynamic range over various ambient light conditions.
- The improvement of the detection limit reached approximately three orders of magnitude under the ambient light condition.

9.2 Future works.

This research is an early stage of development a compact odor sensing system based on insect olfactory receptor and fluorescent instrumentation system robust against disturbance. From both developed instrumentation prototype and measurement procedure, it is possible to implement a robust, real time, and sensitive instrumentation system. However, several improvements should be made.

1. Image and lock-in processing was performed off-line using Matlab on a laptop PC which made the system slower and less compact. Another researcher in our group is implementing the image and lock-in technique processing into a FPGA platform. This will make improvement on speed, power dissipation, and compactness.
2. Several functional blocks of the system can be still optimized such as power of the laser for excitation light and the distance among the optical blocks to have more compact and less power dissipation.
3. Although the image of the cell was processed, only the fluorescent intensity was taken into account. This is because only one type of cells was used. Using the image data, observation can be extended to extraction of individual cell with high sensitivity.
4. More than one type of OR in one image can be involved to form a sensor array. Thus the system can be used to implement a compact and sensitive electronic nose.

Bibliography

1. A.D. Wilson, M. Baietto, **Applications and Advances in Electronic-Nose Technologies**, Sensors 9 (2009), pp. 5099-5148.
2. T. M. Dymerski, T. M. Chmiel, and W. Wardencki, **Invited Review Article: An odor-sensing system – powerful technique for food stuff studies**, Review of Scientific Instruments 82, 111101 (2011).
3. R.E. Baby, M. Cabezas, E.N. Walsöe de Reca, **Electronic nose: A useful tool for monitoring environmental contamination**. Sens. Actuat. B: Chem. 69 (2000), pp. 214-218.
4. A. P. F. Turner and N. Magan, **Electronic Noses and Disease Diagnostics,** Nature Reviews, Vol. 2, No. 2, 2004, pp. 161-166.
5. **J. Gardner**, J. **Yinon** (Eds.), **Electronic Noses & Sensors for the Detection of Explosives**, NATO Science Series II. Springer 2004.
6. K. Arshak, E. Moore, G.M. Lyons, J. Harris and S. Clifford, **A review of gas sensors employed in electronic nose applications**, Sensor Review, Volume 24, Number 2 (2004) pp. 181–198.
7. Y.K. Oh, Y. Lee, J. Heath, and M. Kim, **Applications of Animal Biosensors: A Review**, IEEE Sensor Journal, Vol. 15, No. 2, Feb. 2015.
8. G.H. Dodd, P.N. Bartlett and J.W. Gardner, in J.W. Gardner and P.N. Bartlett (Editors), **Sensors and Sensory Systems for an Electronic Nose, NATO ASI Series E**: Applied Sciences, Vol. 212, Kluwer, Dordrecht, 1992.
9. M.A. Craven, J.W. Gardner, P.N. Bartlett, **Electronic noses - development and future prospects**, trends in analytical chemistry, vol. 15, no. 9, 7996, pp. 486-493.
10. W.F. Wilkens and J.D Hatman, **An electronic analog for olfactory process**, Ann. NY Acad Sci. 1964, 116, pp. 608-12.
11. J. W. Gardner and P. N. Bartlett, **A Brief History of Electronic Noses**, Sensors an Actuators B, Vol. 18-19, No. 1-3, 1994, pp. 211-220.
12. U. Tomši˘c and I. Muševi˘c, **Detection of explosives: Dogs vs. CMOS capacitive sensors**, Faculty of Mathematics and Physics, Univ. Ljubljana, Ljubljana, Slovenia, Tech. Rep., SEMINAR1a 1st year,2nd cycle, 2013.
13. Y. Niimura, **On the Origin and Evolution of Vertebrate Olfactory Receptor Genes: Comparative Genome Analysis Among 23 Chordate Species,** Genome Biol Evol (2009), 1, pp. 34-44.

14. L. Buck and R. Axel, **A novel multigane family may encode odorants receptors: a molecular basis for odor recognition**, Cell, Vol.65, No.1, pp.175-187 (1991)
15. D.E Lynn, **Development and characterization of insect cell lines**, Cytotechnology 20, 1996, pp 3-11.
16. T. Mujiono, Y. Sukekawa. T. Nakamoto, H. Mitsuno, R. Kanzaki, N. Misawa, **Odor sensing method using olfactory receptors and fluorescent instrumentation**, Proceeding of the 2015 ASCC – Kota Kinabalu (Malaysia), May 31 – June 3.
17. Jennifer C. Walters, **Accuracy and precissin in quantitative fluorescence microscopy**, J. Cell Bio. Vol. 185 No 7, pp 1135-1148 (2009).
18. M. L. Meade, **Lock-in Amplifier: principles and applications**, Peter Peregrinus Ltd., London, (1983).
19. J. Bridgeman, A. Baker, D. Brown, J.B. Boxall, **Portable LED fluorescence instrumentation for the rapid assessment of potable water quality, Science of The Total Environment**, Vol. 524–525, 15 August 2015, Pages 338–346.
20. L. Du, C. Wu, Q. Liu, L. Huang, P. Wang, **Recent advances in olfactory receptor-based biosens**, Biosensors and Bioelectronics 42 (2013) pp.570–580
21. R.R. Seeley, T.D. Stephens, P. Tate**, Anatomy and Physiology**, 7/e, McGraw Hill
22. L. Turin, Y. Yoshii, **Structure-odor relation: A modern perspective**, in: R. Doty (Ed.) Handbook of olfaction and gustation, Marcel Dekker, Inc. New York, 2002.
23. S. Sankarana, L.R. Khota, S. Panigrahib, **Biology and applications of olfactory sensing system: A review**, Sensors and Actuators B: Chemical, 171– 172 (2012) pp.1– 17.
24. G. Laurent, M. Stopfer, R.W Friedrich, M.I Rabinovich, A. Volkovskii, H.D Abarbanel, **Odor encoding as an active, dynamical process: experiments, computation and theory**. Annu. Rev. Neorsci. 24. Pp. 263-297.
25. B. Malnic, P.A. Godfrey, and L.B. Buck, **The human olfactory receptor gene family**, Proc. Natl. Acad. Sci. USA, 101, (2004), pp. 2584–2589
26. R. Benton, **On the orogin of smell: odorant receptor in insect**, Cell. Mol. Life Sci. 63 (2006), pp. 1579-1585.
27. A. Couto, M. Alenius and B.J. Dickson, **Molecular, anatomical, and functional organization of the Drosophila olfactory system**. Curr. Biol. 15, (2005). Pp. 1535–1547.
28. B.W. Ache, J.M. Young, **Olfaction: diverse species,conserved principles**, Neuron 48, (2005), pp, 417–430.
29. G.H. Dodd, P.N. Bartlett, J.W. Gardner, **Odours-the stimulus for an electronic nose**, in: J.W. Gardner and P.N. Bartlett (Eds.) Sensor and Sensory system for an

electronic nose, NATO ASI Series E: Applied Science, Vol. 212, Kluwer, Dordrecht, 1992, Ch 1.

30. M.A. Craven, J.W. Gardner p, **Electronic noses – development and future prospect**,Trends in analytical chemistty, vol. 15, no. 9, pp. 486 – 493
31. J.W. Gardner, **A brief history of electronics noses**, Sensor and actuators B, 18-19 (1994), pp. 211 – 220.
32. J.S. Kauer, **Contributions of topography and parallel processing to odor coding in the vertebrate olfactory path**, Trends Neurosci., 14 (1991), pp. 79-95..
33. A.P. Turner, N. Magan, **Electronic noses and disease diagnostics**. Nat Rev Microbiol. 2 (2004), pp. 161–166
34. P. Pelosi, K.C. Persaud, in P. Darion (editor), **Gas sensors: Towards an artificial nose. In Sensors and Sensory Systems for Advanced Robotics**, Springer-Verlag: Berlin, Germany, 1988; pp. 361-381.
35. M. Peris and L. Escuder-Gilabert, **A 21st Century Technique for Food Control: Electronic Noses**, Analytica Chimica Acta, Vol. 638, No. 1, 2009, pp. 1-15.
36. T.C. Pearce, S.S. Schiffman, H.T. Nagle, and J.W. Gardner, **Handbook of Machine Olfaction**, Wiley-VCH (2003), Weinheim.
37. H. Bai and G. Shi, **Gas Sensors Based on Conducting Polymers**, Sensors, Vol. 7, No. 3, 2007, pp. 267-307.
38. S. Aathithan, J. C. Plant, A. N. Chaudry and G. L. French, **Diagnosis of Bacteriuria by Detection of Volatile Organic Compounds in Urine Using an Automated Head- space Analyzer with Multiple Conducting Polymer Sensors**, Journal of Clinical Microbiology, Vol. 39, No. 7,
39. A. L. Smith and H. M. Shirazi, **Principles of Quartz Crystal Microbalance/Heat Conduction Calorimetry: Measurement of the Sorption Enthalpy of Hydrogen in Palladium**, Thermochimica Acta, Vol. 432, No. 2, 2005, pp. 202-211
40. G. Xiea, P. Suna, X. Yana, X. Dua and Y. Jianga, **Fabrication of Methane Gas Sensor by Layer-by-Layer Self-Assembly of Polyaniline/PdO Ultra Thin Films on Quartz Crystal Microbalance**, Sensors and Actuators B: Chemical ,Vol. 145, No. 1, 2010, pp. 373-377.
41. L. Fan, H. Ge, S. Y. Zhang, H. Zhang and J. Zhu, **Optimization of Sensitivity Induced by Surface Conductivity and Sorbed Mass in Surface Acoustic Wave Gas Sensor**s, Sensors and Actuators B: Chemical, Vol. 171-172, 2012, pp. 1272-1276.

42. F. D. Lai and H. M. Huang, **Fabrication of High Frequency and Low-Cost Surface-Acoustic Wave Filters Using Near Field Phase Shift Photolithography**, Microelec-tronic Engineering, Vol. 83, No. 4, 2006, pp. 1407-1409.
43. W. Feng, R. Hettiarachchi1, S. Sato, K. Kakushima, M. Niwa, H. Iwai, K. Yamada and K. Ohmoril, **Advantages of Silicon Nanowire Metal-Oxide-Semiconductor Field-Effect Transistors over Planar Ones in Noise Properties**, Japanese Journal of Applied Physics, Vol. 51, No. 4, 2012.
44. J.A. Covington, J.W. Gardner, D. Briand, N.F. de Rooij, **A polymer gate fet sensor array for detecting organic vapours**, Sensors and Actuators B: Chemical, Vol. 77 No. 1-2, pp. 155-162.
45. T. Mujiono Totok, T. Nakamoto, Y. Sukekawa, H. Mitsuno, R. Kanzaki, N. Misawa. **A Cell-Based Odor Sensing System Using Fluorescent Technique and Lock-in Measurement Robust Against Disturbance**, IEEE Sensors 2015, Nov. 2015.
46. F. Zee,F.and J.W. Judy, **Micromachined polymer-based chemical gas sensor array**, Sensors and Actuators B: Chemical, Vol. 72 No. 2, pp. 120-8.
47. Y. Sakurai, H.S. Jung, T. Shimanouchi, T. Inoguchi, S Morita, R. Kuboi, R. and K. Natsukawa, **Novel array type gas sensors using conducting polymers, and their performance for gas identification**, Sensors and Actuators B: Chemical, Vol. 83 (2002) No. 1-3, pp. 270-5.
48. K.J. Albert, and N.S. Lewis, **Cross reactive chemical sensor arrays**, Chem. Rev., Vol. 100, (2000) p. 2595-626.
49. Z.P. Khlebarov, A.I. Stoyanova, and D.I. Topalova, **Surface acoustic wave gas sensors**, Sensors and Actuators B: Chemical, Vol. 8 No. 1 (1992), pp. 33-40.
50. E. Schaller, J.O. Bosset, and F. Escher, **Electronic noses and their application to food**, LebensmittelWissenschaft und-Technologie Vol. 31 No. 4 (1998), pp. 305-16.
51. J. Ricco, R. M. Crooks and G. C. Osbourn, **Surface Acoustic Wave Chemical Sensor Arrays: New Chemically Sensitive Interfaces Combined with Novel Cluster Analysis to Detect Volatile Organic Compounds and Mixtures**, Accounts of Chemical Research, Vol. 31, No.5, 1998, pp. 289-296.
52. J. Hartmann, J. Auge and P. Hauptmann, **Using the Quartz-Crystal-Microbalance Principle for Gas Detection with Reversible and Irreversible Sensors**, Sensors and Actuators B, Vol. 19, No. 1-3, 1994, pp. 429-433.
53. Y.H. Kim, K.J. Choi, **Fabrication and application of an activated carbon coated quartz crystal sensor**, Sensors and Actuators B Vol. 87, (2002) pp. 196-200.
54. H.T. Nagle, R. Gutierrez-Osuna, S.S. Schiffman, T**he how and why of electronic**

hoses, IEEE Spectrum Vol. 35 No. 9, (1998), pp. 22-31.

55. Tai Hyun Park (Editor), **Bioelectronic Nose, Integration of Biotechnology and Nanotechnology**, Springer 2014.
56. H. Williams and A. Pembroke, **Sniffer dogs in the melanoma clinic**, Lancet, vol. 1, no. 8640, p. 734, 1989.
57. R. Monosika, M. Stredanskyb, E. Sturdik, **Biosensors-classification, characteriza- tion and new trends**, Acta Chimica Slovaca, Vol. 5, No. 1, 2012, pp. 109—120.
58. R. Kanzaki, K. Nakatani, T. Sakurai, N. Misawa, and H. Mitsuno, **Physiology of chemical sense and its biosensor application**, in: T. Nakamoto (Ed.) Essential of machine olfaction and taste, Wiley, 2015.
59. P. Mombaerts, **Seven-transmembrane proteins as odorant and chemosensory receptors**. Science 286, (1999), pp. 707–711.
60. Encyclopedia Britannica online, (www.britannica.com)
61. Encyclopedia Britannica online, (www.britannica.com)
62. Mujiono Totok, Yoshinori Suzuki, Takamichi Nakamoto, H. Mitsuno, R. Kanzaki, Nobuo Misawa, **Odor Sensing System Based on Olfactory Receptors and Fluorescent Instrumentation**, IEE of Japan, Sensor Symp, 2014, 20PM3-PS075
63. N. Misawa, H. Mitsuno, R. Kanzaki, and S. Takeuchi, **Highly sensitive and selective odorant sensor using living cells expressing insect olfactory receptors**, PNAS, Vol. 107, pp. 15340–15344 (2010).
64. Mujiono Totok, Yuji Sukekawa, Takamichi Nakamoto, H. Mitsuno, R. Kanzaki, Nobuo Misawa. **Odor sensing method using olfactory receptors and fluorescent instrumentation**, The 10th Asian Control Conference 2015, 2015.
65. C.A.Thomas,Jr., P.A. Springer, G.E Loeb, Y. Berwald-Netter, L.M. Okun, **A miniature microelectrode array to monitor the bioelectric activity of cultured cells**, Exp. Cell Res., Sept. 74, 1, (1972), pp. 61-66.
66. T. Nomura, M. Okuhara, Frequency shift of piezoelectric quartz crystals immersed in organic liquid, Anal. Chim. Acta 142 1982, pp. 281-284.
67. R.L. Rich, D.G. Myszka, **Advances in surface plasmon resonance biosensor analysis**, Curr. Opin. Biotechnol.11, 2000, pp, 54-61.
68. P. Fromherz, A. Offenhausser, T. Vetter, J. Weis, **A neuron-silicon junction- A Retzius cell of the leech on an insulated- gate field-effect transistor**, Science 252 (1991) 1290-1293.
69. D.R. Walt, V. Agayn, K. Bronk, and S. Barnard, **Fluorescent Optical Sensors,** Applied Biochemistry and Biotechnology, VoL 41, (1993), pp 129-138

70. W. Roelofs, A. Comeau, **Sex pheromone perception: electroantennogram responses of the red-banded leaf roller moth**, J. Insect Physiol., 17, (1071), pp. 1969–1982
71. D.G. Hafeman, J.W. Parce, H.M. McConnell, **Light-addressable potentiometric sensor for biochemical systems**, Science 240 (4856), (1988) pp. 1182-1185.
72. Q. Liu, N. Hu, F. Zhang, D. Zhang& K. Hsia, P. Wang, **Olfactory epithelium biosensor: odor discrimination of receptor neurons from a bio-hybrid sensing system**, Biomed Microdevices, 14, (2012), pp. 1055–1061
73. Q. Liu, W. Ye, L. Xiao, L. Du, N. Hu, P. Wang, **Extracellular potentials recording in intact olfactory epithelium by microelectrode array for a bioelectronic nose,** Biosensor and bioelectronics, vol. 25, 10 (2010), pp. 2212-2217
74. Q. Liu, W. Ye, L. Xiao, N. Hu, H. Cai, Y. Yu, P. Wang, **Olfactory receptor cells respond to odors in a tissue and semiconductor hybrid neuron chip**, Biosensors and Bioelectronics 26 (2010), pp. 1672–1678.
75. Q. chen, L. Xiao, Q. Liu, S. Ling, Y. Yin, Q. Dong, P. Wang, **An olfactory bulb slice-based biosensor for multi-site extracellular recording of neural networks**, Biosensors and Bioelectronics 26 (2011) pp. 3313–331
76. K.C. Park KC, S.A. Ochieng, J. Zhu, T.C. Baker, **Odor discrimination using insect electroantennogram responses from an insect antennal array,** Chem Senses. May;27(4), (2002), pp. 343-352.
77. E, Neher, M**olecular biology meets microelectronics**, *Nature Biotechnology* **19**, 114 (2001), pp 114.
78. Q. Liu, H. Cai, Y. Xu,Y. Li, R. Li, P. Wang, **Olfactory cell-based biosensor: A first step towards a neurochip of bioelectronic nose**, Biosensors and Bioelectronics, 22 (2009), pp. 318–322.
79. M. Huotari, V. Lantto, **Measurements of odours based on response analysis of insect olfactory receptor neurons**, Sensors and Actuators B, 127, (2007), pp.284–287.
80. C. Wu, P. Chen, H. Yu, Q. Liu, X. Zong, H. Cai, P. Wang, **A novel biomimetic olfactory-based biosensor for single olfactory sensory neuron monitoring**, Biosensors and Bioelectronics,24 (2009), pp. 1498–1502
81. A. Corcellia, S. Lobassoa, P. Lopalcoa, M. Dibattistab, R. Aranedac, Z. Peterlind, S. Firestein, **Detection of explosives by olfactory sensory neurons**, Journal of Hazardous Materials, 175 (2010), pp. 1096–1100.
82. N. Tanada, T. Sakurai, H. Mitsuno, D.J. Bakkum, R. Kanzakiac, H. Takahashi, **Dissociated neuronal culture expressing ionotropic odorant receptors as a**

hybrid odorant biosensor—proof-of-concept study, Analyst, 137, (2012), pp. 3452–3458.

83. H.J. Ko, T.H. Park, **Piezoelectric olfactory biosensor: ligand specificity and dose-dependence of an olfactory receptor expressed in a heterologous cell system**, Biosensors and Bioelectronics, 20 (2005), pp. 1327–1332.
84. H.J. Ko, T.H. Park, **Dual signal transduction mediated by a single type of olfactory receptor expressed in a heterologous system**, Biol. Chem., 387(1) (2006), pp, 59-68.
85. H. Mitsuno, T. Sakurai, S. Namiki, H. Mitsuhashi, R. Kanzaki, **Novel cell-based odorant sensor elements based on insect odorant receptors**, Biosensor and bioelectronics, 65 (2015), pp. 287-294.
86. L. Du, C. Wu, Q. Liu, L. Huang, P. Wang, **Recent advances in olfactory receptor-based biosensors**, Biosensors and Bioelectronics, 42 (2013), pp. 570–580.
87. J.M. Vidic, J. Grosclaude, M. Persuy, J. Aioun, R. Salesse, E. Pajot-Augy, **Quantitative assessment of olfactory receptors activity in immobilized nanosomes: a novel concept for bioelectronic nose**, Lab on a chip, 8 (2006), pp. 1026-1032.
88. T.Z. Wu, **A piezoelectric biosensor as an olfactory receptor for odour detection: electronic nose**, Biosensors and Bioelectronics, 14 (1999), pp. 9-18.
89. H.Yoon, S.H. Lee, O.S. Kwon, H.S. Song, E.H. Oh, T.H. Park, J. Jang, **Polypyrrole Nanotubes Conjugated with Human Olfactory Receptors: High-Performance Transducers for FET-Type Bioelectronic Noses**, Angew. Chem. Int. Ed.2009, 48, 2755–2758.
90. L. Kaiser, J. Graveland-Bikker, D. Steuerwald, M. Vanberghem, K. Herlihy, S. Zhang, **Efficient cell-free production of olfactory receptors: Detergent optimization, structure, and ligand binding analyses**, PNAS, vol. 105, no. 41 (2008), pp. 15726–15731.
91. Y. Houa, N. Jaffrezic-Renaulta, C. Marteleta, A. Zhangb, J. Minic-Vidicc, T. Gorojankinac, M.A. Persuyc, E. Pajot-Augyc, R. Salessec, V. Akimovd, L. Reggianid, C. Pennettad, E. Alfinitod, O. Ruize, G. Gomilae, J. Samitiere, A. Errachide, **A novel detection strategy for odorant molecules based on controlled bioengineering of rat olfactory receptor I7**, Biosensors and Bioelectronics, 22 (2007), pp. 1550–1555.
92. T.H. Kim, S.H. Lee, J. Lee, H.S. Song, E.H. Oh, T.H. Park, S. Hong, **Single-Carbon-Atomic-Resolution Detection of Odorant Molecules using a Human Olfactory Receptor-based Bioelectronic Nose**, Adv. Mater. 21 (2009), pp. 91–94.

93. S. Sankarana, S. Panigrahia, S. Mallik, **Olfactory receptor based piezoelectric biosensors for detection of alcohols related to food safety applications**, Sensors and Actuators B, 155 (2011) pp. 8–18.
94. George M. Whitesides, **The origins and the future of microfluidics,** Nature 442, (27 July 2006), pp. 368-373.
95. S. K. Sia, G.M. Whitesides, **Microfluidic devices fabricated in poly(dimethyl siloxane) for biological studies**, Electrophoresis 24 (2003), pp. 3563–3576.
96. J. Noh, H.C. Kim, T.D Chung, **Biosensors in microfluidic chips**, Top Curr Chem 304 (2011), pp. 117–152.
97. K.K. Liu, R.G. Wu 2, Y.J. Chuang 3, H.S. Khoo, S.H. Huang, F.G. Tseng, **Microfluidic Systems for Biosensing**, Sensors, 10 (2010), pp. 6623-6661.
98. X.A. Figueroa, G.A. Cooksey, S.V. Votaw, L.F. Horowitz, A. Folch, **Large-scale investigation of the olfactory receptor space using a microfluidic microwell array**, Lab Chip. 10(9) (2010), pp. 1120-1127.
99. D. Coling D, B. Kachar, **Principles and application of fluorescence microscopy**, Current Protocols in Neuroscience 2*:* (2007)**,** pp. 2.1-2.24.
100. Matthew J. Aernecke, David R. Walt, **Optical-fiber arrays for vapor sensing**, Volume 142, Issue 2, 5 November 2009, Pages 464–469.
101. J. Lippincott-Schwartz, G.H. Patterson, **Development and Use of Fluorescent Protein Markers in Living Cells**, Science, Vol 300, 4 April 2003, pp. 87-91.
102. G. Grynkiewicz, M. Poenie, and R.Y. Tsien, **A new generation of Ca2+ indicators with greatly improved fluorescent properties**, The Journal of Biological Chemistry, Vol.260, March 25, pp. 3440-3450 (2005)
103. J.B. Edel, N.P. Beard, O. Hofmann, J.C. deMello, D.D.C. Bradley, A.J. deMello, **Thin-film polymer light emitting diodes as integrated excitation sources for microscale capillary electrophoresis**, Lab Chip 4 (2004)136.
104. T.H. Wilmshurst, **Signal Recovery from Noise in Electronic Instrumentation**, 2nd ed, Taylor&Francis Group: New York, NY, USA, 1990.
105. A De Marcellis, G. Ferri, A. D'Amico, C. Di Natale, and E. Martinelli, **A fully analog lock-in amplifier with automatic phase alignment for accurate measurement of ppb gas concentration**, IEEE Sensors J., Vol.12, No.5, (2012), pp.1377-1383.
106. P.M. Maya-Hernández, L.C. Álvarez-Simón, M.T. Sanz-Pascual, B. Calvo López, **An Integrated Low-Power Lock-In Amplifier and Its Application to Gas Detection**, Sensors 14 (2014), pp. 15880-15899.

107. L. Novak, P. Neuzil, J. Pipper, Y. Zhang and S. Lee, **An integrated fluorescent detection for lab-on-chip applications**, The Royal Society of Chemistry (Lab Chip), 7 (2007), pp. 27-29.
108. G. Mariott, S. Mao, T. Sakata, J. Ran, D. K. Jackson C. Petchprayoon, T. J. Gomez, E. Warp, O. Tulyathan, H. L. Aaron, E. Y. Isacoff, and Y. Yan, **Optical lock-in detection imaging microscopy for contrast-enhanced imaging in living cells**, PNAS November 8, (2008), vol. 105, no. 46, pp. 17789-17794.
109. M. Benzo, A. Mantovani, A. Pittarello, **Measurement of Odour Concentration of Immissions using a New Field Olfactometer and Markers' Chemical Analysis**, Chemical engineering transaction, 30 (2012), pp. 103-108.
110. ST. CROIX SENSORY INC, 2003, <www.fivesenses.com/Prod_NasalRanger. cfm>, accessed 1.8.2016
111. IDES CANADA INC, 2012, <www.scentroid.com>, accessed 1.8.2016.
112. M. Benzo, G. Gilardoni, **Successful application of thermal desorption GC/MS – olfactometry technique to the identification of main odorants in complex mixtures of volatile compounds**, Chemical Engineering Transactions, 15, (2008), pp. 199-206.
113. C. McGinley, **Enforceable Permit Odour Limits**, The Air and Waste Management Association Environmental Permitting Symposium II, (2000), Chicago, USA.
114. Y. Tanaka, T. Nakamoto, T. Moriizumi, **Study of highly sensitive smell sensing system using gas detector tube combined with optical sensor**, Sensor and Actuator B 119 (2006), pp. 84-88.
115. T. Kawaguchia, D.R. Shankarana,, S.J. Kima, K. Matsumotoc, K. Toko, N. Miura, **Surface plasmon resonance immunosensor using Au nanoparticle for detection of TNT**, Sensors and Actuators B 133 (2008) 467–472.
116. NICHIA CORP., NDS1316E Engineering Sample data sheet.
117. NICHIA CORP., NDS4116E Engineering Sample data sheet.
118. ELM Technology, ELM185BB Laser Diode Driver data sheet.
119. HAMAMATSU, G2711-01 GaAsP Photodiode data sheet
120. Linear Technology, LT1001 Precision Operational Amplifier data sheet.
121. Bitran, SC-52C CMOS Camera Manual.

List of publications:

Journal Paper

1. **Mujiono Totok**, Yuji Sukekawa, Takamichi Nakamoto, Hidefumi Mitsuno, Nakajima Yuko, Ryohei Kanzaki, Nobuo Misawa. **Lock-in measurement technique in fluorescent instrumentation system for cell-based odor sensor**, IEEJ Trans. SM, Vol.136, No.3, 2016, pp. 83-89
2. Yuji Sukekawa, **Totok Mujiono**, Takamichi Nakamoto, Hidefumi Mitsuno, Yuko Nakajima, Ryohei Kanzaki, Nobuo Misawa, **Development of Automated Flow Measurement System for Cell-based Odor Sensor**, Trans IEE of Japan, accepted for publication (in Japanese).
3. **Totok Mujiono**, Yuji Sukekawa, Takamichi Nakamoto, Hidefumi Mitsuno, Maneerat Termtanasombat, Ryohei Kanzaki, Nobuo Misawa, **Sensitivity improvement of applying lock-in technique in fluorescent instrumentation for cell-based odor sensor**, Sensor and Material Journal, accepted for publication

International Conference (Refereed paper)

1. **Mujiono Totok**, Yuji Sukekawa, Takamichi Nakamoto, H. Mitsuno, R. Kanzaki, Nobuo Misawa. **Odor sensing method using olfactory receptors and fluorescent instrumentation**, The 10th Asian Control Conference 2015, 2015.

International Conference

1. **Mujiono Totok**, Takamichi Nakamoto, Yuji Sukekawa, H. Mitsuno, R. Kanzaki, Nobuo Misawa. **A Cell-Based Odor Sensing System Using Fluorescent Technique and Lock-in Measurement Robust Against Disturbance**, IEEE Sensors 2015, Nov. 2015.
2. Yuji Sukekawa, **Totok Mujiono**, Takamichi Nakamoto, Hidefumi Mitsuno, Yuko Nakajima, Ryohei Kanzaki, Nobuo Misawa, **Automated flow measurement for cell-based odor sensing system**, Biosensors 2016, 014.
3. Yuji Sukekawa, **Totok Mujiono**, Takamichi Nakamoto, Hidefumi Mitsuno, Ryohei Kanzaki, **Spatially parallelized lock-in measurement technique for cell-based odor biosensor**, International Symposium on Olfaction and Taste, 2016, Yokohama, P2-073.

Domestic Conference

1. **Mujiono Totok**, Yoshinori Suzuki, Takamichi Nakamoto, H. Mitsuno, R. Kanzaki, Nobuo Misawa. **Odor Sensing System Based on Olfactory Receptors and Fluorescent Instrumentation**, IEE of Japan, Sensor Symp, 2014, 20PM3-PS075
2. **Mujiono Totok**, Takamichi Nakamoto, H. Mitsuno, R. Kanzaki. **Lock-in measurement technique in optical measurement system for olfactory receptor-based odor sensor**, The 2015, annual meeting record, IEE of Japan, 3-085
3. **Mujiono Totok**, Yuji Sukekawa, Takamichi Nakamoto, H. Mitsuno, Maneerat Termtanasombat, Ryohei Kanzaki, Nobuo Misawa, **Detection limit of OR-based odor sensor using lock–in fluorescent instrumentation**, The 2016, annual meeting record, IEE of Japan, 3-104
4. Yuji Sukekawa, **Totok Mujiono**, Takamichi Nakamoto, Hidefumi Mitsuno, Yuko Nakajima, Ryohei Kanzaki, Nobuo Misawa, **Study on flow measurement system for cell-based odor sensor**, The papers of technical meeting on chemical sensor, IEE of Japan, 2015, CHS-15-024 (in Japanese).
5. Yuji Sukekawa, **Totok Mujiono**, Takamichi Nakamoto, Hidefumi Mitsuno, Yuko Nakajima, Ryohei Kanzaki, Nobuo Misawa, **Measurement system of cell-based odor sensor using space division parallel lock-in measurement**, The 2016, annual meeting record, IEE of Japan, (in Japanese).